The galactic dynamo and its relation to the propagation of ultra-high-energy cosmic rays

White, Michael P.

The Galactic Dynamo and its Relation to the Propagation of Ultra-High-Energy Cosmic Rays

A Thesis Submitted to the University of Durham
for the Degree of Doctor of Philosophy

by

Michael P. White, BSc (London)

January 1977

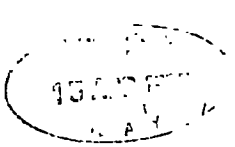

Ad Majorem Dei Gloriam

Abstract

The problem of the origin and nature of the galactic magnetic field is of fundamental interest. The astrophysical consequences of this field are far-reaching, being particularly relevant to the unsolved problem of the origin of cosmic rays. An analysis is made of the small-scale and large-scale features of the distribution of arrival directions of ultra-high-energy cosmic rays in the hope of deducing information about their sources and the strength and degree of irregularity of galactic and intergalactic magnetic fields. The outcome of these statistical searches is negative.

After a review of the basic ideas of the turbulent dynamo, techniques are developed for performing numerical experiments upon the galactic dynamo. The results of these experiments indicate that dynamo action can occur in the galaxy and a steady solution is most easily excited. The dependence of the models upon boundary conditions and relevant astrophysical parameters is investigated. An attempt is made to simulate the nonlinear effect of suppression of turbulence by the magnetic field, which is incorporated into the model proposed for the Galaxy.

The propagation of ultra-high-energy cosmic rays is examined for this model. It is found that these particles cannot be of Galactic origin if they are protons, in agreement with the results obtained from conventional field models.

Comparisons are made between the predictions of the dynamo models and the observed synchrotron radiation from the Galaxy and external galaxies which shed some light upon the nature of the intergalactic medium.

Preface

The work presented in this thesis was carried out during the period 1973-76 while the author was a research student under the supervision of Dr J.L. Osborne in the Physics Department of the University of Durham. During this period the author visited the Central Research Institute for Physics, Budapest (November-December 1975) having discussions with Mr. P. Kiraly on the problem of the galactic dynamo. Visits have also been made to Professor P.H. Roberts and Dr. A.M. Soward at the School of Mathematics, University of Newcastle during the period 1975-76 while working on the dynamo problem.

The results of the author's earlier work, which included collaboration with Mr. P. Kiraly, presented in Chapters Two and Three, have been published in the following papers:

Kiraly P and White M 1975 J. Phys. A Math Gen 8 1336-48

Kiraly P et al 1975 J. Phys A Math Gen 8 2018-31

Kiraly P et al 1975 Nature 255 619-20

Contents

Chapter One. Introduction

The subject of cosmic magnetic fields had its beginnings with William Gilbert, the chief physician in attendance to Queen Elizabeth I, who in 1600 published a treatise asserting that the earth's magnetic field was that of a dipole, like a uniformly magnetized lodestone. Until Hale (1908) discovered by means of the Zeeman effect that sunspots were associated with magnetic fields of the order of 1000 Gauss, the earth had remained the only celestial body known to be surrounded by a magnetic field. Although the physical principles required for magnetohydrodynamics had been established before the publication of Maxwell's electromagnetic theory, magnetohydrodynamic phenomena have only become manifest through observing the large-scale phenomena occurring in the cosmos. The largest scales upon which magnetic fields have been observed are found in galaxies.

Some years after Hale's discovery Larmor (1919) suggested that sunspot magnetic fields could be explained by a self-excited dynamo mechanism. In this theory, the motion of the highly conducting solar gases across the lines of force of a weak seed field was supposed to generate electric currents which amplify this field and sustain it. Larmor envisaged the motion and the magnetic field to have axial symmetry about the vertical axis of the sunspot but Cowling (1934) criticized this theory, producing his non-existence theorem to the effect that axisymmetric motions cannot maintain an axisymmetric steady field. As magnetohydrodynamics developed interest was renewed in the major unsolved problem of the origin of the earth's magnetic field. Through the work of Bullard and Gellman (1954), and others referenced therein, it became clear that the dynamo mechanism provided the best hope of formulating a theory for the maintenance of the geomagnetic field.

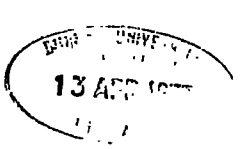

However, it was not until some years later that rigorous proofs for the existence of homogeneous hydromagnetic dynamos were established by Herzenberg (1958) and Backus (1958).

As progress was made in understanding the terrestial and solar magnetic fields it was possible to turn attention to the problem of the Galactic magnetic field. The advent of radio astronomy and cosmic ray astrophysics emphasized the importance of such a study. The first suggestion of a galactic magnetic field appears to have been made by Alfven in 1937 (Kaplan and Pikelner, 1970). Later this was substantiated somewhat by Fermi (1947) and Richtmeyer and Teller (1949) in connection with the study of the motion of cosmic rays, their isotropy, and possibilities for acceleration. In fact, the initial motivation for the study of the galactic dynamo presented here arose from problems connected with the isotropy and origin of ultra-high-energy cosmic rays.

Evidence for the existence of a magnetic field in the Galaxy was first found from the polarisation of starlight by Hiltner (1949), suggesting that this polarisation was caused by scattering from dust grains aligned in the Galactic magnetic field. The results indicated that the magnetic field was parallel to plane of the Galaxy. Later the Zeeman effect was used by Bolton and Wild (1957) for studying the field. Splitting of the 21 cm absorption line is observed when clouds of neutral hydrogen are seen in the line of sight of strong radio sources. However, Zeeman effect measurements tend to give information about the fields in localised regions of the Galaxy and cannot be used to test global aspects of field models. Faraday rotation of extragalactic and galactic sources also provides means of observing the field. The plane of polarisation of polarised radiation is rotated as it passes through the interstellar plasma in a magnetic field.

In view of the ambiguities arising from such observations (Seielstad et al 1964) they are unreliable indicators of the field. The most reliable observations of the field are provided by the Faraday rotation of polarised radio emission from pulsars. Observations of such rotation measures (Manchester, 1974) suggest that the field in the local region (about 1 kpc from earth) consists of a longitudinal component of strength $2.2 \pm 0.4\ \mu G$ directed toward $l^{II} = 94^{o} \pm 11^{o}$, together with superimposed irregularities of comparable field strength. Synchrotron radiation from the Galaxy, which is discussed in greater detail in Chapter Eight, provides a means of observing the large-scale features of the magnetic field. Davies (1965) made the earlier measurements using this method.

The observational situation of the large-scale isotropies of the distribution of arrival directions of ultra-high-energy cosmic rays is summarized in Chapter Two. This is followed by a detailed analysis of the small-scale features of this distribution in Chapter Three. As well as testing cosmic ray origin hypotheses, such an investigation can yield information upon the strength and structure of galactic and intergalactic magnetic fields. Attention is then turned to the problem of origin and nature of the galactic magnetic field, introducing some of the basic concepts of dynamo theory in Chapter Four. The numerical techniques necessary for investigating the galactic dynamo are developed in Chapter Five. These techniques are largely a generalization of those already established in connection with investigations of terrestial and solar dynamos. The simple dynamo model formulated in Chapter Five is developed in Chapter Six, including an attempt to incorporate nonlinear effects. Using the field model constructed, the propagation of ultra-high-energy cosmic rays in the Galaxy is investigated.

Before making concluding remarks in Chapter Nine, a comparison is made of the models and the observations of non-thermal radio emission from the Galaxy and external galaxies.

References

Backus, G.E. 1958 Ann Phys 4 372

Bolton, J.G and Wild, J.P. 1957 Astrophys J. 125 296

Cowling, T.G. 1937 MNRAS 94 39

Davies, R.D. 1965 Proc. 9th Int. Conf. on Cosmic Rays (London), (Institute of Physics and the Physics Society) Vol 1 35

Fermi, E. 1949 Phys. Rev. 75 1169

Hale, G.E. 1908 Astrophys J. 28 100

Herzenberg, A. 1958 Phil. Trans. Roy. Soc. London, A 250 543

Hiltner, W.A. 1949 Astrophys J. 109 471

Kaplan, S.A and Pikelner, S.B. 1970 "The interstellar medium" Havard University Press Cambridge, Mass. p 225

Larmor, J. 1919, Brit. Assoc. Reports, 159

Manchester, R.N. 1974 Astrophys J. 188 637

Richtmeyer, R.D and Teller, E. 1947 Phys. Rev. 75 1729

Seielstad, G.A. et al 1964 Astrophys J. 142 53

Chapter Two. The Anisotropy of Ultra-High-Energy Cosmic Rays: Large-Scale Features

2.1 Introduction

One of the most intriguing features of cosmic ray physics is the high degree of isotropy of arrival directions of the primaries throughout the energy range where interplanetary effects are thought to be negligible (i.e above a few hundred GeV for protons). Below 10^{17} eV all plausible source candidates are several Larmor radii away, and particles may be expected to undergo several random scatterings before reaching Earth.

In a 3μG interstellar magnetic field the Larmor radius (r_L) for protons is $\sim$ dimensions of typical field irregularities (30 pc) at 10^{17} eV, $\sim$ half-thickness of the disk (300 pc) at 10^{18} eV, and $\sim$ comparable to the distance between adjacent Galactic arms (3 kpc) at 10^{19} eV. Galactic source candidates (supernovae, supernova remnants, pulsars) are no longer many Larmor radii away at these energies, it is reasonable to expect an increasingly anisotropic distribution for the Galactic component of cosmic rays, and one might hope to identify sources at the highest energies. The distances of extragalactic source candidates (extragalactic supernovae, rich clusters of galaxies, radio and Seyfert galaxies, quasars, intense x-ray sources) are several orders of magnitude larger, but the magnetic field in intergalactic space might be sufficiently weak so that individual sources emerge.

For nuclei of given total energy $r_L \propto Z^{-1}$, so for heavier nuclei the distribution is more isotropic and individual sources are more difficult to see. If some of the primaries are neutral, then there should be some sharp peaks in the actual distribution of arrival directions, although the observed distribution of the peaks would be broadened by errors in the measured directions of primaries ($\sim 5°$).

The large-scale features of the distribution of cosmic rays $\gtrsim 10^{19}$ eV are now considered.

2.2 The Isotropy of Cosmic Rays with Energies $\gtrsim 10^{19}$ eV

The arrival directions of the 87 largest air showers ($E > 1.5 \times 10^{19}$ eV) available at that time were analysed by Linsley and Watson (1974) and the distribution found to be isotropic. A few months later the data was extended (20 showers from Yakutsk and 12 with 10^{19} eV $< E < 1.5 \times 10^{19}$ eV from Haverah Park being added, bringing the total to 119) and it has been claimed by a joint paper (Krasilnikov et al 1974) of Haverah Park, Volcano Ranch, and Yakutsk that these data give some statistical evidence for a huge anisotropy, harmonic analysis being carried out for selected declination intervals, grouping the data into 2h RA bins.

Kiraly (Kiraly and White, 1975) has given a detailed account of the statistical aspects of this proposed anisotropy, finding no strong evidence in its favour. These findings are summarized as follows. The impressive significance levels published by Krasilnikov et al represented 'a posteriori' statistics both from the point of view of choosing the method of harmonic analysis and also from the point of view of selecting those declination intervals where either the first or the second harmonic has a fairly high significance. Making attempts to simulate the selection effects involved, chance probabilities were calculated for χ^2 analysis, analysis for high maxima in individual bins, as well as harmonic analysis. The results indicated that the statistical evidence for a genuine anisotropy was weak.

Later at the 14th International Cosmic Ray Conference (Munich, 1975) Krasilnikov revealed that there was a mistake in the published arrival directions of Yakutsk, and supplied revised values.

This further weakened the evidence for anisotropy. At the conference six more events were added to the world statistics from Haverah Park (Edge et al, 1975). Figure 2.1 shows the total 125 events, displayed on an equal-area Hammer projection. The parametric equations for this projection are derived in Appendix I. The Galactic plane, Galactic centre (GC) and Galactic anti-centre (GAC) are also shown. Our subsequent analyses pertain to this set of data.

2.3 Correlations with Relevant Regions in the Galaxy and Supercluster

The statistical expectation of the number of showers coming from a given region G of the sky is calculated in the following way. For each observed shower a line is drawn of constant δ (see figure 2.2) and the ratio of the section inside G to the total length (2π) is calculated. Assuming complete isotropy, then these ratios can be interpreted as the probabilities p_i of the i^{th} shower falling inside G. The change in observational coverage with δ does not affect these probabilities.

The statistical expectation for the number of showers n which fall inside G is

$$\langle n \rangle = \sum_{i=1}^{N} p_i \qquad (2.3.1)$$

N is the number of observed showers whose lines intersect G. The standard deviation of n is given by

$$\sigma^2 = \langle (n - \langle n \rangle)^2 \rangle = \sum_{i=1}^{N} p_i (1 - p_i) \qquad (2.3.2)$$

Setting

$$\bar{p} = \frac{1}{N} \sum_{i=1}^{N} p_i \qquad \delta p_i = p_i - \bar{p} \qquad (2.3.3)$$

(2) becomes

$$\sigma^2 = \sum_{i=1}^{N} (\bar{p} + \delta p_i)(1 - \bar{p} - \delta p_i) = N\bar{p}(1 - \bar{p}) - \sum_{i=1}^{N} \delta p_i^2 \qquad (2.3.4)$$

The standard deviation of n is always smaller than it would be for a binomial distribution with the same N and $p = \bar{p}$ (except in the limiting case $p_i = p$ for all values of i. Lines lying completely inside G give no contribution to σ^2 .

Table 2.1 shows the observed and expected numbers of showers in some relevant regions of the Galaxy and Supercluster. The Supercluster appears to be a flattened system of groups of bright galaxies. de Vaucouleurs suggests that the space distribution of 55 nearby groups give clear evidence for this flattening. The agreement between the observed and expected is good.

2.4 Discussion

The largest deviation in table 2.1 is the 1.60 deficiency connected with the Galactic plane. This deviation is not significant in itself, but it does put some upper limits on any genuine enhancement connected with the Galactic plane. This does not exclude a Galactic origin, but places some restrictions on the choice of field model and charge composition of the primaries required, in order to avoid discrepancy. For conventional models of the field it was shown by Karakula et al (1972) and Osborne et al (1973) that the observed angular distributions at somewhat lower energies do not fit with the hypothesis that the primaries are protons produced in the Galaxy. The observational evidence for the field is very vague outside our local neighbourhood of about 2 kpc in the Galactic plane. The local field points approximately in the direction of the inward spiral arm, but the irregularities make the interpretation uncertain (Berge and Seielstad 1967, Manchester 1974, Vallee and Kronberg 1973).

In the case of a universal origin one might expect some enhancement from the direction of the plane of the supercluster, in particular from the Virgo cluster (Strong et al 1975). The observed deficiency (-1.20) does not favour this hypothesis.

In the next chapter a comprehensive search for small-scale anisotropies is carried out.

TABLE 2.1

Region		Galaxy			Supercluster		
		Observed	Expected	(obs-exp)/σ	Observed	Expected	(obs-exp)/σ
∓30° band around equator		54	63.1	-1.6	59	64.9	-1.2
Northern Hemisphere		58	53.9	+0.8	10	10.1	-0.0
Around centre	30° circle	7	8.1	-0.4	7	7.8	-0.3
	60° circle	30	28.8	+0.3	31	30.0	+0.2
	90° circle	52	53.9	-0.4	63	60.9	+0.4
Around anticentre	30° circle	7	7.9	-0.4	7	7.0	+0.0
	60° circle	31	33.2	-0.5	33	29.3	+0.8

References

Bell, C.J. et al 1973 Proc 13th Int Conf on Cosmic Rays, Denver 4, 2525

Berge, G.L. and Seielstad, G.A. 1967 Astrophys. J. 148, 367

Edge, D.M. et al 1975 Proc 14th Int. Conf on Cosmic Rays, Munich 2, 604

Karakula, S. et al 1972 J. Phys. A:Gen Phys. 5, 904

Kiraly, P. and White, M. 1975 J. Phys. A:Math Gen 8, 1336

Krasilnikov, D.D. et al 1974 J. Phys. A: math, Nucl. Gen 7 L176

Linsley, J. 1963 Proc 8th Int Conf on Cosmic Rays, Jaipur, 4, 77

Linsley, J. and Watson, A.A. 1974 nature, Lond 249, 816

Manchester, R.N. 1974 Astrophys. J. 188, 637

Osborne, J.L. et al 1973 J. Phys. A: Math, nucl. Gen 6, 421

Strong, A.W. et al 1974 J. Phys. A: Math, nucl. Gen 7,1767

Vallee, J.P. and Kronberg, P.P. 1973 Nature Phys. Sci 246, 49

de Vaucouleurs, G. 1976 Vol IX Stars and Stellar systems 'Galaxies and the Universe ed. Sandage, A. et al p 592.

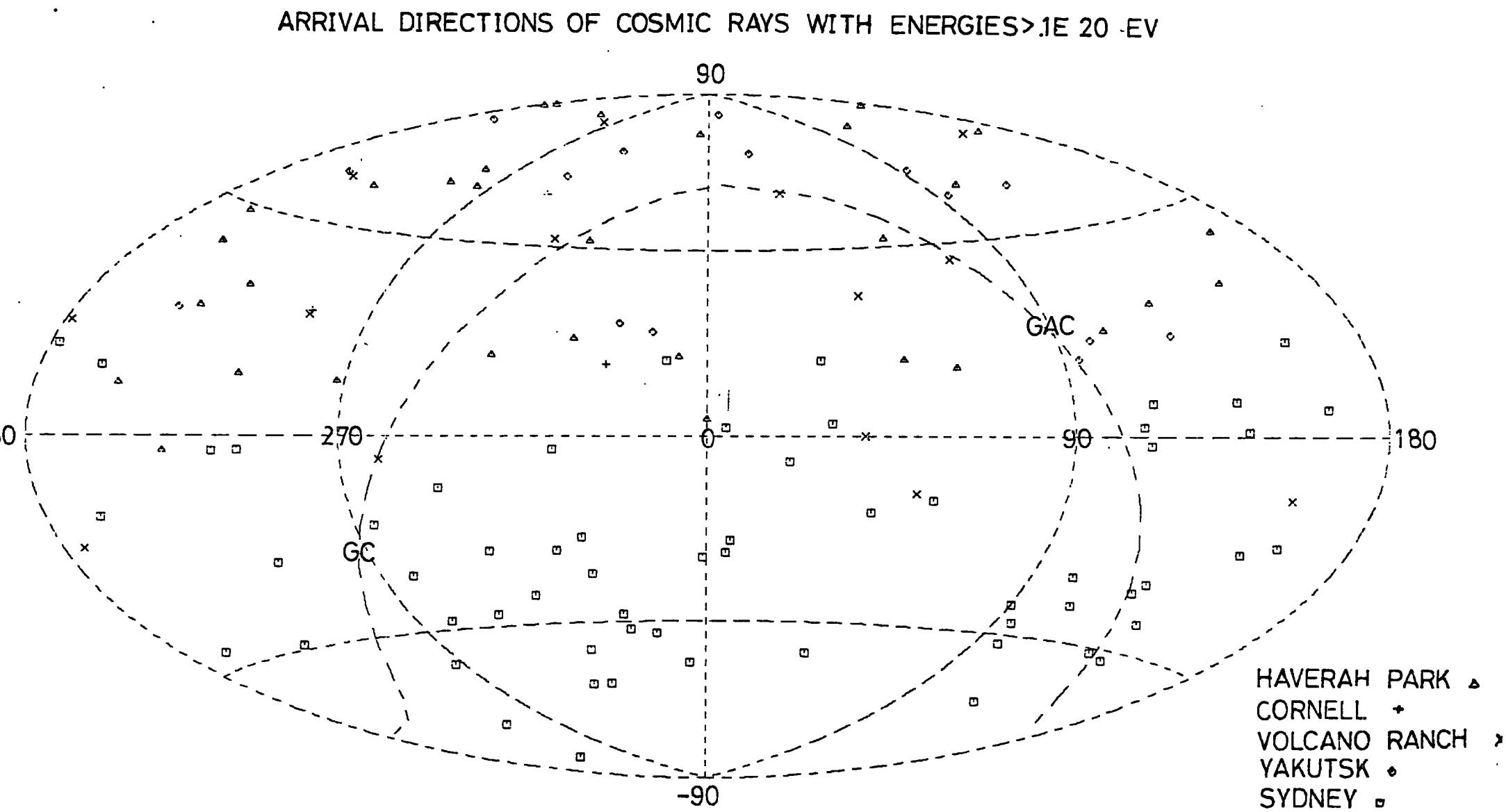
ARRIVAL DIRECTIONS OF COSMIC RAYS WITH ENERGIES>.1E 20 EV
90
270
0
90
180
-90
GAC
GC
HAVERAH PARK
CORNELL
VOLCANO RANCH
YAKUTSK
SYDNEY

FIG 2.1

THE CONTRIBUTIONS OF THE OBSERVED SHOWERS TO THE EXPECTATION INSIDE G

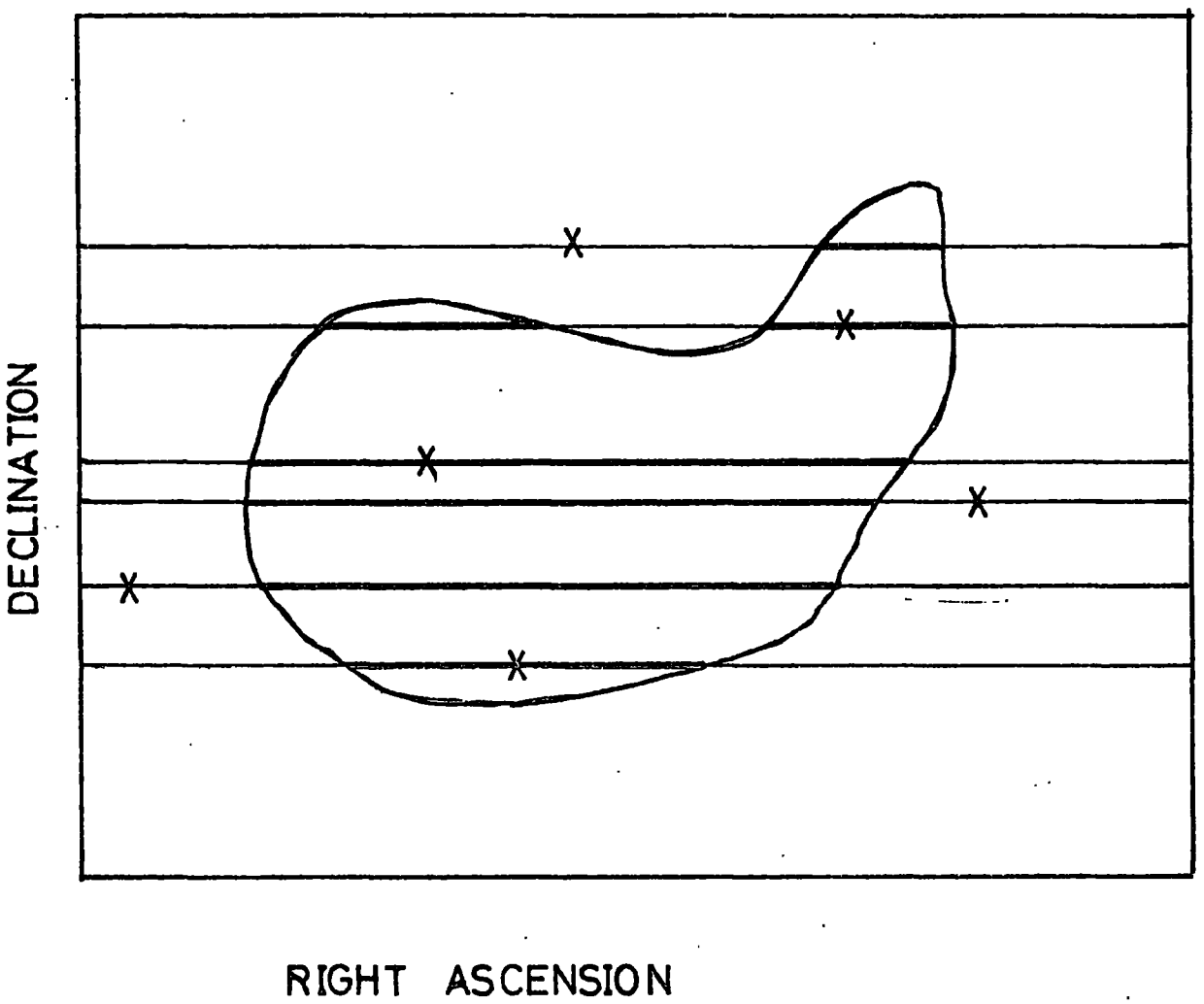

FIG 2.2

Chapter Three. The Anisotropy of Ultra-High-Energy Cosmic Rays: Search for Correlations with Astronomical Objects

3.1 Introduction

Searches are made for correlations of arrival directions with astronomical objects. Because of the existence of a Galactic magnetic field, attention is only devoted to charged particles of the highest energies ($> 10^{19}$ eV).

The ultra-high-energy primary cosmic rays which give rise to extensive air showers are usually considered to be protons and heavier nuclei, but the composition is uncertain. Emphasis is laid on primary protons.

Although the neutron is unstable it can travel significant distances if it is sufficiently energetic. On a galactic length scale, decay ceases to be of importance at energies $> 10^{16}$ eV . It is only at energies approaching 10^{20} eV that nearby extragalactic sources can be expected to produce detectable neutrons.

Neutrinos could produce the air showers if the nucleon-neutrino cross-section rises sufficiently fast with energy. Berezinskii and Zatsepin (1970) have made this proposal in order to account for air showers with energies beyond 10^{20} eV while maintaining a universal origin for cosmic rays.

3.2 Preliminary Analysis

The most straightforward method of looking for intensity enhancements around suspected sources of a given type is to calculate the statistically expected number of showers falling within a certain angular distance of the sources and compare it with the observed values. The technique has been described in Chapter Two, but now the given region of sky is not contiguous but consists of the union of all circles of given radius centred on the source candidates.

The results are presented in table 3.1. The cosmic ray data used has been discussed in Chapter Two. Limiting angular distances of 5° and 10° have been chosen, the first representing the experimental uncertainty in the arrival directions of the showers, while the second makes some allowance for deflection effects.

Table 3.1 gives some indications for enhancements in the directions of extragalactic supernovae and quasars, but none of the data are statistically significant and their overall distribution is roughly what one would expect for random fluctuations.

The method adopted is completely unbiased in the sense that the expectation value of $(Obs-Exp)/\sigma$ is zero for an isotropic distribution of the arrival directions, whatever the celestial distribution of the 'source candidates'. Thus, if the hypothesis of isotropy is checked separately for various types of source candidates, then any directional correlations among candidates of different types have no immediate effect, although the $(Obs-Exp)/\sigma$ values are slightly correlated.

The distribution of the adopted source candidates on the celestial sphere is not completely isotropic, the deviations being due partly to genuine concentrations and partly to observational coverage effects. An incomplete coverage does not introduce any bias, but it obviously impairs the efficiency of the search.

It is somewhat arbitrary to decide which sources of a given type should be included in the analysis. In some cases the sources can be ranked in decreasing order of expected contributions (i.e a 'figure of merit' can be introduced), and one might include only those sources with the highest 'figure of merit'. In other cases the expected contributions are quite uncertain and those objects which are nearest or brightest in some well defined waveband can be selected.

The samples analysed in table 3.1 which comprise the largest sets of objects used in later analyses are not quite homogeneous from this point of view as will be seen from later discussions.

3.3 Correlation with Galactic Pulsars and Supernova Remnants

The 118 pulsars used in the preliminary analysis are those with known dispersion measures (DM), taken from an unpublished compilation of J H Seiradakis (1974, 'Jodrell Bank Catalogue of Pulsars'). The whole set of pulsars shows a negative correlation with the arrival directions of showers.

The effects of subdividing the list of pulsars according to a figure of merit have been examined. For this quantity $(DM \times P)^{-2}$ is taken (following Aguirre 1974) where P is the pulsar period. The period dependence follows from the Gunn and Ostriker (1969) model in which the rate at which particles are injected into the pulsar wave zone is proportional to P^{-2}. DM is proportional to the distance of the pulsar. Various threshold values were examined and it was found that in all cases the observed number was less than the chance number. This is apparently a reflection of the fact, mentioned in Chapter Two, that there is a deficit of cosmic rays within 30^{o} of the Galactic plane, while there is an excess of pulsars in this region.

With regards to the figure of merit, two points are made. Firstly, the Gunn and Ostriker model goes on to predict that 10^{19} eV particles, if produced at all, would be produced only when the pulsar is very young, yet in our search the bulk of pulsars have deduced ages from 10^{5} to 10^{8} years. Secondly, the figure of merit has a range of a factor of 10^{5} for the observed pulsars. It is apparent that, if some of the observed cosmic rays do come from pulsars, this could not be the only factor affecting the flux; the flux from the four 'brightest' pulsars would be about 10 times greater than that from all the others combined, yet none of the 'observed coincidences' involves these pulsars.

From the catalogue of supernova remnants of Ilovaisky and Lequeux (1972) 28 have been selected which are, according to their adopted diameter-surface brightness relation, within 3 kpc of the earth. This includes a complete sample of those with diameters less than 30 pc and thus with ages less than about 3×10^4 years and a large proportion of those with diameters up to 50 pc (age $\lesssim 10^5$ years). We regard the list as a relatively complete sample of the probable sites of pulsars, within 3 kpc, which are considerably younger than the observed pulsars considered above. Table 3.1 reveals little indication of an excess cosmic ray intensity around these objects.

3.4 Propagation Effects

Before discussing the results of the extragalactic searches it is reasonable to ask whether such coincidences should be expected at all. The answer depends upon the nature of the cosmic ray particles, on the strength and configuration of Galactic and intergalactic magnetic fields as well as on the cosmic ray intensities of the individual sources.

For neutral primaries there are no angular deflections and time delays (relative to optical photons) and the only limiting factor is intensity. Neutrons cannot contribute on account of their short lifetime. Although ultra-high-energy cosmic rays and neutrinos are not known to be copiously produced in identifiable sources, the remote possibility warrants some search for angular coincidences. For heavy nuclei as primaries, no coincidences are expected because of the huge deflections caused by the Galactic magnetic field. For protons the deflections are not so prohibitive and a closer scrutiny of propagation effects is justified.

The Galactic deflection suffered by a 10^{19} eV proton arriving from the direction of the Galactic pole is $\sim 3^{o}$ if the field has a maximum strength of 3 μG near the Galactic plane and falls off exponentially with a scale height of 150 pc. The direction of the field is assumed to be parallel to the plane. For protons with higher energies, the deflections decrease as E^{-1}. The time delays suffered inside the Galaxy are of the orders of years for 10^{19} eV and perpendicular incidence, but increase rapidly for protons arriving at lower Galactic latitudes. For higher energies, the time delay decreases as E^{-2}. Thus for this field model (neglecting intergalactic fields) intensity enhancements within 5^{o} or 10^{o} circles around the sources might be observed. The small time delays might also allow us to detect intensity increases around the directions of recently recorded extragalactic explosions, e.g supernova outbursts. The whole argument is dependent upon the very uncertain Galactic field structure.

Knowledge of the magnitude and structure of the intergalactic field is even more uncertain. For a model a series of cells had been taken in which the field reversed itself completely from one cell to the next. Skilling (1974, private communication) criticized this model, pointing out that it was not an adequate representation of a random magnetic field. So instead a model consisting of independent cells with randomly orientated fields has been taken. The model is described in Appendix II. For protons arriving with small total deflection angles we find

$$\beta \simeq 2 \cdot 7 K E_{19}^{-1} D^{1/2} \qquad (3.4.1)$$

$$\delta \simeq 1800 K^2 E_{19}^{-2} D^2 = 250 \beta^2 D \qquad (3.4.2)$$

where $$K^2 = H^2 l \qquad (3.4.3)$$

H is the magnitude of the field (nG), ℓ the cell size (Mpc), K a scattering constant, δ the root mean square time delay (years), β the angular deflection (degrees), and E_{19} the energy in units of 10^{19} eV. By fixing the energy and either β or δ, the scattering constant can be expressed as a function of D. In figure 3.1 the functions are plotted for $E_{19} = 3$ and $\beta = 5^{o}$, $\delta = 10^{6}$ yr and 10 yr. Close directional correlations with objects active on the timescale of 10^{6} years might be observed for K and D values in the regions 3 and 4. In 4 the time delays are so short that association of cosmic ray particles with recently observed explosions (e.g supernovae) might be observed. In region 2 the angular deflections or time delays prevent the detection of close directional correlations. Finally region 1 is beyond the 'diffusion horizon' and particles from such sources cannot reach us because their velocities of diffusion towards us are counterbalanced by the recessional velocity due to the Hubble expansion.

A further 'propagation effect' is the decrease of flux with distance. Assuming that the angular deflections are small, the flux should decrease at least as fast as D^{-2}. Since we have no firm identification of the sources of the observed ultra-high-energy cosmic rays the source intensities cannot be estimated. One might ask, however, about the minimum source intensities needed to give rise to a detectable effect. The physical plausibility of the resulting intensities is useful in deciding whether some marginally significant statistical results should be taken seriously.

The detected flux of cosmic rays above 10^{19} eV is a few particles per 10 km^{2} st yr, with a considerable uncertainty mainly due to the difficulties in the estimation of the primary energy (Bell et al 1973, Edge et al 1973).

The total detection area-time product providing the present world statistics is ~ 300 km^2 yr (Bell et al 1973). In order to give a marked excess above the background we estimate that a typical source should contribute definitely more than 1 particle per 10 km^2 per 10 yr (perpendicular to the line of sight), even if there are sources of similar intensity in the sample. Accepting this as a lower limit and taking a typical particle energy as 2×10^{19} eV, the total rate of energy production in the form of particles above 10^{19} eV is 10^{38} D^2 erg s^{-1}, where D (Mpc) is the distance of the source. It is of course difficult to imagine a source in which most of the cosmic rays are accelerated to ultra-high energies. It is more likely that the total energy output in the form of relativistic particles should be at least 10^4 times higher than the above estimates corresponding to a power spectrum with a differential exponent of 2.4. In figure 3.2 these energy requirements are compared with the measured luminosities of a few particularly active objects. These luminosities refer to some limited regions of the electromagnetic spectrum but it is unlikely that the total rate of energy production in the objects should be more than two orders of magnitude higher than these estimates.

3.5 Extragalactic Supernovae

Supernova (SN) explosions, the most violent phenomena occurring in stars, have long been considered as obvious candidates for producing cosmic rays. While Galactic SN probably do give some (and perhaps even a dominant) contribution to the local flux at moderate energies, it is very much in doubt whether there is a sufficiently high production rate above 10^{19}eV for extragalactic SN to give a noticeable local flux. According to a proposal by Colgate (1975) there might be such a possibility.

In his model the cosmic rays are generated by the same type of source (tentatively identified with SN) throughout the whole energy spectrum, the contributions to the local flux being mostly Galactic except at the highest energies, where the extragalactic flux becomes predominant.

In the present search for correlations between SN and cosmic rays the SN data have been taken from 'The Master List of Supernovae Discovered since 1885' maintained by the Palomar group (Sargent et al 1974). The distances of the parent galaxies of the observed SN have been calculated from the corrected recessional velocity values of Sandage and Tammann (1975 a, b, c) using a Hubble constant of 60 km s^{-1} Mpc^{-1}. The times of arrival and energies of the cosmic ray showers observed at Haverah Park (A A Watson, private communication) and at Volcano Ranch (J Linsley, private communication) have also been used in the course of the evaluation.

The search has been carried out in three stages. First, all those SN were included for which the recessional velocity of the parent galaxy was known and less than 2500 km s^{-1} (92 SN). The coincidence criteria included the proper time sequence (SN earlier) and an angular deviation of less than 5°. For the 89 shower directions ($E > 1.5 \times 10^{19}$ eV) published by Linsley and Watson (1974) somewhat more coincidences have been found than statistically expected; furthermore, the average (and median) distance to the SN involved in the coincidences was lower than expected for random right ascensions of the showers. None of these deviations is, however, statistically significant in itself, and extension of the numbers of showers to 125 ($E > 10^{19}$ eV) has not strengthened the evidence either.

The comparison of expected and observed numbers of coincidences given in table 3.1 shows a slight excess. In the second stage the analysis was restricted to correlations with SN observed at high Galactic latitudes ($|b^{II}| > 45^{\circ}$) and at smaller distances ($D < 16.6$ Mpc corresponding to a limiting corrected recessional velocity of 1000 km s^{-1}). This sample included only 22 SN, but most of the genuine effect is expected from this subset. A somewhat complicated evaluation using the methods of maximum likelihood has been used and is described in Appendix III. It has yielded the following significances: 4% for energies above 1.5×10^{19} eV and 10% for energies above 10^{19} eV. Finally in the third stage a very small sample of SN was taken (11 SN satisfying the conditions $|b^{II}| > 45^{\circ}$, $D < 10$ Mpc). The maximum likelihood significance was similar to that found before (8%). Although the maximum likelihood method admittedly implies some arbitrariness in the construction of the likelihood function it has the advantage that one obtains some estimates for the unknown parameters, in our case for the 'intensity parameter' (the number or total energy of ultra-high-energy particles produced in a SN) and for the 'propagation parameter' K we have discussed. Of course, these estimates are physically meaningful only if the effect is genuine and not merely a statistical fluctuation. According to these estimates the total energy produced in the form of particles with energies above 10^{19} eV should be about 3×10^{47} erg (i.e 10^{40} particles with an average energy of approximately 2×10^{19} eV) with a propagation parameter of approximately 5×10^{-2} nG $Mpc^{\frac{1}{2}}$. It is interesting to note that the local flux calculated from all extragalactic SN explosions in the universe would have the same order of magnitude as the observed flux if one accepts the above 'intensity parameter' for all SN.

The predominantly extragalactic SN origin of the highest-energy primaries encounters some difficulties however. One is the lack of any intensity enhancement around the Virgo cluster. The number of SN in that region shows a definite excess and thus an enhanced intensity would be expected even if the time delays are too long to associate the particles with individual SN explosions. There is a more important difficulty with the transition between the two energy regions, one where Galactic and the other where extragalactic SN give the main contribution. For straight-line propagation the time-averaged flux from Galactic SN should be roughly two orders of magnitude higher than the extragalactic SN contribution. Now it might happen that at very high energies a 'preferential bending out' of the Galactic particles on the one hand and a fluctuation in time on the other, as proposed by Colgate, largely reduces the flux of Galactic origin. At somewhat lower energies, however, the much more intense Galactic flux should surely dominate the extragalactic one and a smooth power spectrum as observed would seem unlikely under such circumstances. We also note that the energy required for the production of particles above 10^{19} eV is very high (3×10^{47} erg), and the production spectrum should be close to the flattest spectrum allowed by Colgate in order to have realistic values for the total energy of cosmic rays produced by a supernova. The statistical indications in favour of the effect being genuine are much too weak to counterbalance these difficulties.

3.6 Strong Extragalactic Radio Sources

Although very little is known about the production mechanism of ultra-high-energy cosmic rays, the best extragalactic source candidates appear to be the objects showing violent activity on the scale of whole galaxies. One such class of objects is characterized by very intense non-thermal radio emission, generated by the synchrotron radiation of relativistic electrons.

In spite of their huge distances, the radio brightness of the strongest extragalactic sources is comparable with the brightest Galactic sources, and it might well happen that they are also efficient ultra-high-energy cosmic ray producers.

The search for coincidences was carried out by using an all-sky catalogue of strong radio sources at 408 MHz (Robertson 1973). The catalogue covers the whole sky except a $\mp 10°$ band around the Galactic plane and a few localized regions. The number of sources above the lower flux limit of 10 Jy is 160 (1 Jy = 10^{-26} W m^{-2} Hz^{-1}). In order to restrict the sample, we have raised the lower threshold to 50 Jy. The total flux of the 13 sources thus included in the analysis far exceeds that of the remaining 147 sources. The brightest extragalactic radio source, Cyg A, is not included in the sample because of its low Galactic latitude.

Of the 13 sources, 11 are radio galaxies and two are quasars. The nearest (and brightest) object included is the radio galaxy Cen A, which has claimed to be the first identified source of high-energy ($E > 3 \times 10^{11}$ eV) γ rays (Grindley et al 1975). The results of table 3.1 suggest no cosmic ray excess in the vicinity of the sources.

3.7 Extragalactic X-Ray Sources

This class of objects is more heterogeneous than that of the bright radio sources, and also the set of identifications with optical objects is much less complete. A representative sample of x-ray sources published by Rowan-Robinson and Fabian (1975) has been adopted. The sample contains those 39 'extragalactic' ($|b^{II}| > 10°$) sources which fall in the zone of complete coverage of the Abell catalogue of clusters of galaxies and have fluxes higher than 3 counts s^{-1} as measured by the Uhuru satellite.

This threshold corresponds to an energy flux of about 5×10^{-11} erg cm^{-2} s^{-1} in the 2-10 keV x-ray interval. Out of the 39 sources only 17 are more or less reliably identified, most of them with Abell clusters.

The x-ray spectrum of cluster sources is not known well enough to decide whether the radiation is generated by the Compton scattering of relativistic electrons on the 2.7 K background or by thermal bremsstrahlung in a hot gas filling the clusters. While in the first case the presence of relativistic particles gives some justification for our search, the thermal bremsstrahlung interpretation gives no direct indication for violent acceleration processes. Again the results (table 3.1) show no cosmic ray excess in the vicinity of the sources.

3.8 Galaxies with Seyfert or Seyfert-like Spectra

The objects known as Seyfert galaxies are defined by a combination of spectral and morphological criteria. The spectral features (broad high-excitation lines and an enhanced continuum) give evidence of fast gas motions and other violent processes, similar to those occurring on even larger scales in quasars.

The search for coincidences has been based on a catalogue compiled by Vorontsov-Vel'yaminov and Ivanisevic (1974), which includes not only typical Seyferts but also various transitional objects intermediate between Seyfert galaxies and other types. Out of the 95 galaxies listed those 32 have been selected which are within a distance of 100 Mpc (i.e $cz < 6000$ km s^{-1}). There is not much indication of an excess cosmic ray intensity around these sources.

3.9 Quasars

Quasars are characterized by a stellar appearance (i.e very small angular diameter), broad emission lines, strong ultraviolet and infrared continua, and, what is more important, by large redshifts.

The quasars can be subdivided into those which are radio sources (generally termed QSS) and those which have similar optical properties but are radio quiet (QSO). If the redshifts are cosmological the radio luminosities of QSS are comparable with the most luminous radio galaxies. It is estimated that the QSS group comprises only a few per cent of all quasars. Some quasars are variable on short time scales, indicating small spatial extensions of either the quasars themselves or of some bright constituents emitting a substantial part of the radiation.

There is still some controversy about the origin of the redshifts of quasars. The consensus of opinion is in favour of an interpretation in terms of recessional velocities due to the Hubble expansion, but some authors favour much smaller distances (see Field et al 1973). Accepting the majority view, quasars are intrinsically extremely luminous objects and this luminosity is due to very violent, strongly non-thermal processes. In such circumstances very efficient particle acceleration can be expected, but the reduction of flux due to propagation effects makes the possibilities of detection very doubtful.

The quasar data have been taken from a catalogue compiled by de Veny et al (1971) containing 202 objects. The majority of these are QSS, being optical identifications of radio sources in the Cambridge and Parkes catalogues, but some radio-quiet objects are included. Restricting the analysis to the 'nearby' 110 quasars ($z < 1$) some excess coincidences have been found (table 3.1) although the affect is not significant. By taking the 55 nearest quasars only, the excess increases for the 5° circles (1.83 σ) but decreases for the 10° circles (0.67 σ). A subdivision into narrower redshift intervals shows that most of the excess is caused by quasars with redshifts between 0.3 and 0.4, and not by those with the smallest redshifts. We take this as an indication for a statistical origin of the excess.

As we have mentioned, the cosmological origin of redshifts is not unanimously accepted. One of the main proponents of small quasar distances, Arp (1974) has compiled a list of ten quasars suspected to be associated with the Local Group of galaxies. We have found 8 cosmic ray coincidences around these objects (5° circles), while the expected number is 2.4. Such an excess has a fairly low probability (0.4%).

3.10 Discussion

The searches carried out give no firm evidence for the association of the arrival directions of ultra-high-energy cosmic rays with the sets of source candidates. There are, however, some indications for positive effects which, if substantiated, might turn out to give much information about the origin and composition of cosmic rays and about some important astrophysical parameters such as the magnitude and degree of irregularity of Galactic and intergalactic magnetic fields.

From a purely statistical point of view, the best indication points to a quasar origin. If quasars are at cosmological distances, then the energies required in the form of particles with $E > 10^{19}$ eV would be almost prohibitively high (see figure 3.2). Although the observed correlations might be easier to interpret in terms of a non-cosmological origin of redshifts, the statistical evidence is insufficient (chance probability 0.4%) to justify a definite suggestion in this controversial field.

The present observational limits on the large-scale anisotropy above 10^{19} eV appears to exclude a Galactic origin for a predominantly proton composition. In view of our ignorance of the Galactic magnetic field, however, this is not the case for heavy primaries. For an extragalactic origin there are virtually no restrictions on the composition. Because of the importance of the galactic magnetic field we turn our complete attention toward it.

In the next chapter some of the fundamental ideas of dynamo theory are introduced, upon which our model of the galactic magnetic field will be founded. Later, when a model has been constructed, we return to some of the problems considered in this chapter.

TABLE 3.1

Source Candidates		5° bins			10° bins		
		Observed	Expected	(obs-exp)/σ	Observed	Expected	(obs-exp)/σ
Galactic Pulsars	119	11	17.8	-1.8	40	46.2	-1.2
Galactic Supernova Remnants	28	8	6.4	+0.7	17	19.2	-0.6
Extragalactic Supernovae	92	12	9.2	+1.0	33	28.0	+1.1
Extragalactic Radio Sources	13	3	2.8	+0.2	8	10.6	-0.9
Extragalactic x-ray Sources	39	6	9.7	-1.3	30	31.4	-0.3
Seyfert Galaxies	32	8	7.8	+0.1	18	23.0	-1.2
Quasars	110	21	17.0	+1.1	55	44.7	+2.2

References

Aguirre, C. 1974 J. Phys. A: Math. Nucl. Gen 7 1474-82

Arp, H. 1974 High Energy Astrophysics and its Relation to Elementary Particle Physics eds K Brecher and G Setti (Cambridge, Mass: MIT Press) pp 1-76

Bell, C.J. et al 1973 Proc. 13th Int. Conf. on Cosmic Rays, Denver vol 4 (Denver: University of Denver) pp 2525-8

Berezinskii, V.S. and Zatsepin, G.T. 1970 Sov. J. Nucl. Phys. 10 696-701

Colgate, S. 1975 Phys. Rev. Lett. 34 1177-80

De Veny, J.B. et al 1971 Publ. Astron. Soc Pacific 83 611-25

Edge, D.M. et al 1973 Proc. 13th Int. Conf. on Cosmic Rays, Denver vol 4 (Denver: University of Denver) pp 2513-7

Field, G.B. et al 1973 The Redshift Controversy (Reading, Mass: Benjamin)

Grindlay, J.E. et al 1975 Astrophys. J. 197 L9-12

Gunn, J.E. and Ostriker, J.P. 1969 Phys. Rev. Lett. 22 728-31

Ilovaisky, S.A. and Lequeux, J. 1972 Astron. Astrophys 18 169-85

Kiraly, P. and White, M. 1975 J. Phys. A: Math. Gen 8 1336-48

Krasilnikov, D.D. et al 1974 J. Phys. A: Math. Nucl. Gen 7 L176-80

Lapikens, J. 1975 J. Phys. A: Math. Gen. 8 838-52

Linsley, J. and Watson, A.A. 1974 Nature 249 816-7

Robertson, J.G. 1973 Aust. J. Phys. 26 403-16

Rowan-Robinson, M. and Fabian, A.C. 1975 Mon. Not. R. Astron. Soc 170 199-217

Sandage, A. and Tammann, G.A. 1975a Astrophys. J. 194 223-43

Sandage, A. and Tammann, G.A. 1975b Astrophys. J. 194 559-68

Sandage, A. and Tammann, G.A. 1975c Astrophys. J. 196 313-8

Sargent, W.J.W. et al 1974 Supernovae and Supernova Remnants Astrophysics and Space Science Library vol 45 ed C.B. Cosmovici (Dordrecht: Reidel) pp 33-49

Vorontsov-Vel'yaminov, B.A. and Ivanisevic, G. 1974 Sov. Astron. 18 174-9

INTERGALACTIC PROPAGATION CHARACTERISTICS

a) diffusion horizon
b) deflection=5^{0}
c) time delay=10^{6}yr
d) time delay=10yr

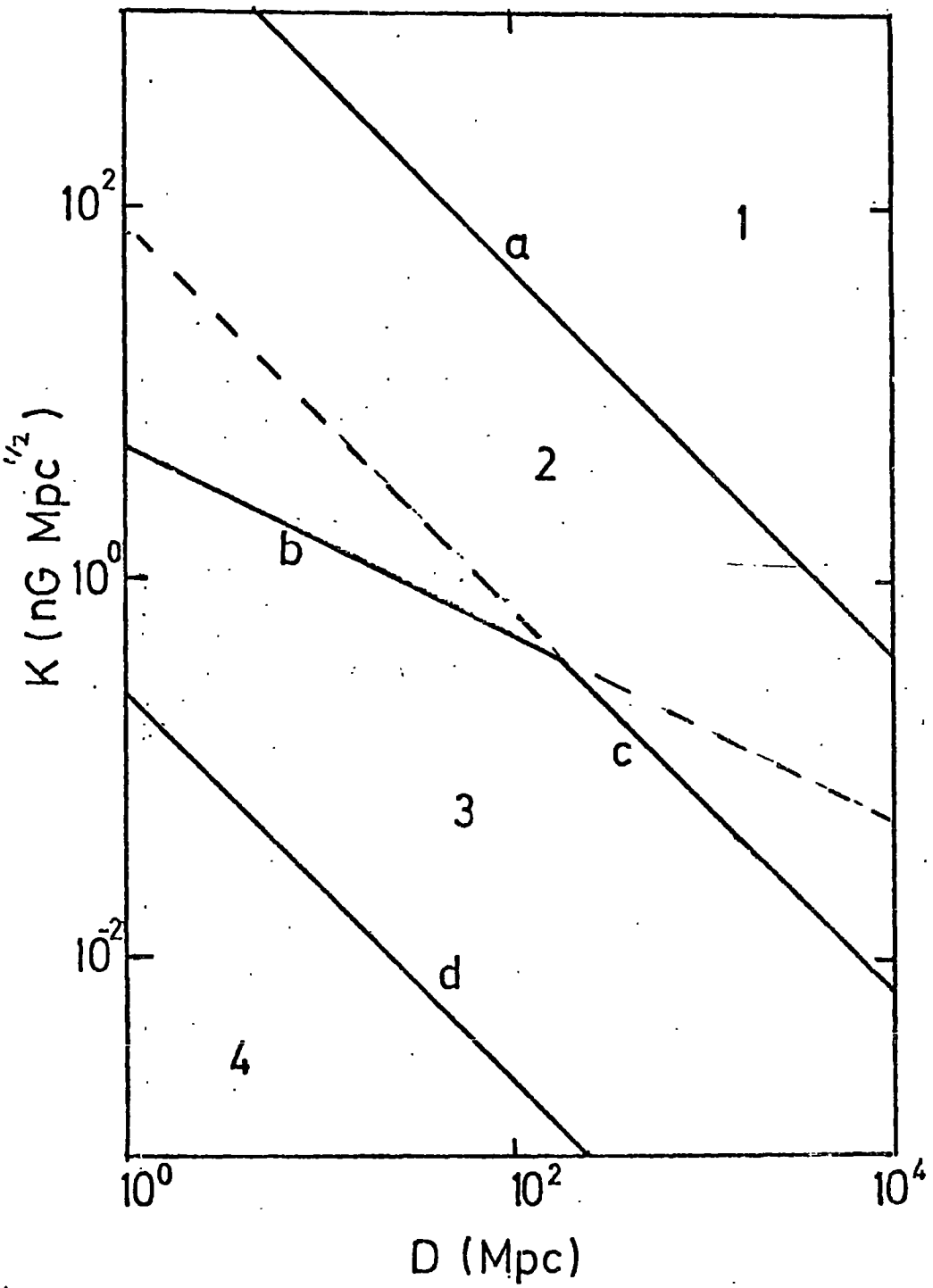

FIG 3.1

Luminosities and distances of some selected source candidates compared to minimum energy requirements. The lower line represents the minimum power output required in the form of particles with energies above 10^{19} eV in order to give rise to observed correlations. The upper line is the estimated minimum output required in cosmic rays of all energies. Luminosities are presented in the radio (Δ, 10^{7} -10^{11} Hz), X-ray (×, 2-10 keV) and optical (O) wavebands. The optical data given refer to non-thermal sources (Seyfert galaxies and quasars).

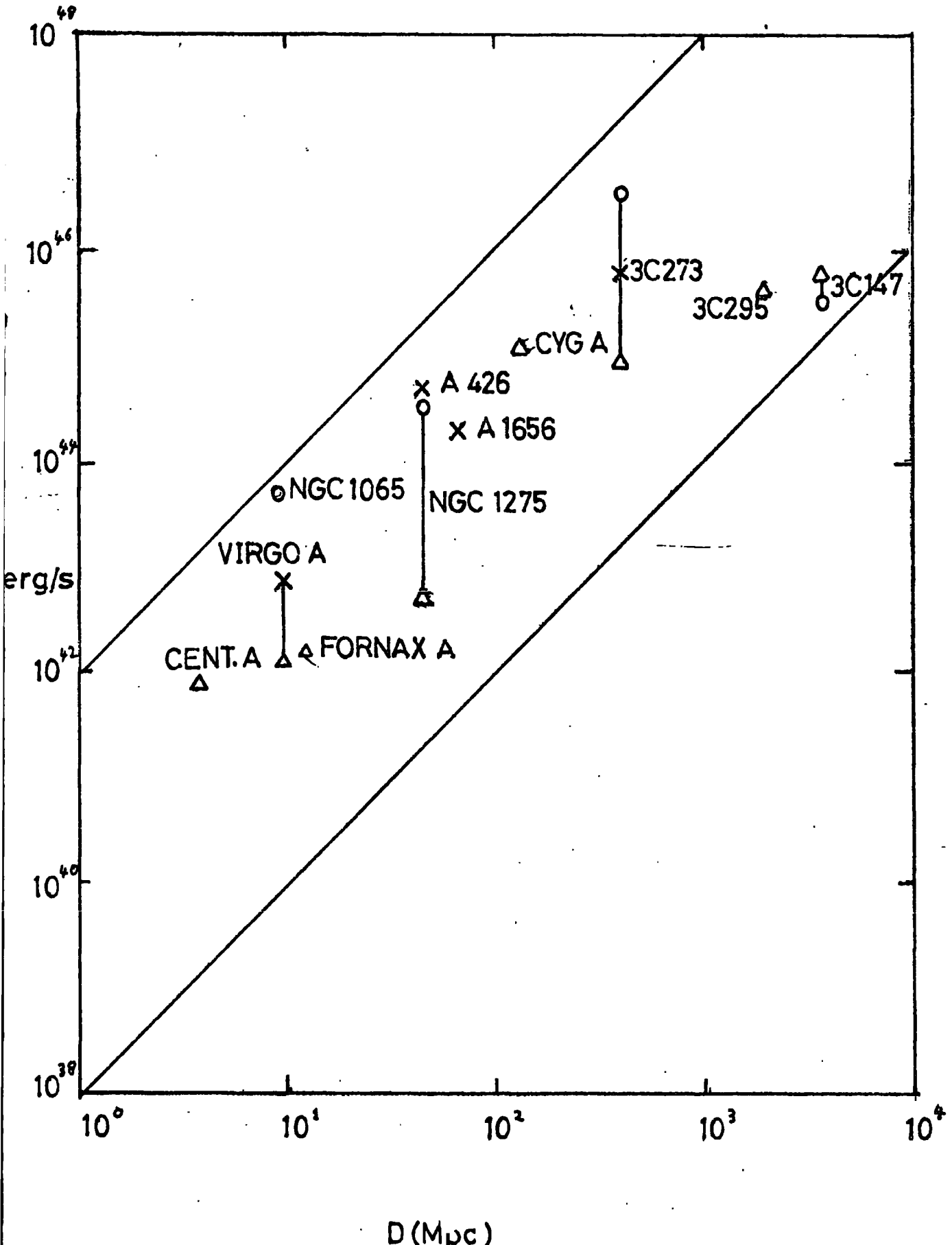

FIG 3.2

Chapter Four. The Turbulent Dynamo

4.1 Introduction

The problem of understanding the origin and nature of the galactic magnetic field is one to which no satisfactory solution has yet been given. One approach argues that the magnetic field is of primordial origin. Although this notion is certainly unattractive, it is, nevertheless, difficult to eliminate it. Piddington (1970) is the main proponent of this viewpoint.

Another approach, which provides the most plausible solution, is based upon dynamo theory. Parker (1955) has pioneered some of the fundamental ideas of this theory, but the mathematical formalism has been largely developed by Steenbeck, Krause, and Radler. Their work appears in German, but a translation of their most important papers has been made by Roberts and Stix (1971).

Dynamo theory ascribes the maintenance of the magnetic field to the flow of currents, induced in the fluid, as a result of its motions across the lines of force. The complete problem is nonlinear, and extremely difficult. Electric currents induced in the fluid as a result of its motions modify the field, and at the same time their flow in the magnetic field create mechanical forces which modify the motion (Cowling, 1957). In other words, the governing equations are coupled, a Lorentz term involving the magnetic field appearing in the equation of motion, and an induction term depending on the fluid velocity appearing in the equation for the magnetic field.

Progress has been made by linearizing the problem which involves making the small field assumption. This requires that the magnetic field is sufficiently small, so that the Lorentz term, which is quadratic in magnetic field strength, may be ignored, thus allowing the governing equations to be decoupled.

One can then prescribe the fluid motions and solve the induction equation for the magnetic field. This is the approach of the kinematic dynamo problem, and will be the subject of much of the discussion below.

4.2 Basic Equations

The equations are the ordinary electromagnetic equations, modified to take account of the interaction between the motion and the magnetic field. Maxwell's displacement currents are ignored. This is justified if the time scale of variation of the field is long compared with the light-crossing time of the system. Thus the electromagnetic state of the system alters only slightly in the time taken for light to cross it. We will find that this is a very good assumption for the cases we consider.

If $\underset{\sim}{j}$ is the current density, $\underset{\sim}{B}$ the magnetic field, and $\underset{\sim}{E}$ the electric intensity, then

$$\underset{\sim}{\nabla} \wedge \underset{\sim}{E} = -\frac{\partial \underset{\sim}{B}}{\partial t} \qquad (4.2.1)$$

$$\underset{\sim}{\nabla} \wedge \underset{\sim}{B} = \mu \underset{\sim}{j} \qquad (4.2.2)$$

$$\underset{\sim}{\nabla} . \underset{\sim}{B} = 0 \qquad (4.2.3)$$

μ, the magnetic permeability, is assumed to be constant.

If the material has velocity $\underset{\sim}{u}$, the electric field it experiences is $\underset{\sim}{E} + \underset{\sim}{u} \wedge \underset{\sim}{B}$. Thus if σ is the electrical conductivity, Ohm's Law becomes

$$\underset{\sim}{j} = \sigma (\underset{\sim}{E} + \underset{\sim}{u} \wedge \underset{\sim}{B}) \qquad (4.2.4)$$

σ, for the moment, is assumed to be constant.

The fluid is bounded by a fixed surface, S, which separates the conducting volume, V, from a vacuum region, Va. Continuity demands that

$$\langle \underset{\sim}{B} \rangle = 0 \qquad \text{on } S \tag{4.2.5}$$

where the angular bracket denotes the leap in the enclosed quantity.

The induction equation follows from (1), (2), and (4).

$$\frac{\partial \underset{\sim}{B}}{\partial t} = \underset{\sim}{\nabla} \wedge (\underset{\sim}{u} \wedge \underset{\sim}{B}) + \tilde{\eta} \nabla^2 \underset{\sim}{B} \tag{4.2.6}$$

where

$$\tilde{\eta} = 1/\mu\sigma \tag{4.2.7}$$

is the magnetic diffusivity.

We will now consider the two limiting cases of (6). If the fluid is at rest ($\underset{\sim}{u} = 0$) the equation becomes

$$\frac{\partial \underset{\sim}{B}}{\partial t} = \tilde{\eta} \nabla^2 \underset{\sim}{B} \tag{4.2.8}$$

This diffusion equation indicates that the field leaks through the fluid, resulting in the decay of the field. Dimensionally (8) indicates that the time of decay

$$t_d \sim L^2/\tilde{\eta} \tag{4.2.9}$$

where L is the scale of the region where currents flow. For cool interstellar gas clouds $\tilde{\eta} \sim 10^{22}$ cm^2 s^{-1} (Cowling, 1957). For a typical galactic length scale of 100 pc this leads to a diffusion time of 3×10^{11} years, which is longer than the lifetime of the galaxy.

We will find, however, that when turbulence is taken into account, the rate of dissipation of a magnetic field is affected drastically.

For the other limiting case of (6) the fluid is in motion but has negligible electrical resistance. We have

$$\frac{\partial \underset{\sim}{B}}{\partial t} = \underset{\sim}{\nabla} \wedge (\underset{\sim}{u} \wedge \underset{\sim}{B}) \qquad (4.2.10)$$

An analogy can be drawn between this equation and the one for vorticity of nonviscous flows, which suggests that the lines of force are "frozen" to the fluid.

When both terms on the right-hand side of (6) are important the lines of force tend to be carried about the the fluid and, at the same time, diffuse through it. One can set up a magnetic Reynolds number (Cowling, 1957) by the equation

$$R = L U / \tilde{\eta} \qquad (4.2.11)$$

where U is typical of the velocities present in the fluid. For transport of the field to dominate its diffusion $R \gg 1$.

4.3 The Kinematic Dynamo Problem

The kinematic dynamo problem is that of determining, whether a flow, $\underset{\sim}{u}$, assigned within a conducting body of fluid, can amplify or maintain the magnetic field within it, without the need for external sources of field. Therefore

$$|\underset{\sim}{B}| = O(r^{-3}) \quad \text{as} \quad t \to \infty \qquad (4.3.1)$$

where r is the distance from some origin within the body. The condition that the field does not decay with time is

$$|\underset{\sim}{B}| \not\to 0 \quad \text{as} \quad t \to \infty \qquad (4.3.2)$$

Outside the conducting region we have

$$\nabla \wedge \underset{\sim}{B} = 0 \qquad (4.3.3)$$

Difficulties with the problem are illustrated by the presence of non-existence theorems, which prohibit the existence of dynamos possessing convenient symmetrical structures. Cowling's Theorem (Cowling, 1933) is the most far-reaching of these, and precludes the possibility of dynamo action sustaining an axisymmetric magnetic field. Early attempts by Bullard and Gellman (1954) to solve the problem in a sphere for non-axisymmetric velocities produced a series of models, all of which proved incapable of sustaining a magnetic field. The failure of convergence of the solutions had led the early workers to suspect the existence of a 'super-Cowling's Theorem', to the effect that no stationary flow could maintain a magnetic field. Fortunately, this is now known to be incorrect! In, fact it would appear that any motion of "sufficient vigour and complexity" (Roberts, 1971), will act as a kinematic dynamo. It was for this reason that attention was turned to turbulent motions, the first suggestions being made by Parker (1955).

4.4 Effects of Turbulence Upon a Magnetic Field

Turbulence, occurring in rotating, electrically conducting fluid, is accompanied by unusual electrodynamic effects. Sweet (1950) was the first to suggest that the influence of turbulence upon a magnetic field could be described by an altered conductivity. This causes the magnetic diffusivity to increase by some orders of magnitude, thus enhancing the decay of the magnetic field. Another effect, which is of crucial interest, is the ability of turbulence to amplify any small magnetic field initially present, and maintain it indefinitely.

A theory of electrodynamics for turbulent fluids, known as 'mean field electrodynamics' has been developed by Steenbeck, Krause, and Radler (see Roberts and Stix, 1971, for translation). This theory is likely to be of the greatest importance in cosmic electrodynamics. It is supposed that there is no external source of magnetic field, the only source being the electric current distribution within the fluid itself. Fields introduced into a turbulent medium vary in space and time. Let F be such a fluctuating field, which is considered as a random function. The corresponding mean field, which is defined as the expectation value of F in an ensemble of identical systems is $\bar{F}$. F' denotes the difference.

The problem of mean field electrodynamics is to determine $\bar{\underset{\sim}{B}}$ as a solution to the induction equation, when some of the properties of u' are known. On averaging, Maxwell's equations, since they are linear in $\underset{\sim}{B}$, are unchanged, but Ohm's Law acquires a new term.

$$\bar{\underset{\sim}{j}} = \sigma (\bar{\underset{\sim}{E}} + \bar{\underset{\sim}{u}} \wedge \bar{\underset{\sim}{B}} + \overline{\underset{\sim}{u}' \wedge \underset{\sim}{B}'}) \qquad (4.4.1)$$

If $\underset{\sim}{u}'$ and $\underset{\sim}{B}'$ are correlated in such a way that the turbulent electromotive force (E.M.F)

$$\mathcal{E} = \overline{\underset{\sim}{u}' \wedge \underset{\sim}{B}'} \qquad (4.4.2)$$

is non-zero, then the turbulence supplies energy which modifies the electromagnetic state of the system. This is the crucial point of the theory. We shall illustrate the most important relations which follow by an elementary derivation for a special case, which Steenbeck and Krause have given (Roberts and Stix, 1971).

Steenbeck and Krause make the following assumptions:

(i) The conducting fluid lies in a global field $\underset{\sim}{\bar{B}}$, which varies 'slowly' with time. The turbulent velocity field, $\underset{\sim}{u}'$, is assumed to have zero mean ($\underset{\sim}{\bar{u}}' = 0$). In practice, this motion would vary continuously in space and time, but for simplicity it is supposed that it consists of a sequence of motions, each constant over a time interval t_0, and each continuously varying in space. At the end of each interval, the motion is abruptly replaced by another motion which is uncorrelated with it. The mean correlation time τ, of u' is therefore

$$\tau = t_0/2 \qquad (4.4.3)$$

(ii) The correlation time, τ, is small compared with the electromagnetic diffusion time, based on the correlation length, λ, of the turbulent velocity field, i.e,

$$\tau \ll \mu\sigma\lambda^2 \qquad (4.4.4)$$

(iii) The turbulent velocity is so small that, in calculating $\overline{\underset{\sim}{u}' \wedge \underset{\sim}{B}'}$ one neglects terms smaller than those quadratic in $\underset{\sim}{u}'$.
This requires that

$$v_{rms}\,\tau \ll \lambda \qquad (4.4.5)$$

where v_{rms} is the root mean square (rms) turbulent velocity.

(iv) The turbulent velocity field is isotropic. There is no preferred direction on average, and all the mean values derived from the velocity field remain constant under any rotation of the coordinate system, including cyclic permutation of axes.
Ohm's Law is

$$\underset{\sim}{j} = (\underset{\sim}{\nabla} \wedge \underset{\sim}{B})/\mu = \sigma(\underset{\sim}{E} + \underset{\sim}{u}' \wedge \underset{\sim}{B}) \qquad (4.4.6)$$

Applying the curl operator one finds

$$\tilde{\eta}\,\underset{\sim}{\nabla}\wedge\underset{\sim}{\nabla}\wedge\underset{\sim}{B} = -\tilde{\eta}\,\nabla^2\underset{\sim}{B} = -\frac{\partial \underset{\sim}{B}}{\partial t} + \underset{\sim}{\nabla}\wedge(\underset{\sim}{u}'\wedge\underset{\sim}{B}) \qquad (4.4.7)$$

It is only necessary to estimate $\underset{\sim}{B}'$ in the linear $\underset{\sim}{u}'$ approximation, since $\overline{\underset{\sim}{u}'\wedge\underset{\sim}{B}'}$ is to be computed as far as terms quadratic in $\underset{\sim}{u}'$. Only that part of $\underset{\sim}{B}'$, namely B'_{cor}, which is correlated with $\underset{\sim}{u}'$ is required. It is necessary to retain only that part of $\underset{\sim}{B}'$ which is generated by the particular $\underset{\sim}{u}'$ motion, in any one of the sequence of $\underset{\sim}{u}'$ motions. According to (ii) the left-hand side of (7) may be neglected. Assumption (i) allows integration of (7) to give

$$B_{cor} = t\,\underset{\sim}{\nabla}\wedge(\underset{\sim}{u}'\wedge\bar{\underset{\sim}{B}}) \qquad (4.4.8)$$

and so

$$\underset{\sim}{u}'\wedge\underset{\sim}{B}'_{cor} = t\,\underset{\sim}{u}'\wedge\underset{\sim}{\nabla}\wedge(\underset{\sim}{u}'\wedge\bar{\underset{\sim}{B}}) \qquad (4.4.9)$$

Averaging (9) over a time of length to Steenbeck and Krause have obtained

$$\overline{\underset{\sim}{u}'\wedge\underset{\sim}{B}'} = \overline{\underset{\sim}{u}'\wedge\underset{\sim}{B}'_{cor}} = \tau\,\overline{\underset{\sim}{u}'\wedge\underset{\sim}{\nabla}\wedge(\underset{\sim}{u}'\wedge\bar{\underset{\sim}{B}})} \qquad (4.4.10)$$

Supposing the global field $\bar{\underset{\sim}{B}}$ is uniform in the x-direction, they find that the mean emf in the direction parallel to $\bar{\underset{\sim}{B}}$ is

$$(\overline{\underset{\sim}{u}'\wedge\underset{\sim}{B}'})_x = -\frac{1}{3}\,\overline{\underset{\sim}{u}'\cdot(\underset{\sim}{\nabla}\wedge\underset{\sim}{u}')}\,\tau\,\bar{B}_x \qquad (4.4.11)$$

Assumption (iv) has been invoked to reach (11). It is also shown, that, because of (iv), components of the mean emf in directions perpendicular to $\bar{\underset{\sim}{B}}$ vanish.

Supposing next that $\bar{\underset{\sim}{B}}$ is not uniform, but has constant derivatives in the volume which is averaged, then an analogous calculation reveals the additional term

$$-\frac{1}{3}\,\overline{\underset{\sim}{u}'^2}\,\tau\,\underset{\sim}{\nabla}\wedge\bar{\underset{\sim}{B}} = -\frac{1}{3}\,\mu\,\overline{\underset{\sim}{u}'^2}\,\tau\,\bar{j} \qquad (4.4.12)$$

which is added to the global emf.

The total contribution to the global emf from turbulent motions (to an order quadratic in $\underset{\sim}{u}'$) is

$$\overline{\underset{\sim}{u}'\wedge\underset{\sim}{B}'} = \alpha\,\bar{\underset{\sim}{B}} - \beta\,\underset{\sim}{\nabla}\wedge\bar{\underset{\sim}{B}} \qquad (4.4.13)$$

where

$$\alpha = -\frac{1}{3}\,\overline{\underset{\sim}{u}'.\,\underset{\sim}{\nabla}\wedge\underset{\sim}{u}'}\,\tau \qquad (4.4.14)$$

$$\beta = \frac{1}{3}\,\overline{\underset{\sim}{u}'^2}\,\tau \qquad (4.4.15)$$

The same results hold for a velocity field which is a continuous function of time.

Turbulence can, under certain circumstances, modify the mean electromagnetic field. This phenomenon is described by the first term on the right-hand side of (13) and is called the α-effect. According to (14) the necessary condition for the existence of an α-effect is that $\underset{\sim}{u}'.\,\underset{\sim}{\nabla}\wedge\underset{\sim}{u}'$ does not vanish.
If $u'.\,\underset{\sim}{\nabla}\wedge\underset{\sim}{u}'$ is positive (negative) the turbulent motion possesses right-handed (left-handed) helicity. Only a non-mirror symmetric turbulent velocity field possesses $\alpha \neq 0$. The value of β does not depend upon the existence of pseudo-isotropic turbulence.

Ohm's Law, for mean fields, becomes

$$\bar{j} = \sigma\left(\bar{\underset{\sim}{E}} + \alpha\,\bar{\underset{\sim}{B}} - \mu\beta\,\bar{j}\right) \qquad (4.4.16)$$

or

$$\bar{j} = \sigma_T (\bar{E} + \alpha \bar{B}) \qquad (4.4.17)$$

where

$$\sigma_T = \sigma/(1 + \mu\sigma\beta) \qquad (4.4.18)$$

and

$$\tilde{\eta}_T = 1/\mu\sigma_T = \tilde{\eta} + \beta \qquad (4.4.19)$$

are respectively the turbulent conductivity and the turbulent magnetic diffusivity. For strongly turbulent flows for which $\beta >> \tilde{\eta}$

$$\tilde{\eta}_T \approx \tfrac{1}{3} \bar{u}'^2 \tau \qquad (4.4.20)$$

It is useful to consider how well assumptions (i)→(iv) are obeyed in the interstellar medium. Following Parker (1971) we take the life-time of a turbulent eddy as 2×10^7 years ($\Rightarrow \tau \sim 6 \times 10^{14}$ s) and a scale length $\lambda \sim 100$ pc. $\mu\sigma \sim 10^{-22}$ cm^{2}s^{-1} (see section 4.2) so $\mu\sigma\lambda^2 \sim 10^{19}$ s and (4) is obeyed.

Generally, for turbulent motions, one supposes that $v_{eff}\tau \sim \lambda$ (the above estimate of τ is based upon this). Assumption (iii) is therefore is not readily satisfied. In view of the more serious extrapolations we shall be making, this may not be very important.

The assumption (iv) of isotropic turbulence is an idealization. In the next section we shall follow Parker's argument which suggests that rotation can provide the required helicity for the interstellar turbulence. However, this rotation will also destroy the assumed isotropy. The rotation will imply a preferred direction to the turbulence and further terms governing the global emf will occur. The additional terms would appear not to be as significant as the one involving the α-effect (Roberts and Stix, 1971).

4.5 Magnetic Field Regeneration in the Galaxy

Taking (4.17) and the averaged Maxwell's equations the induction equation

$$\frac{\partial \bar{\underset{\sim}{B}}}{\partial t} = \underset{\sim}{\nabla} \wedge (\bar{\underset{\sim}{u}} \wedge \bar{\underset{\sim}{B}}) + \underset{\sim}{\nabla} \wedge \alpha \bar{\underset{\sim}{B}} + \tilde{\eta}_T \nabla^2 \underset{\sim}{B} \qquad (4.5.1)$$

which follows is called the dynamo equation.

Toroidal shear can create a toroidal magnetic field from a poloidal one. If the turbulence is non-mirror symmetric, then the α-effect which occurs can create a poloidal magnetic field from a toroidal one. A self-sustaining cycle occurs which is described by (1).

We shall turn to Parker's arguments (Parker, 1971a) which justify the assumed lack of mirror symmetry, and illustrate the α-effect. The fate of a rising eddy of fluid, in a horizontal turbulent layer, which is rotating about a vertical axis, and contains an approximately horizontal magnetic field, is considered. The pressure of the fluid decreases with height, and the fluid moves in vigorous short-lived, small-scale eddies. Figure 4.1 illustrates the situation. As an eddy rises into a region of lower pressure it expands and the forces $(-2 \underset{\sim}{\Omega} \wedge \underset{\sim}{u})$ associated with this expansion create a circulatory velocity, or swirl. Clearly, a correlation exists between the vertical velocity of the eddy and its sense of swirl. Moreover, this correlation is the same for a sinking eddy, since it is compressed as it falls. Thus the turbulence possesses a preferred sense, or helicity. Parker has called turbulence with this property "cyclonic". Bearing (4.14) in mind it appears that α is positive (negative) in the northern (southern) galactic hemisphere.

The effect of these motions on the magnetic field is illustrated. Since the motion is small-scale, the magnetic field is uniform across an eddy. Also, since the motion is vigorous and short-lived, the perfect conductivity picture holds. This is equivalent to assumption (ii) in the previous section. The vertical motion will bend the field line into an $\int\!\!\!\!\!\!\Omega$ shape, (see figure 4.2) and the vorticity about it will twist it out of its plane. Ampères Law tells us that the current associated with this out-of-plane loop will have a component parallel to the field. Imagining a large number of these loops, and supposing a period of rest after each motion, over which the fields created can diffuse over the mean distance separating loops, then the small-scale currents can produce an average large-scale current, parallel to $\underline{B}$. This toroidal current can generate a poloidal field, as we require for the cycle.

The α -effect can also generate a toroidal field from a poloidal one, and dynamos functioning on the α -effect alone are called α^2-dynamos. The model Parker has proposed for the galaxy involves differential rotation also, and is called the $\alpha\omega$-dynamo. Non-uniform rotation can generate toroidal field very efficiently, work being performed against the tension in the magnetic field while extending the lines of force into the toroidal direction (Parker, 1976). This work appears as energy in the field. The α -effect, however, is much less efficient. Turbulent eddies are of a dissipative nature and loose most of their energy into heat. It is therefore usual to neglect the production of toroidal field by the α -effect in the $\alpha\omega$-dynamo.

α has the dimensions of velocity and Parker has argued that its magnitude is essentially given by the cyclonic velocity within an eddy. This is plausible, when (4.14) is considered.

4.6 Turbulent Diffusion in the Galaxy

Expression (4.20), which gives the turbulent magnetic diffusivity for homogeneous isotropic turbulence, is a result of mean field electrodynamics.. Parker (1971b) has calculated a similar result, from a different view-point. He argues that the probability distribution for the magnetic field carried in a turbulent fluid varies with time in a manner identical to that expected of a scalar field. The results suggest

$$\tilde{\eta}_T \simeq 0.15\, u' \lambda \qquad (4.6.1)$$

where λ is the scale of the largest eddies and u' the rms turbulent velocity. Taking u' as 6 kms^{-1} (again Parker, 1971a) one finds

$$\tilde{\eta}_T \sim 3 \times 10^{25}\ cm^2 s^{-1} \qquad (4.6.2)$$

This suggests a characteristic diffusion time, t_d, of

$$t_d \sim \lambda^2/\tilde{\eta}_T \sim 2 \times 10^9\ yrs \qquad (4.6.3)$$

λ, the scale of the largest eddies is taken as the half-thickness of the gaseous disk. This value is some orders of magnitude smaller than that obtained by considering ambipolar diffusion, and is less than the age of the galaxy ($\sim 2 \times 10^{10}$ years). It would appear, then, that the possibility of primordial origin for the field is unlikely.

4.7 Discussion

An elementary derivation of the dynamo equation has been provided, based upon mean field electrodynamics. The results can be justified with greater rigour than we have given credit for, and the reader interested in the mathematical formalism is referred to Roberts and Stix (1971).

It is apparent that dynamo action can occur (i.e the systematic transfer of energy from a turbulent velocity field to the magnetic field) if the turbulent velocity field lacks mirror symmetry. Moffatt (1970) has justified this result with some degree of rigour for the case where the magnetic Reynold's number $Rm \ll 1$. His approach, however, does not reveal the effects of turbulence upon the magnetic diffusivity, since $\tilde{\underset{\sim}{B}}$ is taken as approximately uniform in the region considered.

The problem of turbulent diffusion has been mentioned. Piddington (1972) has repudiated the concept of turbulent diffusion, imagining that magnetic field stresses suppress it completely. He has also speculated that this suppression of turbulence blocks dynamo action in the galaxy. This suggestion is criticized in Chapter Six.The next chapter mainly concerns itself with setting up the techniques necessary for the numerical experiments, with which we shall investigate the galactic dynamo.

References

Bullard, E.C and Gellman, H. 1957 Phil. Trans. A 247 213

Cowling, T.G. 1933 M.N.R.A.S. 94 39

Cowling, T.G. 1957 Magnetohydrodynamics Interscience New York

Moffatt, H.K. 1970 J. Fluid Mech. 41 435

Parker, E.N. 1955 Astrophys. J. 122 293

Parker, E.N. 1971a Astrophys. J. 163 255

Parker, E.N. 1971b Astrophys. J. 163 279

Parker, E.N. 1975 Role of Magnetic Fields in Physics and Astrophysics edit. V. Canute Annals of the N.Y. Academy of Sciences 257 241

Piddington, J.H. 1970 Australian J. Phys. 23 731

Piddington, J.H. 1972 Cosmic Electrodynamics 5 129

Roberts, P.H. 1971 Lectures in Applied Mathematics W.H. Reid Ed. 14 129 American Mathematical Society Providence R.I.

Roberts, P.H. and Stix, M. 1971 The Turbulent Dynamo N.C.A.R. Tech. Note, TN/1A-60.

Sweet, P.A. 1950 M.N.R.A.S. 110 69

SWIRL OF RISING AND SINKING EDDIES

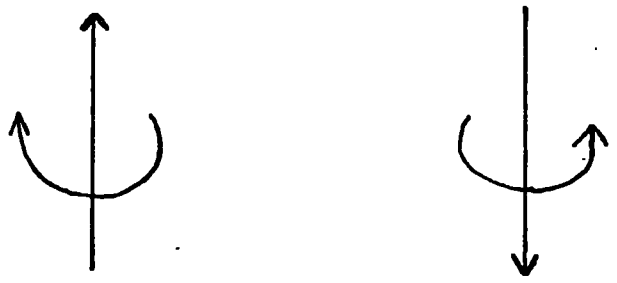

(a) (b)

FIG 4.1

MAGNETIC FIELD LOOP FORMED BY RISING EDDY

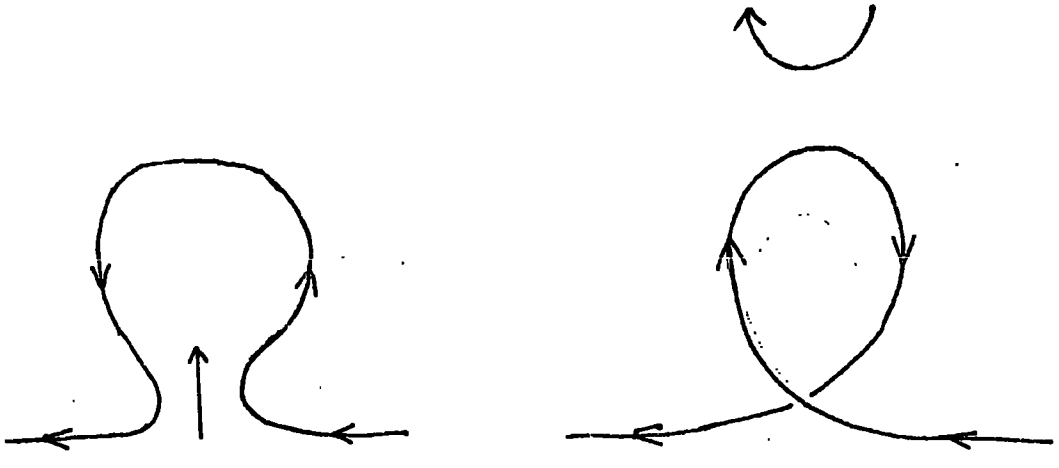

(a) (b)

FIG 4.2

Chapter Five. The Simple Galactic $\alpha\omega$-dynamo Model

5.1 Introduction

Parker (1971 a, b) has solved the dynamo equation analytically, using a restrictive "slab" geometry. Stix (1975) has pointed out that this does not allow boundary conditions to be imposed upon a closed surface, and has suggested that an oblate spheroidal geometry is more appropriate. He has then proceeded to solve the dynamo equation numerically, in this geometry, using the conventional eigenvalue-problem approach. The work reported here represents the next step in the development of the problem. Using an initial-value problem formulation, a considerably more flexible numerical framework is constructed, in which the dynamo equation is solved. In particular, this approach, unlike the eigenvalue approach, allows important nonlinear effects to be incorporated. It also provides a valuable check on the results obtained from the eigenvalue approach.

In fact, some disagreement is found between the results presented here and those of Stix. Discussions over this matter with P H Roberts and A M Soward (April, 1976) have led the latter to evaluate, analytically, an asymptotic relation (section 5.7) which favoured the results presented here. Repetition of part of Stix's calculations has also led to good agreement with the results of the initial-value problem approach. Recently (August, 1976) Stix has informed the author (private communication) of an error in his calculations, which, when corrected, resolves the discrepancy.

The importance of obtaining independent confirmation of the results will be appreciated once the complexity of the numerical problem is described. One has to be especially cautious of results derived purely from numerical means. For example, rounding errors arising incidentally from the finite difference method used in solving the differential equation, or through a series expansion of the magnetic field, can give rise to stray electric fields, which result in "numerical" dynamo action. (Roberts, 1967). Thus, independent checks, particularly with analytical results, allow astrophysical and computational effects to be distinguished.

5.2 Decomposition of the Dynamo Equation

The dynamo equation, as we have seen, for the $\alpha\omega$-dynamo is

$$\frac{\partial \underset{\sim}{b}}{\partial t} = \underset{\sim}{\nabla} \wedge (\underset{\sim}{u} \wedge \underset{\sim}{b}) + \underset{\sim}{\nabla} \wedge (\alpha \underset{\sim}{b}) + \tilde{\eta} \nabla^2 \underset{\sim}{b} \qquad (5.2.1)$$

where $\underset{\sim}{b}$ is the global magnetic field, $\underset{\sim}{u}$ the global velocity field, α a function describing the α-effect, and $\tilde{\eta}$ the turbulent magnetic diffusivity. Dividing the magnetic field into a toroidal (azimuthal) part and a poloidal (meridional) part are set

$$\underset{\sim}{b} = \underset{\sim}{B}_{TOR} + \underset{\sim}{B}_{POL} \qquad (5.2.2)$$

Attention is restricted to axisymmetric solutions largely as a matter of mathematical expediency, although some physical justification exists, which will be discussed later. In this case, since the field has zero divergence, one may write

$$\underset{\sim}{B}_{POL} = \underset{\sim}{\nabla} \wedge \underset{\sim}{A} \qquad (5.2.3)$$

where $\underset{\sim}{A}$ is purely toroidal. The usefulness of this division (originally due to Lamb) lies in the fact that the curl of a toroidal field is a poloidal one, and the curl of a poloidal field is a toroidal one, and that the divergenceless property of the field is automatically satisfied. Since the small-scale field is non-axisymmetric, Cowlings Theorem is not violated.

The toroidal and poloidal components of the dynamo equation can now be equated separately.

$$\frac{\partial \underset{\sim}{B}_{TOR}}{\partial t} = \underset{\sim}{\nabla} \wedge (\underset{\sim}{\mu} \wedge \underset{\sim}{B}_{TOR}) + \nabla \wedge \alpha \underset{\sim}{B}_{POL} + \tilde{\eta} \nabla^2 \underset{\sim}{B}_{TOR} \qquad (5.2.3)$$

$$\frac{\partial \underset{\sim}{B}_{POL}}{\partial t} = \underset{\sim}{\nabla} \wedge (\alpha \underset{\sim}{B}_{TOR}) + \tilde{\eta} \nabla^2 \underset{\sim}{B}_{POL} \qquad (5.2.4)$$

The $\underset{\sim}{\mu}$ field is assumed to be purely toroidal. Rewriting $\underset{\sim}{B}_{TOR}$ as $\underset{\sim}{B}$ and integrating (4) we have

$$\frac{\partial \underset{\sim}{B}}{\partial t} = \underset{\sim}{\nabla} \wedge (\underset{\sim}{\mu} \wedge |\underset{\sim}{\nabla} \wedge \underset{\sim}{A}|) + \tilde{\eta} \nabla^2 \underset{\sim}{B} \qquad (5.2.5)$$

$$\frac{\partial \underset{\sim}{A}}{\partial t} = \alpha \underset{\sim}{B} + \tilde{\eta} \nabla^2 \underset{\sim}{A} \qquad (5.2.6)$$

where, in (5) the regeneration of the field by the α-effect has been neglected. This, as we have pointed out, is justified if the generation by differential rotation is the dominant induction mechanism. No toroidal gradient appears in (6) since this must vanish for an axisymmetric case. Equation (5) describes the generation of toroidal field from poloidal field by differential rotation, and equation (6) describes the generation of poloidal field from toroidal field by the α-effect.

For dynamo action, the rotation must not be a solid body rotation, otherwise the first term of (5) would vanish. This conclusion can also be inferred from the invariance of Maxwell's equations under rigid rotation. It is also worth noting that neither the sign nor the magnitude of the field can be predicted from a simple linear model.

5.3 Oblate Spheroidal Coordinates

The geometry which appears appropriate to describing the galaxy is introduced. The oblate spheroidal coordinate system is formed by rotating the two-dimensional elliptic coordinate system, which consists of confocal ellipses and hyperbolas, about the minor axes of the ellipses. The z -axis is the axis of revolution, and the interfocal distance is denoted by d.

These coordinates (Flammer, 1957) are related to the rectangular coordinates by the following transformations

$$x' = d/2\left[(1-\eta^2)(\xi^2+1)\right]^{1/2}\cos\phi \tag{5.3.1}$$

$$y = d/2\left[(1-\eta^2)(\xi^2+1)\right]^{1/2}\sin\phi \tag{5.3.2}$$

$$z = d/2\,\eta\,\xi \tag{5.3.3}$$

with

$$-1 \le \eta \le 1,\quad 0 \le \xi \le \infty,\quad 0 \le \phi \le 2\pi \tag{5.3.4}$$

The system is illustrated in figure 5.1.

The surface ξ = constant > 0 is a flattened ellipsoid of revolution with major axis of length $d(\xi^2 + 1)^{1/2}$, and minor axis of length $d\xi$. The surface $\xi = 0$ is a circular disk of radius $a = d/2$, lying in the (x', y) plane, and centred upon the origin. The surface $|\eta|$ = constant < 1 is a hyperboloid of revolution of one sheet with an asymptotic cone whose generating line passes through the origin and is inclined at an angle $\theta = \cos^{-1}\eta$ to the z-axis. The degenerate surface $|\eta| = 1$ is the z-axis. The surface $\eta = 0$ is the (x', y) plane, except for the circular disk $\xi = 0$. The surface ϕ = constant is the plane through the z-axis, making the angle ϕ with the (x', z) plane.

(η, ξ, ϕ) form a right-handed orthogonal curvilinear coordinate system. In the limit $d \to 0$ the oblate spheroidal system reduces to the spherical coordinate system. For d finite, the surface ξ = constant becomes spherical as ξ approaches infinity; thus

$$1/2\, d\xi \to r \quad , \quad \eta \to \cos\theta \quad \text{as} \quad \xi \to \infty$$

where r and θ are spherical coordinates.

The scale factors defined by

$$dx'^2 + dy^2 + dz^2 = h_\eta^2 d\eta^2 + h_\xi^2 d\xi^2 + h_\phi^2 d\phi^2 \tag{5.3.5}$$

are

$$h_\eta = \frac{d}{2}\left(\frac{\xi^2 + \eta^2}{1 - \eta^2}\right)^{1/2} \tag{5.3.6}$$

$$h_\xi = \frac{d}{2}\left(\frac{\xi^2 + \eta^2}{\xi^2 + 1}\right)^{1/2} \tag{5.3.7}$$

$$h_\varphi = \frac{d}{2}\left[(1-\eta^2)(\xi^2+1)\right]^{1/2} \tag{5.3.8}$$

For future reference it is useful to note that

$$\underset{\sim}{\nabla}\wedge\underset{\sim}{B} = \left\{ \frac{1}{h_\xi h_\varphi}\frac{\partial}{\partial\xi}(h_\varphi B),\ -\frac{1}{h_\eta h_\varphi}\frac{\partial}{\partial\eta}(h_\varphi B),\ 0 \right\} \tag{5.3.9}$$

where

$$\underset{\sim}{B} = (0,\ 0,\ B) \tag{5.3.10}$$

5.4 Scaling of the Equations

Units of length and time are taken as R and $R^2/\tilde{\eta}$, where R is the semi-major axis of the spheroid. The ratio of the minor axis to the major axis of the spheroidal is

$$V = b/R = \xi_0(1+\xi_0^2)^{1/2} \tag{5.4.1}$$

where ξ_0 is the value of ξ at the surface boundary. Transforming ξ to $x\xi_0$ the distance from the axis of symmetry is

$$s = b\left[(x^2+\xi_0^{-2})(1-\eta^2)\right]^{1/2} \tag{5.4.2}$$

When the coordinate system is introduced to, and this scaling applied to equations (2.5) and (2.6), two dimensionless parameters, associated with the two induction effects, appear. These are R_α and R_ω where

$$R_\alpha = \alpha_0 R/\tilde{\eta} \qquad R_\omega = \omega_0 R^2/\tilde{\eta} \tag{5.4.3}$$

α_0 and ω_0 characterize typical magnitudes of the respective effects.

Since we expect $|R_\omega/R_\alpha| >> 1$, the physical magnitude of the toroidal field will be greater than that of the poloidal field. It is, however, numerically convenient to have these field quantities about the same order of magnitude, so A and B are rescaled in the following manner

$$A = (|R_\alpha/R_\omega|)^{1/4} A' \qquad B = (|R_\omega/R_\alpha|)^{1/4} B' \tag{5.4.4}$$

Dropping the primes on A and B, equations (2.5) and (2.6) become

$$\frac{\partial B}{\partial \bar{t}} = -\frac{S R_m}{b^3(x^2+\eta^2/\beta_0^2)}\left[\frac{\partial \tilde{\omega}}{\partial \bar{x}}\frac{\partial (sA)}{\partial \bar{\eta}} - \frac{\partial \tilde{\omega}}{\partial \bar{\eta}}\frac{\partial (sA)}{\partial \bar{x}}\right]$$

$$+ \frac{1}{b^3(x^2+\eta^2/\beta_0^2)}\left[(x^2+\beta_0^{-2})^{1/2}\frac{\partial^2}{\partial \bar{x}^2}((x^2+\beta_0^{-2})^{1/2}B) + (1-\eta^2)^{1/2}\frac{\partial^2}{\partial \bar{\eta}^2}((1-\eta^2)^{1/2}B)\right] \tag{5.4.5}$$

$$\frac{\partial A}{\partial \bar{t}} = R R_m B + \frac{1}{b^3(x^2+\eta^2/\beta_0^2)}\left[(x^2+\beta_0^{-2})^{1/2}\frac{\partial^2}{\partial \bar{x}^2}((x^2+\beta_0^{-2})^{1/2}A) + (1-\eta^2)^{1/2}\frac{\partial^2}{\partial \bar{\eta}^2}((1-\eta^2)^{1/2}A)\right] \tag{5.4.6}$$

$$\omega = \omega_0 \tilde{\omega}(x,\eta) \qquad \alpha = \alpha_0 \tilde{\alpha}(x,\eta) \tag{5.4.7}$$

$$u = s\omega \tag{5.4.8}$$

$$R_m = (|R_\alpha R_\omega|)^{1/2} \tag{5.4.9}$$

The angular velocity distribution and α-effect distribution are prescribed in (7). The only dimensionless parameter which appears in equations (5) and (6) is the magnetic Reynolds number, R_m, given in ( ). The dynamo number, P, is defined as

$$P = R_\alpha R_\omega \tag{5.4.10}$$

5.5 Boundary Conditions

Equations (4.5) and (4.6) determine the toroidal components $A(x, \eta, t)$ and $B(x, \eta, t)$ of fields A and B, once the boundary conditions are specified. We take a homogeneous oblate spheroid, outside of which, we suppose there is vacuum. No currents can cross the surface of the spheroid (defined by x = 1) so $(\nabla \wedge \underset{\sim}{b})_x = 0$ on x = 1. According to (3.9) the toroidal field must also vanish on the surface, so

$$B = 0 \qquad \text{at} \quad x = 1 \tag{5.5.1}$$

The second boundary condition on the surface arises from the continuity of the magnetic field within the spheroid to the source-free potential field outside it.

The potential field is a consequence of our neglect of retardation effects due to the finite velocity of light. Both components of the poloidal field must be continuous at $x = 1$, so not only must A be continuous, but also its normal derivative (see equation (3.9)). Thus

$$\langle A \rangle = \left\langle \frac{\partial A}{\partial x} \right\rangle = 0 \quad at \quad x = 1 \tag{5.5.2}$$

where the angular bracket denotes the leap in the enclosed quantity.

Outside the conducting spheroid the condition is given by

$$\underset{\sim}{\nabla} \wedge \underset{\sim}{B}_{pol} = -\nabla^2 \underset{\sim}{A} = \underset{\sim}{\nabla} \wedge \underset{\sim}{\nabla} \wedge \underset{\sim}{A} = 0 \tag{5.5.3}$$

which becomes, in our coordinate system

$$(x^2 + \beta_0^{-2}) \frac{\partial^2 A}{\partial x^2} + 2x \frac{\partial A}{\partial x} + \frac{\beta_0^{-2}}{(x^2 + \beta_0^{-2})} A + (1 - \eta^2) \frac{\partial^2 A}{\partial \eta^2}$$

$$- 2\eta \frac{\partial A}{\partial \eta} - \frac{\eta}{(1 - \eta^2)} A = 0 \tag{5.5.4}$$

The requirement that no external sources are present is fulfilled by the condition

$$A \to 0 \quad as \quad x \to \infty \tag{5.5.5}$$

In general one would demand $A = 0(x^{-2})$ as $x \to \infty$, for a unique solution to Laplace's equation. This additional constraint is unnecessary since A contains no arbitrary scalar gradient.

On the axis of symmetry ($\eta = 1$), since both A and B are norms of azimuthal vectors, axisymmetry will demand that they both vanish. The remaining conditions to be satisfied are those on the equator.

The global velocity field is assumed to have mirror-symmetry about the equator, which is physically realistic for the galaxy. The α -effect is taken to be an odd function of latitude, since it describes a pseudo-scalar (helicity). One can also appreciate this by observing that the Coriolis forces, which give rise to the lack of mirror symmetry, and hence the α -effect, change sign at the equator.

Under these conditions Roberts (1972) has examined the symmetry properties of the solutions for the magnetic field. He has found that they break down into two separate families, one for which A is an odd function of latitude and B an even function, called the quadrupole family, and another for which A is even and B odd, called the dipole family. For negative dynamo numbers stationary quadrupole and oscillating dipole solutions are preferred. The situation is reversed for positive dynamo numbers. Figure 5.2 illustrates the boundary conditions.

5.6 Numerical Techniques

The techniques described here are largely a generalization of the techniques employed by Jepps (1975) in his approach to the solar dynamo. The problem is of such a nature that, if the state of the physical system is arbitrarily specified at some initial time $t = t_o$, a solution exists for $t > t_o$, and is uniquely determined by the equations, together with the boundary conditions.

A spatial mesh is introduced in the (η , x) plane, on which the derivatives of the dependent variables are expressed in a finite-difference form.

Following Jepps, the Dufort-Frankel scheme (1953) is employed to perform the integration. This scheme is explicit and involves three time levels. Making the following approximations

$$A(i\Delta\eta, j\Delta x, \ell\Delta t) = (A_{ij}^{\ell+1} + A_{ij}^{\ell-1})/2$$

$$\frac{\partial A}{\partial t} = (A_{ij}^{\ell+1} - A_{ij}^{\ell-1})/2\Delta t$$

$$\frac{\partial A}{\partial \eta} = (A_{i+1,j}^{\ell} - A_{i-1,j}^{\ell})/2\Delta\eta$$

$$\frac{\partial^2 A}{\partial \eta^2} = (A_{i+1,j}^{\ell} - A_{ij}^{\ell+1} - A_{ij}^{\ell-1} + A_{i-1,j}^{\ell})/\Delta\eta^2 \qquad (5.6.1)$$

and similarly for $\partial A/\partial x$ and $\partial^2 A/\partial x^2$, the finite difference forms of equations (4.5) and (4.6) can be written down. To initiate the integration starting values are required for the first two levels, which can be taken from any desired approximation valid in the limit $\Delta t \to 0$. In particular one can set the arbitrary values at the first time level equal to those at the second time level. As the integration proceeds the boundary conditions are imposed at each time step. Three-point backward difference equations have been found sufficiently accurate to impose conditions such as $\frac{\partial A}{\partial \eta} = 0$ and $\partial A/\partial x = 0$ at the equator.

The condition which presents the most difficulty is that at $x = 1$. Here it is necessary to ensure that equations (4.5), (4.6), and (5.4) are simultaneously satisfied, at each time step. This is complicated since (5.4) spans an infinite domain. Inversion removes this difficulty. One writes $C(x)$ as $A(1/x)$ and equation (5.4) becomes

$$x^4\left[\frac{1}{x^2}+\frac{1}{\beta_0^2}\right]\frac{\partial^2 C}{\partial x^2}+2\left[x^3\left(\frac{1}{x^2}+\frac{1}{\beta_0^2}\right)-x\right]\frac{\partial C}{\partial x}$$

$$+\frac{C}{(\beta_0^2/x^2+1)}+(1-\eta^2)\frac{\partial^2 C}{\partial \eta^2}-2\eta\frac{\partial C}{\partial \eta}-\frac{\eta C}{(1-\eta^2)}=0 \qquad (5.6.2)$$

and the condition at x = 1 becomes

$$\frac{\partial A}{\partial x}=-\frac{\partial C}{\partial x}\,, \qquad A=C \qquad (5.6.3)$$

Noting that the symmetry of the interior solution is inherited by the inverted solution, the other relevant boundary conditions follow readily. The condition on A at $x = \infty$ inverts to C = 0 at x = 0.

A matrix multiplication method is used to determine the boundary values of A for each time step of the integration. This method, which was originally suggested by R Thirlby (unpublished work), and has been used by Jepps, is now described.

For a three-point backward difference approximation of the conditions at x = 1 one finds

$$C(1)=\frac{2}{3}\left\{A(1-\Delta x)+C(1-\Delta x)\right\}$$
$$-\frac{1}{6}\left\{A(1-2\Delta x-C(1-2\Delta x)\right\} \qquad (5.6.4)$$

$$A(1)=C(1) \qquad (5.6.5)$$

The following operations are now necessary in order to achieve the simultaneous solution of equations (4.5), (4.6) and (5.4):

(i) All the values of A and B are determined from the finite-difference form of (4.5) and (4.6) at the interior mesh points on the next time level.

(ii) Equation (5.4) is expressed in a finite-difference form, and using relations (6.4) and (6.5) together with the other relevant boundary conditions, the values of C at all the points on the inverted spatial mesh can be determined. The method of solving this n x n system of finite-difference equations provides some difficulty, which will be discussed below.

(iii) Finally the boundary values of A can be calculated from (6.4) and used to advance the next time step.

The matrix multiplication method allows these operations to be combined into one simpler procedure. We are, at present, only interested in the inverted solution because it determines the boundary values of A. Let the vector whose components are the values of A at the boundary points be A_B, and let the vector whose components are the values of A at the two rows immediately inside the boundary be A_I. The operations outlined above calculate the boundary values A_B given A_I. However, since A_B is a linear function of A_I, a matrix, M, exists such that

$$M A_I = A_B \tag{5.6.6}$$

It is now only necessary to calculate M at the start of the calculation and the boundary values A_B can be found at each time step by matrix multiplication. The matrix M can be calculated column by column, once the following is noted.

If the n^{th} component of A_I is set equal to unity, and all the others set equal to zero, then the boundary values obtained by our operations consist of the n^{th} column of M.

The problem of solving the inverted equation is now discussed. The finite-difference form of this equation gives rise to n x n equations which are solved in common. Successive over-relaxation is usually employed, but this technique converges only if the matrix of the coefficients of the equations is positive definite. This is true for the spherical case, but untrue for the more general oblate spheroidal case. A method involving triangular factorization and back-substitution has been used instead.

To determine the external solution it is first necessary to reconstruct the inverted solution from the final boundary values. This is then interpolated onto a uniform external mesh.

The length of the time step is decreased, and the fineness of the spatial mesh increased, until the solution found is independent of both. The magnetic Reynolds number is prescribed at the beginning of the calculation, and the subsequent development of the field reveals whether the value is sub-critical, critical, or super-critical. For sub-critical (super-critical) values the field exponentially(grows) decays . Determination of critical values is therefore a matter of trial and error.

The calculations have been performed upon the NUMAC IBM 370/168 at the University of Durham. Library programs (of the Nottingham Algorithms Group (NAG)) have been used to perform the triangular factorization and back-substitution, and interpolation procedures. The contouring procedure which is used to display the results has been adapted from a program originally written by F J Rens (Geography Department, University of Michigan).

It was possible to advance the integration using 20 x 20 spatial intervals by 100 steps in 3 seconds C.P.U. time. 10 x 10 interval mesh gave essentially the same results, but the finer mesh was found more convenient for contouring. A time step $\Delta t = 10^{-5}$ was used. This could be increased to $\Delta t = 10^{-3}$ in the spherical limit.

The techniques described enable the development of the magnetic field to be investigated for any given choice of velocity field and α-effect distribution. The final solutions were found not to be sensitive to the initial field distribution. In practice, both A and B were set equal to unity at each interior mesh point.

5.7 Tests in the Spherical Limit ($V \rightarrow 1$)

Throughout the calculations it was found more convenient to use a (θ, x) grid instead of a (η, x) grid (where $\eta = \cos\theta$). The former gives a more uniform coverage in Cartesian coordinates. Letting $f_0 \rightarrow \infty$ produces the spherical limit. Comparison can then be made with results reported by Roberts (1972) on a solar dynamo model suggested by Steenbeck and Krause. The simple model is defined by

$$\alpha = \alpha_0 \cos\theta \qquad \omega = \omega_0 r \tag{5.7.1}$$

Table 5.1 shows a comparison of the magnetic Reynolds numbers and oscillation frequencies obtained for quadrupole symmetry. For the initial-value approach the oscillation frequency is obtained by counting the number of time steps needed to complete a cycle.

TABLE 5.1

Sign of $\alpha_0 \omega_0$	Critical Magnetic Reynolds Number, Rm	Oscillation Frequency
	Roberts (1972)	
+	76.1	55.1
−	85.4	67.4
	Present Work	
+	75.4	54.8
−	81.3	67.8

A 10 x 10 spatial mesh has been used in these calculations. As the integration proceeded the solutions settled down rapidly, giving the expected oscillatory behaviour. The agreement is reassuring. Steady solutions are not excited in the spherical case.

5.8 Stix's Model

Stix has proposed the following distributions for the galactic dynamo

$$\tilde{\alpha} = z/b = x\eta \qquad (5.9.1)$$

$$d\tilde{\omega}/ds = s/R^2 \qquad (5.9.2)$$

(1) is the simplest function which is an odd function of latitude and (2) gives a very rough approximation to the observed differential rotation in the galaxy.

5.9 Tests in the Asymptotic Limit($V \to 0$)

A M Soward has derived the following asymptotic formula (personal communication), from analytical considerations, for the critical dynamo numbers, Pc, of the steady solutions to Stix's dynamo model.

$$V^3 P_c = \frac{27}{\pi} P_{00} \left\{ 1 + V^{2/3} \left(6^{1/3} \lambda \right) + O(V^{4/3}) \right\}$$

(5.9.1)

$$\lambda = 1.01879\cdots$$

(5.9.2)

For the steady dipolar mode $P_c > 0$ and

$$P_{00} = 69.0983 \qquad \nu = 0.836624 \tag{5.9.3}$$

For the steady quadrupolar mode $P_c < 0$ and

$$P_{00} = -12.5572 \qquad \nu = 1.06228 \tag{5.9.4}$$

A comparison between the present work and the asymptotic results is shown in table 5.2.

TABLE 5.2

Critical Dynamo Numbers

Aspect Ratio	Quadrupole Symmetry	Dipole Symmetry
	Asymptotic Results (Soward)	
2/15	-51,000	
1/15	-363,000	2,250,000
	Present Work	
2/15	-63,000	
1/15	-400,000	2,800,000

No steady dipolar mode is excited at V = 2/15. The agreement is satisfactory.

As V is decreased the agreement improves, as one would expect from comparison with results from an asymptotic relation. For values of V less than 1/15 the numerical scheme starts to break down, i.e, the length of time step and fineness of mesh, required for stability, become computationally prohibitive. It is just in this regime where asymptotic results can take over.

5.10 Comparison with Stix's Results

Disagreement had been found between the present work and Stix's results, which motivated A M Soward's derivation of the asymptotic relation. It had become clear that the difference could be explained simply by a factor of V, for the critical dynamo numbers obtained. Stix has now confirmed this (private communication).

Previous to this, part of Stix's calculations had been repeated. It was found that for V = 2/15 the critical dynamo number for the steady quadrupole solution was -58,000. The method used follows directly from Stix's work and is described in Appendix III. This is of some interest, since it suggests an alternative procedure for imposing the boundary conditions for the initial-value problem approach, which would combine the best features of each approach.

5.11 Results

Steady and oscillating solutions have been investigated for both parities (dipolar and quadrupolar) for Stix's model. The results are shown in the following series of pictures. Equispaced contours of constant toroidal field strength are plotted on the right-hand side, and poloidal field lines plotted on the left-hand side.

Poloidal field lines are given by As = constant. We can see this from the following argument (Roberts and Stix, 1971). Field lines are defined by

$$\underset{\sim}{B}_{p\alpha} \wedge \hat{\underset{\sim}{n}} = 0 \qquad (5.11.1)$$

where $\hat{\underset{\sim}{n}}$ is the normal unit vector to the magnetic field $\underset{\sim}{B}_{p\alpha}$. From (3.9) it is evident that $\underset{\sim}{\nabla}(As)$ is perpendicular to $\underset{\sim}{B}_{p\alpha}$. Consequently As = constant will satisfy the definition.

Figures 3-7 show steady solutions. The second solution shows a higher quadrupole mode being excited as the dynamo number is increased. Parker (1971a) has discussed the crowding of field lines which occurs at the boundaries for these modes. This effect becomes much more pronounced as P is further increased. The dipole solution shown in figure 5 is slowly decaying. An aspect ratio V = 2/15 is taken for all of the solutions except those shown in figures 6 and 7. Steady modes at V = 1/15 for both parities are shown there.

Figures 8-13 (14-19) illustrate the oscillating quadrupole (dipole) solution. Phase = 0 is an arbitrary starting point. For the quadrupole (dipole) mode the critical dynamo number is approximately +260,000 (-260,000) and the oscillation frequency is 2617 (1707). $(2\pi\tilde{\eta}/R^2)$

5.12 Discussion

We take, for the galaxy, R = 15 kpc, $\tilde{\eta} \sim 1$ kpc km s^{-1}, ω_0 = -2A (Oort's constant), and α_0 = 0.5 km s^{-1} (which correspond roughly to the numbers used by Parker, 1971a and Stix, 1975) we find

$$R_\omega = \omega_0 R^2/\tilde{\eta} \simeq -7\times10^3, \quad R_\alpha = \alpha_0 R/\tilde{\eta} \simeq 7 \qquad (5.12.1)$$

Thus, $D = (R_\omega R_\alpha) \sim -5 \times 10^4$, which compares favourably with the dynamo numbers computed for the steady quadrupole modes shown in table 5.2. Steady solutions are preferred to oscillating ones, where the dynamo number required for excitation is much higher. For the numbers quoted the oscillation periods correspond to $\sim 10^9$ yr.

The galactic disk, is, however, highly oblate, Taking V = 1/100 we find from the asymptotic formula that Pc = -7×10^7, which is some orders of magnitude larger than the estimate of the observed quantity. The most uncertain parameter involved in the estimate of Pc is probably $\tilde{\eta}$, upon which Pc depends considerably. We note that even if $\tilde{\eta}$ is a factor of 30 less than our estimate the characteristic escape time of the field from the gaseous disk is $\sim 6 \times 10^9$ years, which is less than the age of the galaxy. Stix's conclusion, that the galaxy can act as an $\alpha\omega$-dynamo, and that a steady quadrupole mode is most easily excited, is therefore accepted.

Before formulating a working model for the galactic magnetic field, development are made to the simple model, which are reported in the next chapter.

References

Parker, E.N. 1971a Astrophys J 122 293

Parker, E.N. 1971b Astrophys J 163 279

Stix, M. 1975 Astron and Astrophys 42 85

Roberts, P.H. 1967 An Introduction to Magneto-hydrodynamics, Longmans, Green, London (Chapter 3)

Roberts, P.H. 1971 In Lectures in Applied Mathematics. W.H. Reid, Ed. Vol 14 129. American Mathematical Society Providence, R.I.

Flammer, C 1957 Spheroidal Wave Functions, Stanford Univ press, California

Jepps, S.A. 1975 J. Fluid Mech 67 625

Dufort, E.C. and Frankel, S.P, 1953 Math Tables Aids to Comp 7 135

Roberts, P.H. 1972 Phil Trans Roy Soc London A272, 663

Roberts, P.H, and Stix, M. 1971. The Turbulent Dynamo, N.C.A.R. Technical Note TN11A-60

THE OBLATE SPHEROIDAL COORDINATE SYSTEM

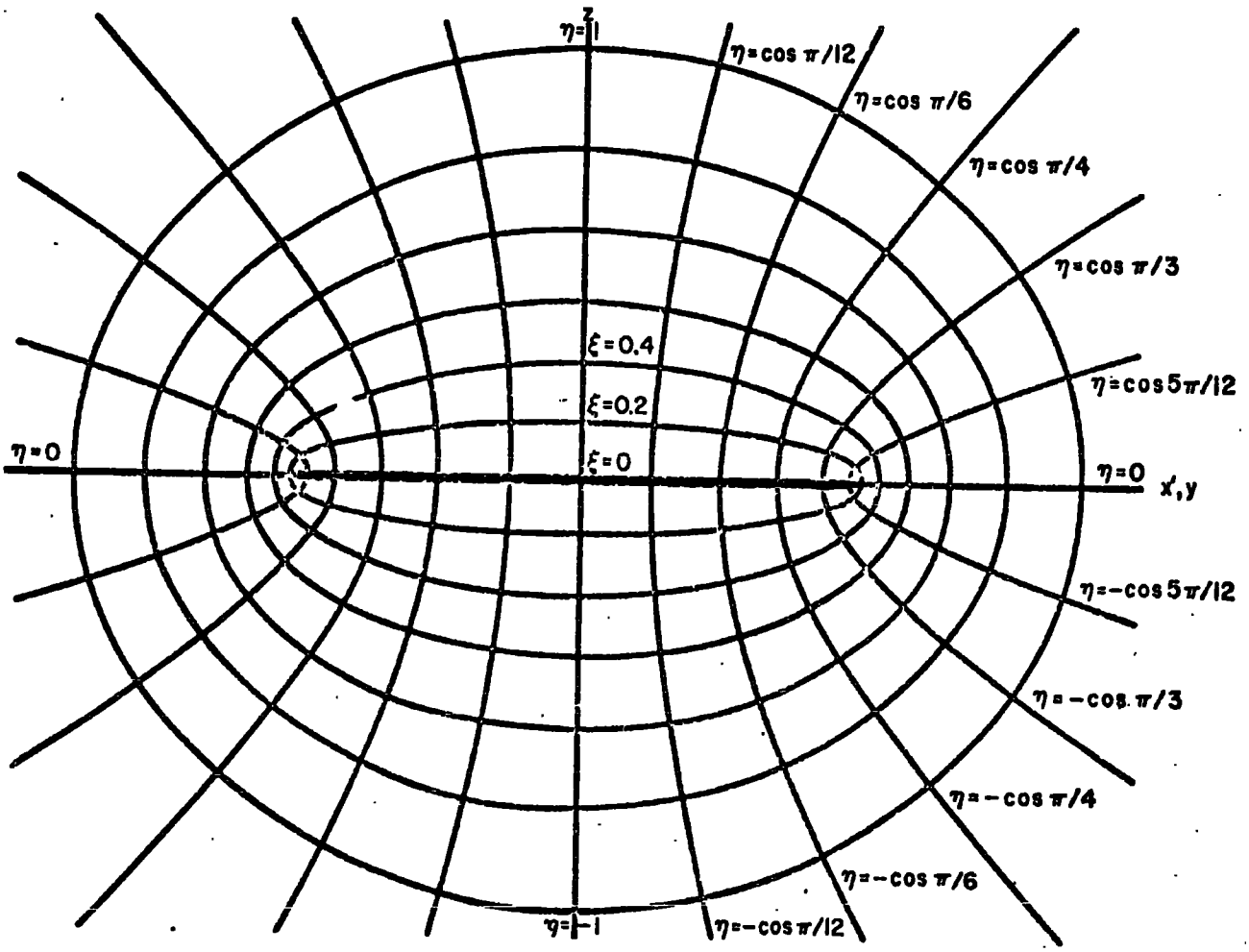

FIG 5.1

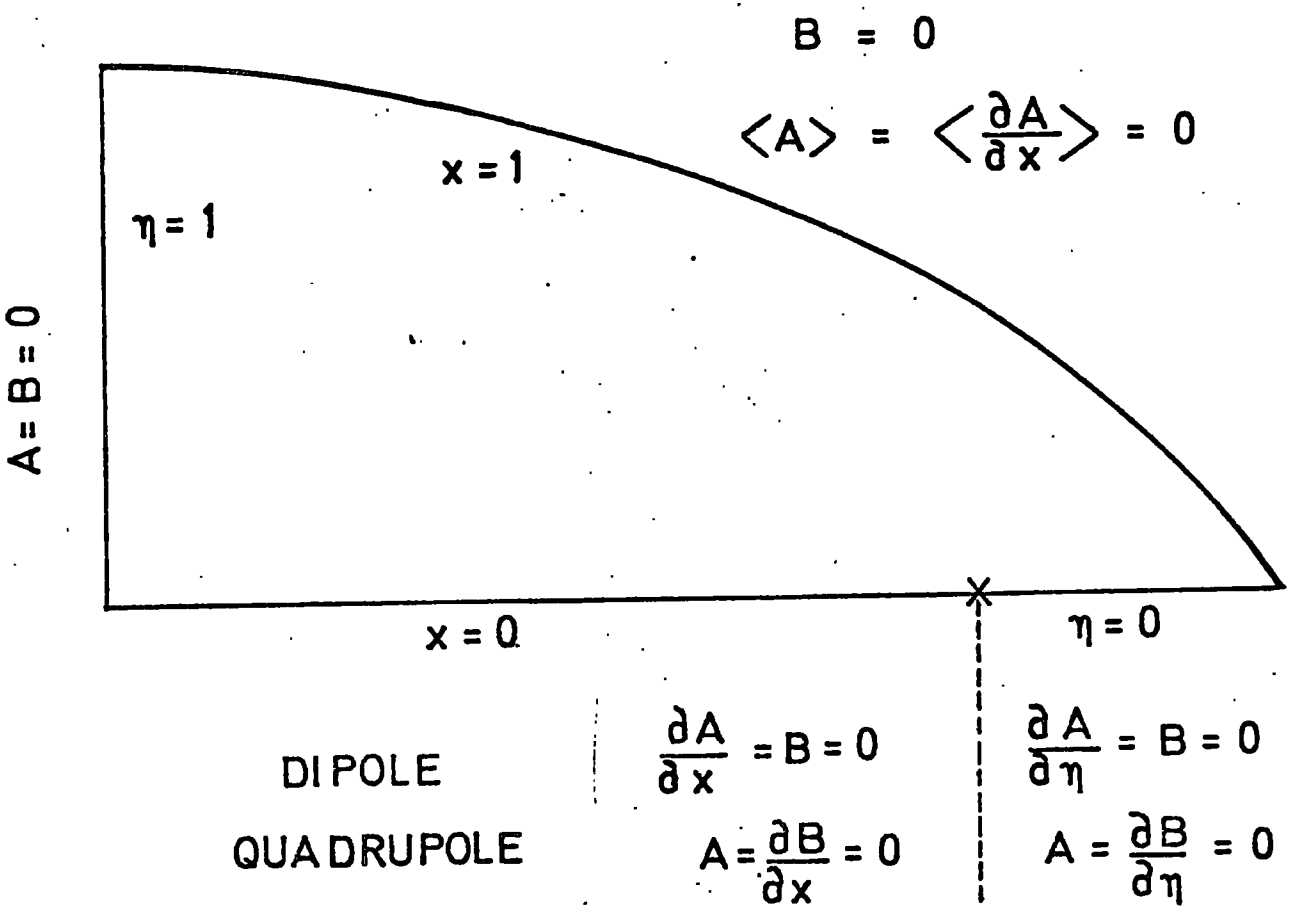

FIG. 5.2

QUADRUPOLE MODE: STEADY SOLUTION
P=-.63E 05

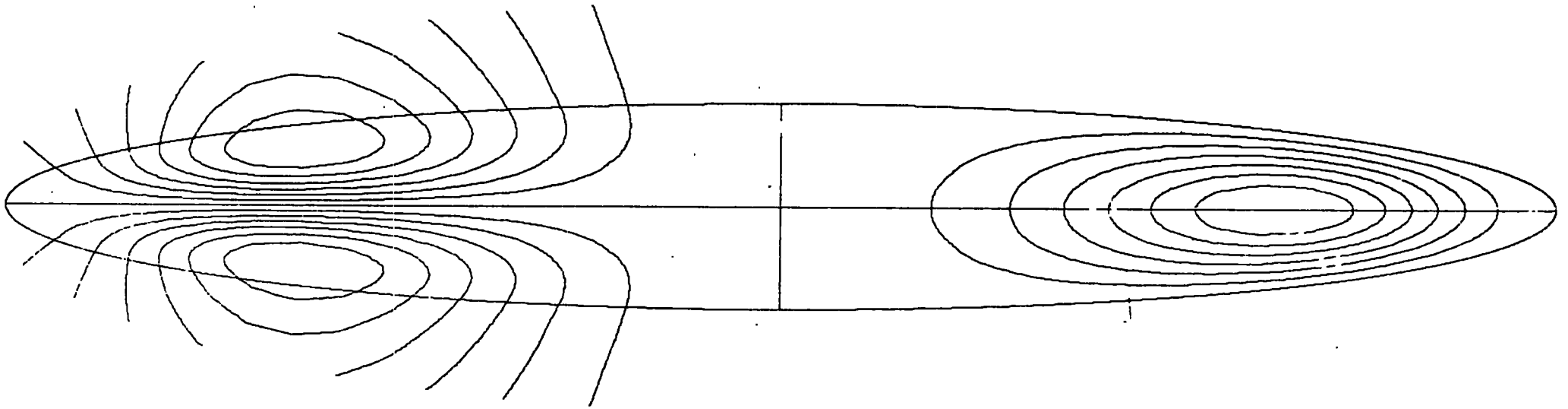

FIG 5.3

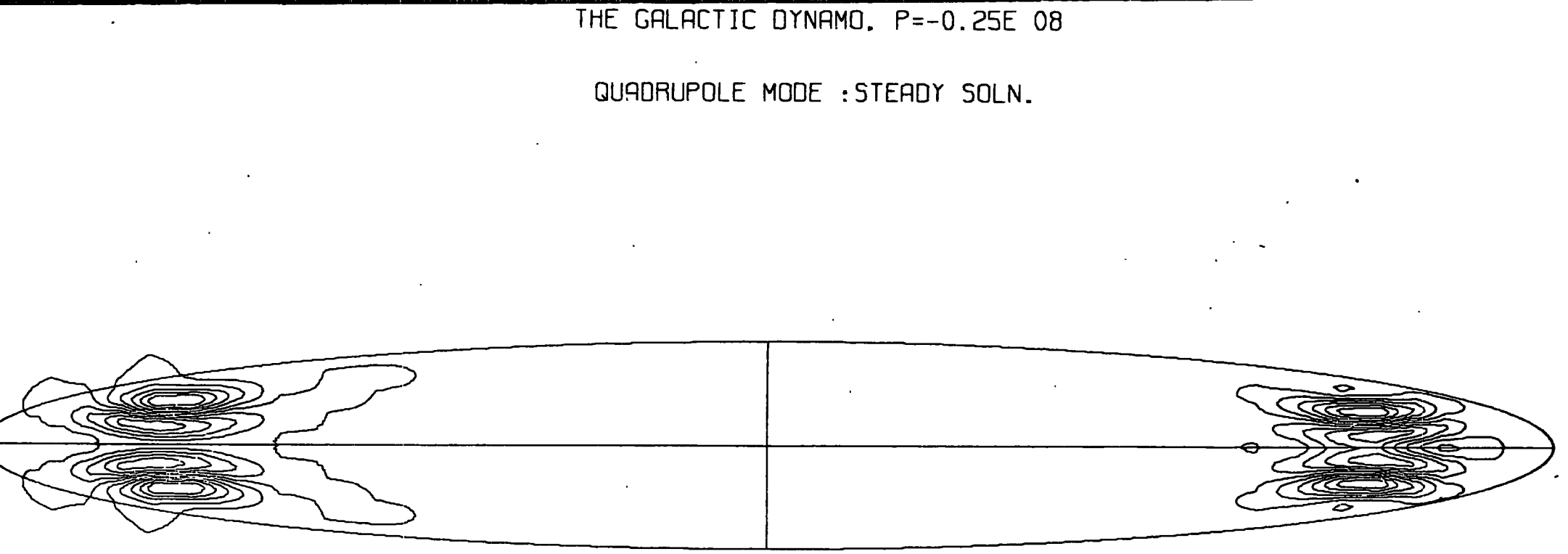

FIG 5.4

DIPOLE MODE :SLOWLY DECAYING SOLN.
P=0.60E 06

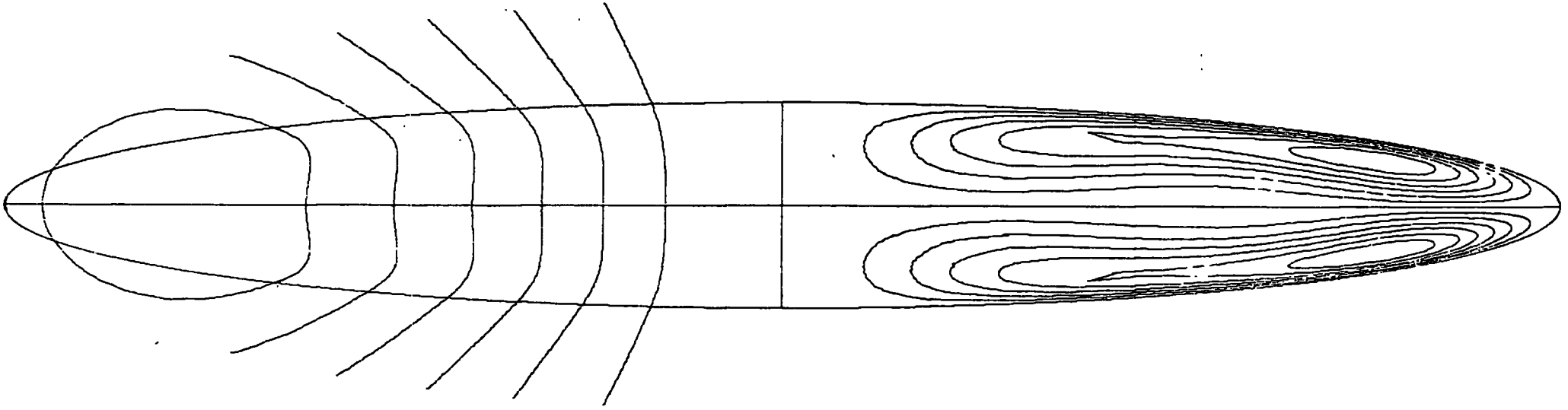

FIG 5.5

QUADRUPOLE MODE: STEADY SOLUTION
P=-.40E 06

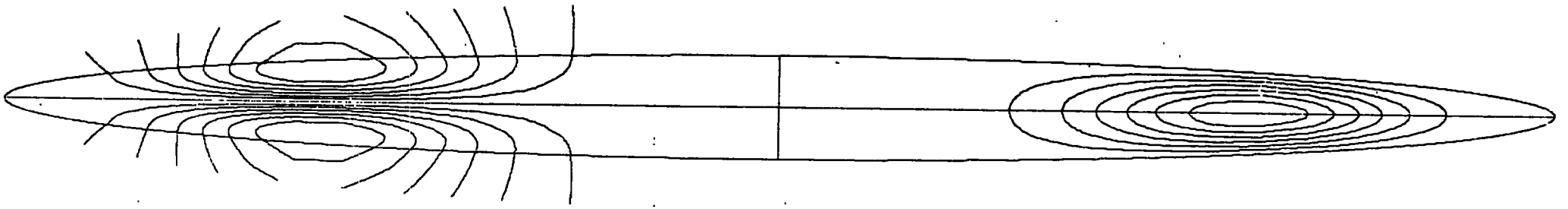

FIG 5.6

DIPOLE MODE:STEADY SOLUTION
P=0.28E 07

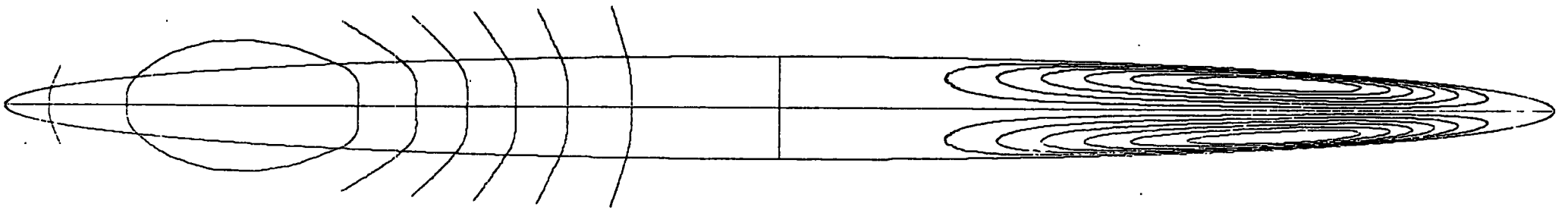

FIG 5.7

QUADRUPOLE MODE: OSCILLATING SOLUTION
P=0.26E 07

PHASE=0

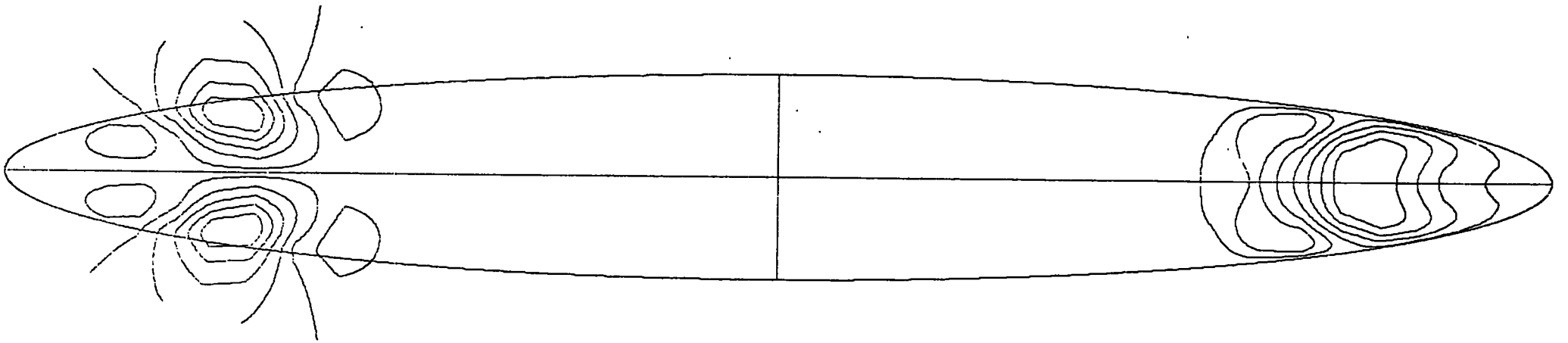

FIG 5.8

PHASE=1/6π

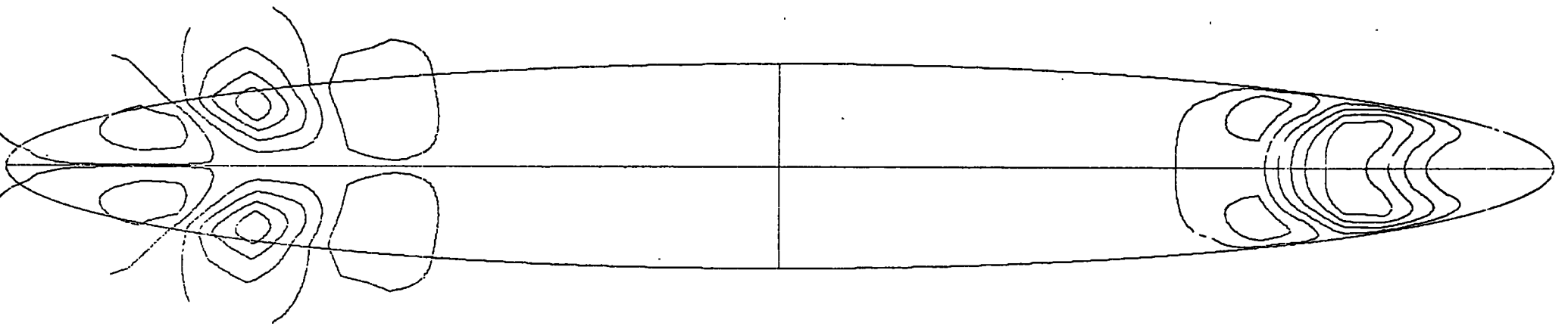

FIG 5.9

PHASE=2/6π

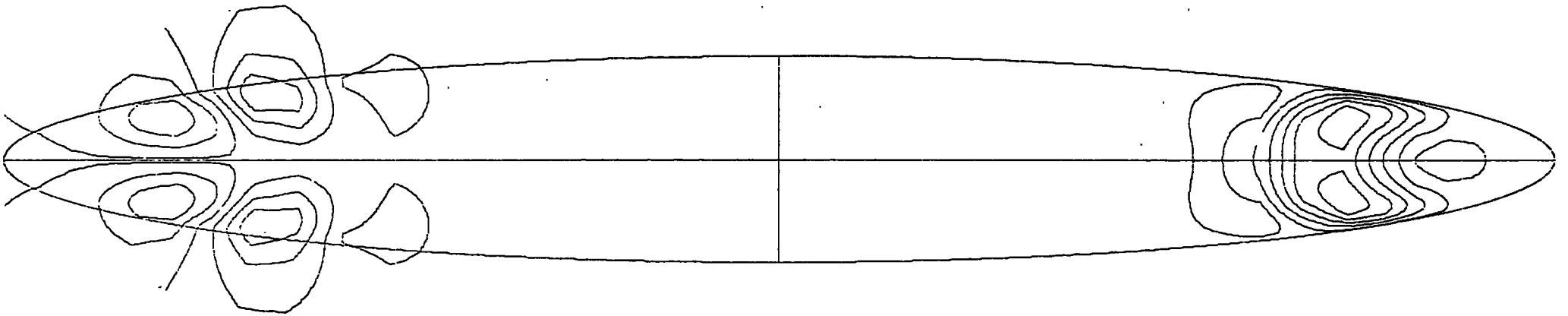

FIG 5.10

PHASE=3/6π

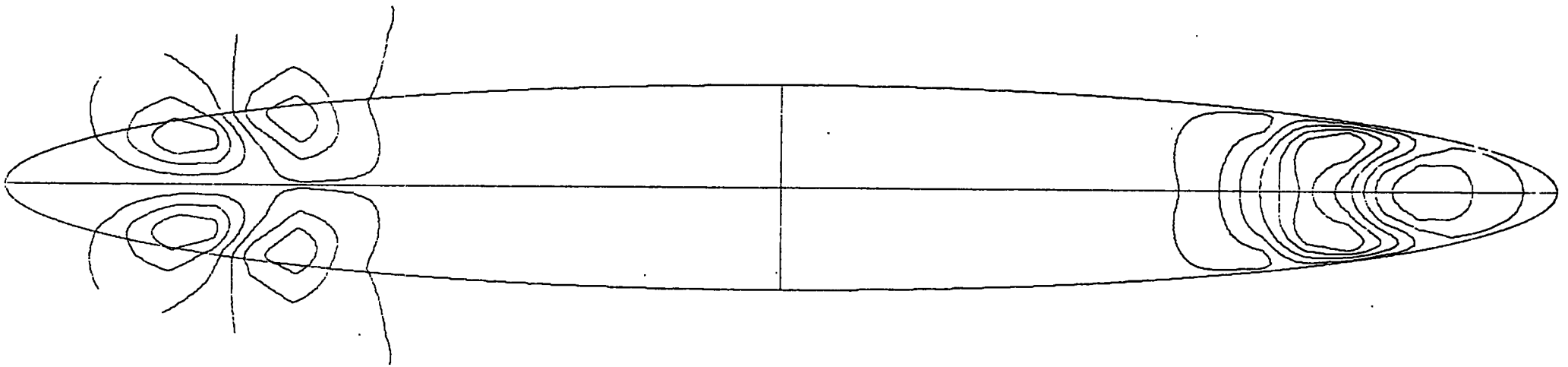

FIG 5.11

PHASE=4/6π

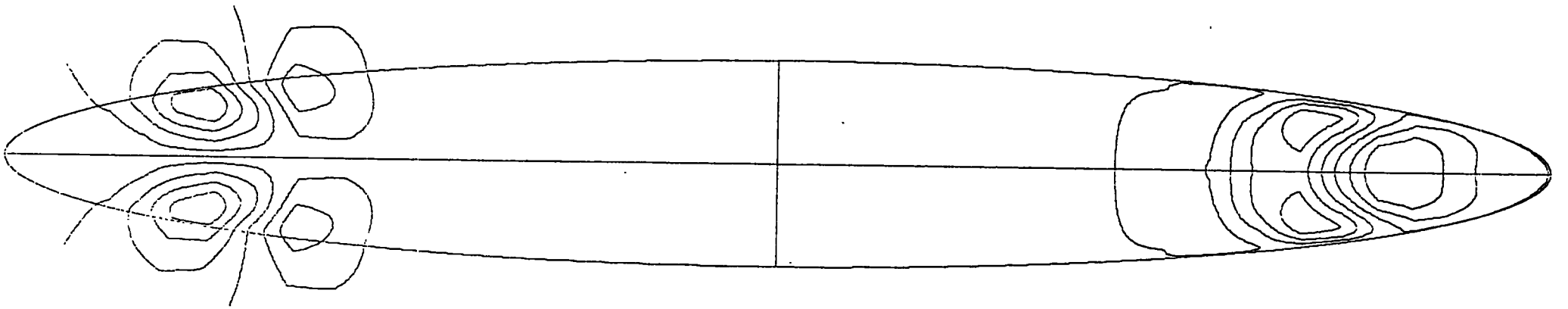

FIG 5.12

PHASE=5/6π

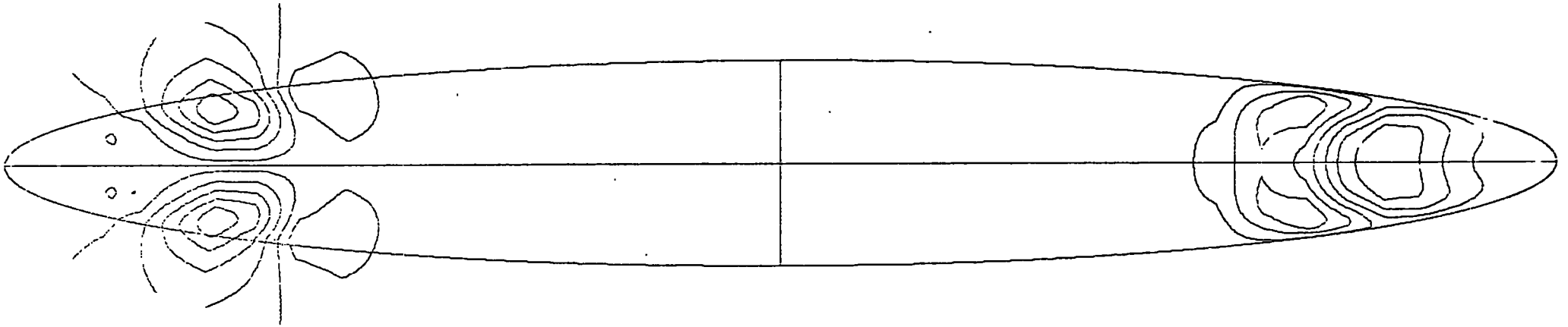

FIG 5.13

DIPOLE MODE: OSCILLATING SOLUTION
P=-.26E 07

PHASE=0

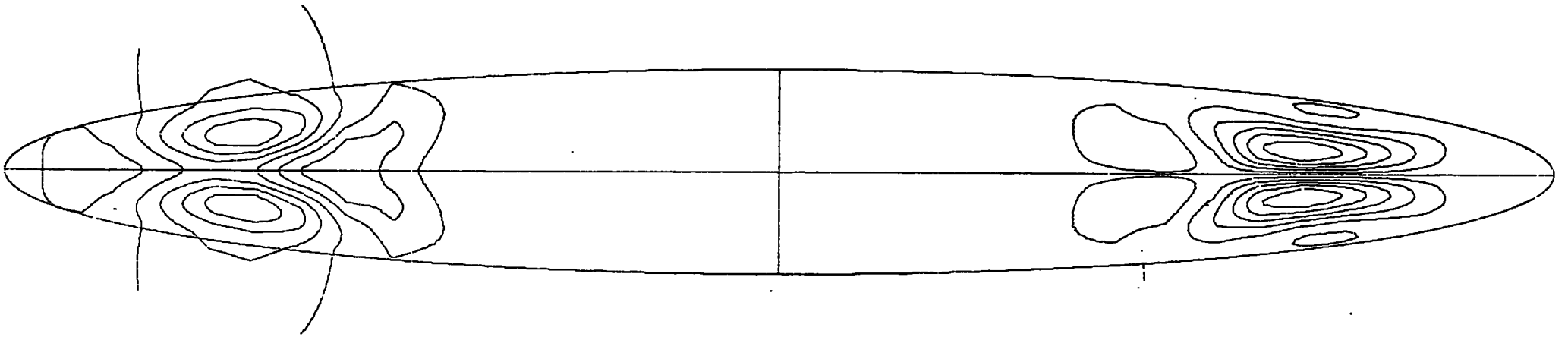

FIG 5.14

PHASE = 1/6 π

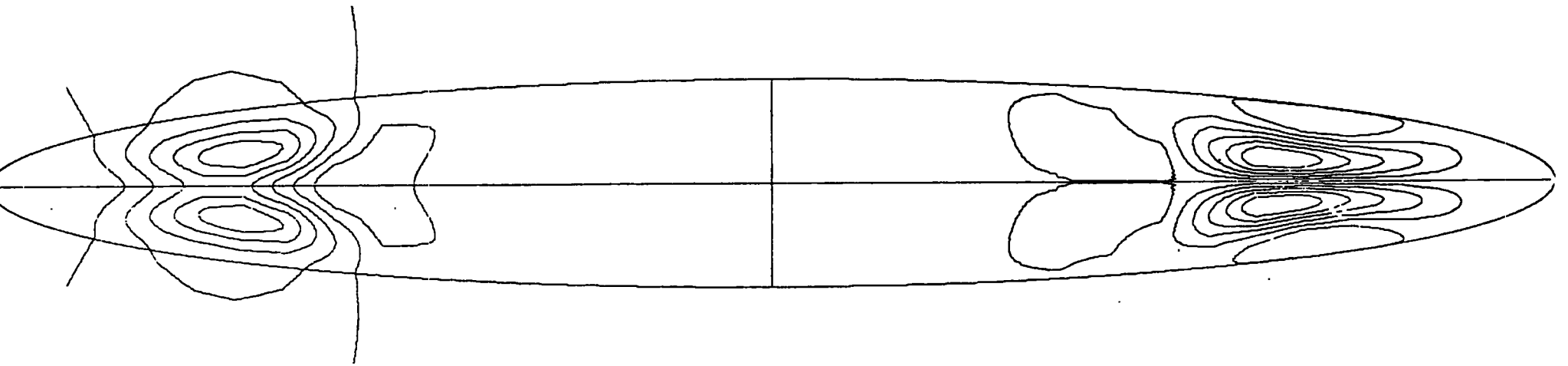

FIG 5.15

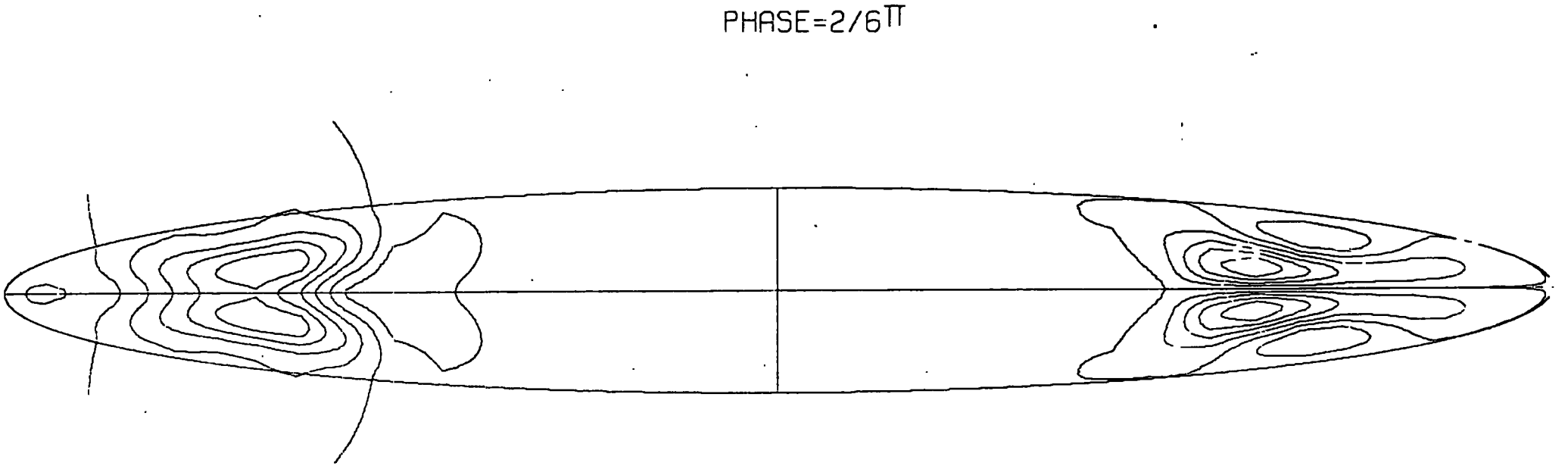

FIG 5.16

PHASE=3/6π

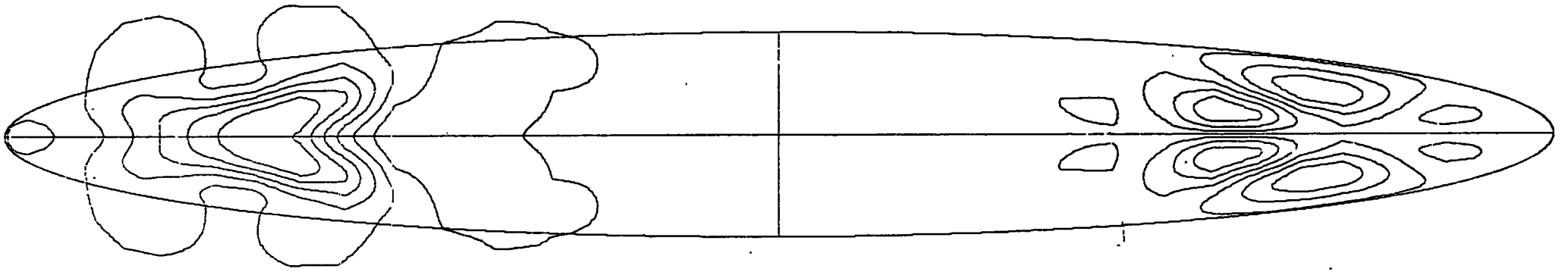

FIG 5.17

PHASE=4/6π

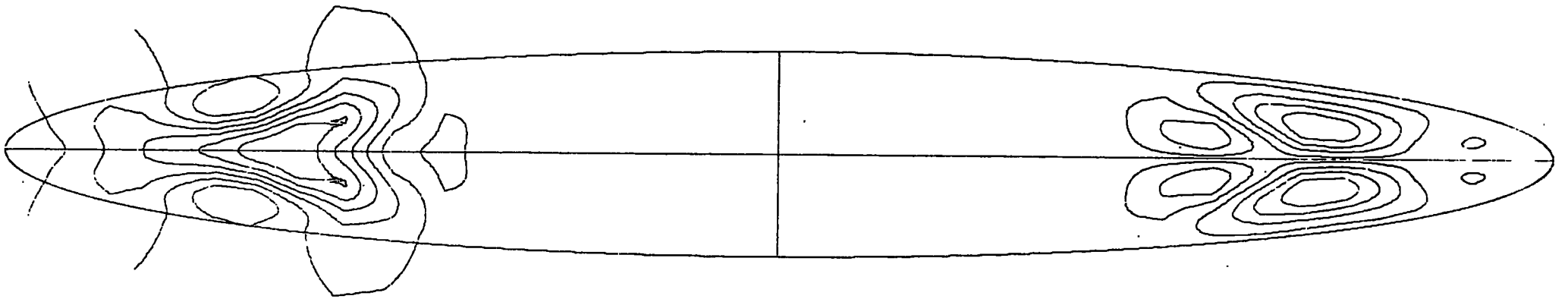

FIG 5.18

PHASE=5/6π

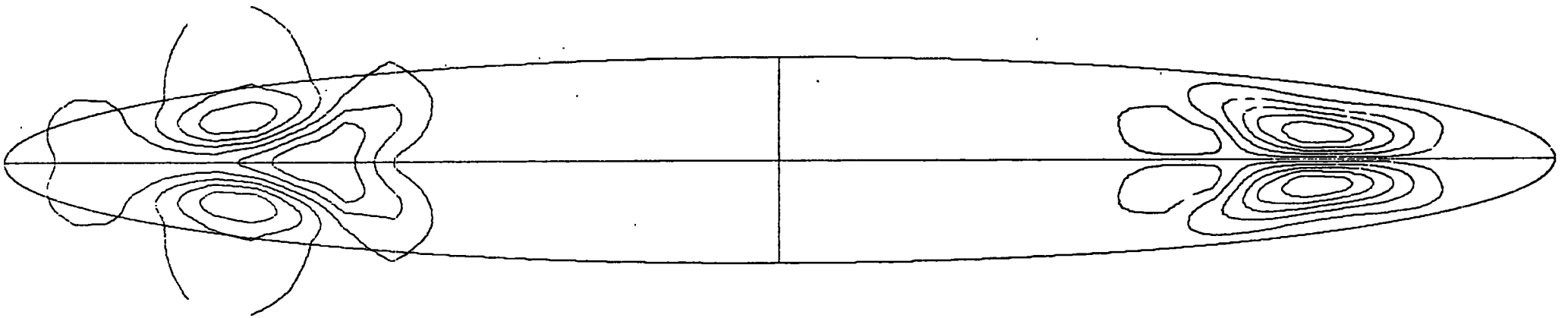

FIG 5.19

Chapter Six. Developments of the Simple Model

6.1 Introduction

Modifications to the simple galactic dynamo model are discussed. It is important to decide how sensitive the results are to the particular forms of $\tilde{\alpha}$ and $d\tilde{\omega}/ds$ employed. In order to simulate the suppression of turbulence by the magnetic field nonlinear models are constructed in which $\tilde{\alpha}$ is a function of B. This prevents the field from suffering the unphysical fate of increasing indefinitely, if the dynamo number is super-critical.

The possibility of the intergalactic medium having a finite conductivity is investigated by adjusting the boundary conditions in a simple manner. Finally a model is proposed for the galaxy which incorporates some of the features we have discussed. Attention is restricted to the steady quadrupole mode in all cases.

6.2 Dependence upon $\tilde{\alpha}$

The distributions of $\tilde{\alpha}$ suggested by Parker (1971), Stix (1975), and the present work are illustrated in figure 6.1. Parker's distribution has discontinuities at $z = 0$ and $|z| = b$ (the surface of the disk). Stix's distribution increases monotonically to the surface, where it is discontinuous. We suggest that the cyclonic velocity of turbulent eddies across the disk (and therefore $\tilde{\alpha}$) has a continuous distribution and take

$$\tilde{\alpha} = 1.5686\cdots e^{-|z'|} \sin \pi z' \qquad (6.2.1)$$

where

$$z' = z/b \,. \qquad (6.2.2)$$

The constant has been chosen so $\tilde{\alpha}$ has unit maximum. The resulting solution when $\tilde{\alpha}$ is changed in this manner is shown in figure 5.2.

Before a comparison can be made of the critical dynamo numbers for each model the following remarks are in order. Parker, as we have pointed out, has employed a 'slab' geometry, but has also employed a different function for $d\omega/ds$ (one in which the gaseous disk obeys Keplerian motion). For sufficiently small values of V, the spatial variation of the field in the s-direction is very small compared to its variation in the z-direction. Therefore, differences arising from the different geometries are likely to be insignificant. Anticipating a result of section 6.6 the following table is compiled.

TABLE 6.1

Critical Dynamo Numbers for some Relevant Models V = 2/15

Parker	Present Work		Stix
-2,500	-8,000+	-40,000	-63,000

+Includes Observed Rotation Curve.

Since Parker's prescription of Keplerian motion for $d\omega/ds$ differs insignificantly from the observed motion, the differences occurring in the first two entries of table 6.1 can be largely ascribed to the different $\tilde{\alpha}$ distributions used (compare (a) and (c) on figure 6.1). The last two entries of table 6.1 reveal that the difference caused by using our $\tilde{\alpha}$ distribution instead of Stix's is slight.

6.3 Suppression of Turbulence by the Magnetic Field

To simulate this suppression, the following dependence of $\tilde{\alpha}$ upon $\underset{\sim}{B}$ is considered

$$\tilde{\alpha}' = N\tilde{\alpha}/(1 + |B|^n) \qquad (6.3.1)$$

Jepps (1975) has investigated cut-off laws of this form for the solar dynamo. Since the Lorentz force is quadratic in B we take n = 2.

The choice of cut-off law is arbitrary, and not based upon any theory of turbulent magneto-hydrodynamics. We find that, for supercritical values of Pc, the magnetic field now stabilizes at a finite value. N is a quantity which gives the degree to which the prescribed dynamo number is supercritical. The dependence of $\tilde{\alpha}'$ is only on the toroidal field, B, which is consistent with the assumption made earlier about the field being predominantly toroidal. This cut-off law is probably unrealistic for small values of B, where no suppression of turbulence is expected.

For these nonlinear models an additional operation is performed at each time step of the integration : the new distribution of $\tilde{\alpha}'$ based upon the current magnetic field distribution is calculated in readiness for the next time step. Results are shown for N = 5 and N = 10 in figures 6.3 and 6.4, respectively. As one expects, the variation in the magnitude of the field is reduced. This nonlinearity will also prevent higher modes of the field from being excited.

6.4 Variation of Diffusivity

As a crude attempt to simulate spiral arm structure in the galaxy the following distribution of $\tilde{\eta}$ has been investigated

$$\eta(r,\theta) = \tilde{\eta}_0 \left(1 + a \sin^2(2\hat{n}s/\lambda)\right) \qquad (6.4.1)$$

where $a = 5 \qquad \lambda = R/4 \qquad (6.4.2)$

Clearly, spiral arm structure cannot be incorporated into a axisymmetric model, so concentric annuli are considered. It is assumed that the diffusivity is a maximum in the 'interarm' region, where there is less conducting matter.

For a spatially dependent $\tilde{\eta}$ the dynamo equation acquires an additional term, becoming

$$\frac{\partial \underset{\sim}{b}}{\partial t} = \underset{\sim}{\nabla} \wedge \underset{\sim}{u} \wedge \underset{\sim}{b} + \underset{\sim}{\nabla} \wedge (\alpha \underset{\sim}{b}) + \tilde{\eta} \nabla^2 \underset{\sim}{b} - \underset{\sim}{\nabla} \tilde{\eta} \wedge \nabla \wedge \underset{\sim}{b} \qquad (6.4.3)$$

A resulting solution is shown in figure 6.5. This solution is not exactly steady, and for such a large value of P 'active degeneration' occurs : the poloidal field is decaying, but the toroidal field is growing. Higher modes do not occur. At an appropriate lower value of P an exactly steady solution can be found.

The mention of spiral structure leads to the question of whether we are justified in considering axisymmetric solutions to the dynamo equation. Braginski (1964) has developed an alternative approach to the dynamo problem, through the nearly symmetric dynamo.

In this case it is supposed that the fluid motions are long-lived and large-scale, in contrast to the short-lived, small-scale motions of the turbulent dynamo. As the degree of asymmetry approaches zero the dynamo number $Pc \rightarrow \infty$ (Roberts, 1972). One expects, then, large dynamo numbers for the excitation of a nearly symmetric dynamo. It is on this expectation that we suggest the galaxy prefers to excite an axisymmetric field.

Soward (1972) has found that for the nearly symmetric dynamo can be explicitly evaluated in terms of the asymmetric flow, and is, surprisingly, closely related to the helicity of flow. If the large-scale asymmetric motions of the galaxy could be predicted (or observed) then one could decide with confidence if nearly axisymmetric fields are excited (Roberts, personal communication).

6.5 An Intergalactic Medium of Finite Conductivity

Here we consider the case where the galactic disk is surrounded by an infinite medium, having the same conductivity as the disk. Then, not only will A and $\partial A/\partial x$ be continuous across the surface of the disk ($x = 1$), but also B and $\partial B/\partial x$. The boundary at $x = 1$ now represents the surface beyond which there are no fluid motions. For steady solutions the additional condition

$$\underset{\sim}{\nabla} \wedge \underset{\sim}{\nabla} \wedge \underset{\sim}{\beta} = 0 \qquad (6.5.1)$$

is satisfied outside the boundary. The boundary conditions for B at $x = 1$ are imposed in a manner identical to that already described for A at $x = 1$.

For those interested in studying oscillating solutions under these boundary conditions the situation is somewhat more complicated, since the equations governing the external solution (such as (1)) would contain time-dependent terms. In this case the following procedure might be adopted:

(i) The equations governing the external solution are inverted and expressed in a finite-difference form.

(ii) The integration may be carried out by time-stepping the inverted and interior equations simultaneously.

(iii) At each time step it is simple to impose the necessary boundary conditions at $x = 1$ (from the continuity requirements) which are used in the next time step.

We have, however, only considered the steady quadrupole solution. The resulting field structure is shown for aspect ratios of 2/15 and 1/15 in figures 6.6 and 6.7, respectively. The dynamo numbers found suggest that the field is easier to excite if the intergalactic medium has a finite conductivity.

Parker (1971) has considered similar boundary conditions for his model, but has allowed the shear to extend to infinity. He has found that the excitation parameter (and therefore dynamo number) is small compared to the estimate of the observed value. In this case he argues that a higher mode is excited, but the reversed fields cannot escape freely (as a result of the finite conductivity of the surrounding medium) and active degeneration occurs. He continues to conclude that the emptiness of the intergalactic medium is an essential part of the galactic dynamo. We reject this conclusion on two accounts: the dynamo number obtained is sensitive to the prescribed α-effect function (see table 6.2): the inclusion of the nonlinear effects we have discussed prevent higher modes from occurring and are therefore likely to save the field from active degeneration.

TABLE 6.2

Critical Dynamo Numbers for Models with Finite Conductivity of Intergalactic Medium V = 1/15

Parker	Present Work	
-750	-15,000	-6,000[+]

[+]Includes Observed Rotation Curve

In table 6.2 we have also included the dynamo number for this model when the observed rotation curve is included. It is more appropriate to compare this number with Parker's result. Given that dynamo action occurs in the galaxy, we conclude there is no evidence for (or against) the intergalactic medium having a finite conductivity. We find, however, that the situation is clearer when we look at external galaxies (Chapter Eight).

6.6 Inclusion of the Observed Galactic Rotation Curve

The galactic rotation curve (Mihalas, 1968) has been approximated to suitable polynomials. Figure 6.8 shows the observed points and the polynomial approximation. From this we can calculate $d\omega/ds$ at each point on the finite-difference mesh. The shear is normalized so that its value at earth is unity. This allows ω_o to be interpreted as -2A, where A is Oorts' constant.

Figures 6.9 and 6.10 show the resulting field for aspect ratios of 2/15 and 1/15, respectively. The dynamo numbers (-8,000 and -20,000) are smaller than those reported in previous models. If the toroidal field strength is normalized to 3 μG at the earth, then, in the case where V = 1/15 the maximum field strength is some three orders of magnitude larger. The nonlinear effects arising from the mechanical forces exerted by such large fields would be important. We therefore allow the turbulence to be suppressed in the manner already described.

6.7 A Proposed Model for the Galaxy

Figure 6.11 shows the radial behaviour of B at z = 0, for three values of N. The field values have been normalized so that the field strength at the earth is 3 μG. We choose N = 6 for our model. This choice is somewhat arbitrary, but it leads to more reasonable values of B towards the galactic centre (French and Osborne, 1976). Also the required dynamo number does not differ significantly from the estimate of the observed value. The solution is shown in figure 6.12. The external solution has been calculated out to a distance of $\sim$ 20 kpc, in readiness for the investigations we describe in the next chapter.

6.8 Discussion

With regards the suppression of turbulence by the magnetic field we first point out that an alternative school of thought exists. Parker (1975) has suggested that the Petschek mechanism for the rapid reconnection of field lines may be important here. As the magnetic field grows and becomes entangled by the turbulent velocity field, fluid is squeezed out between neighbouring ribbons of field, so the field gradients become very large. Under these conditions (Parker, 1975, and references therein) resistive diffusion proceeds rapidly and rapid reconnection of the field occurs, preventing the field from becoming sufficiently large so that field stresses are important. We do not know whether this mechanism or the one considered in section 6.3 dominates. It is clear, however, that if the turbulence is suppressed in the manner we have suggested, it does not block dynamo action, as Piddington (1970) has suggested.

We note that Piddington (1973) has also suggested that spiral structure is of a hydromagnetic origin, challenging density wave theory. Unlike the hydromagnetic model, density wave theory predicts that HI regions should lie along the spiral arms. Lindblad (1974) has pointed out that Oorts' observations (1974) of neutral hydrogen in M51 favour the density wave theory, and remove Piddington's earlier criticism. This point has been substanstiated by higher resolution studies of neutral hydrogen by Allen et al (1974).

The model discussed in section 6.4 serves mainly as a example of the way in which a spatially dependent diffusivity can be incorporated. From equation (4.4.10) we expect the diffusivity to increase with the rms turbulent velocity, and therefore probably towards the galactic centre. We leave the diffusivity constant in the final model, in view of the lack of observational evidence to the contrary.

The back-reaction of the field upon the fluid motions may also influence the large-scale motions. As the field grows it can exert a braking effect upon the differential rotation, reducing its capacity for regeneration. Unfortunately, this effect has proved too difficult to be included in our models. The most successful attempt to include the effect of the magnetic field upon the large-scale flow appears to have been made by Malkus and Proctor (1975). Their work is concerned with spherical α^2-dynamos and illustrates that only the most sophisticated techniques are able to make progress in this nonlinear regime.

References

Allen, R.J. et al 1974 I.A.U. Sym 58, 425

"The Formation and Dynamics of Galaxies" ed J.R. Shakeshaft.

Braginski 1964 Soviet Phys. JETP 20, 726

French, D.K. and Osborne, J.L. 1976 M.N.R.A.S. in press.

Jepps S.A. 1955 Fluid Mech, 67 625

Lindblad, P.O. 1974 I.A.U. Sym 58, 399

Malkus, W.V.R. and Proctor, M.R.E. 1975 J. Fluid Mech 67, 417

Oort, J.H. 1974 I.A.U. Sym 58, 375

Parker, E.N. 1971 Astrophys J. 163, 255

Parker, E.N 1975 Annals of the N.Y. Academy of Sciences 257, 141

"Roles of Magnetic Fields in Physics and Astrophysics" Ed V. Canute

Piddington, J.H. 1970 Australian J. Phys. 23, 731

Piddington, J.H. 1973 M.N.R.A.S. 162, 73

Roberts, P.H. 1972 Phil. Trans. R. Soc Lond. A272, 663

Soward, A.M. 1972 Phil. Trans. R. Soc. Lond. A 272, 431

Stix, M. 1975 Astron. and Astrophys. 42, 85

Mihalas, D. 1968, Galactic Astronomy, Freeman & Co, San Francisco and London

DISTRIBUTIONS OF α

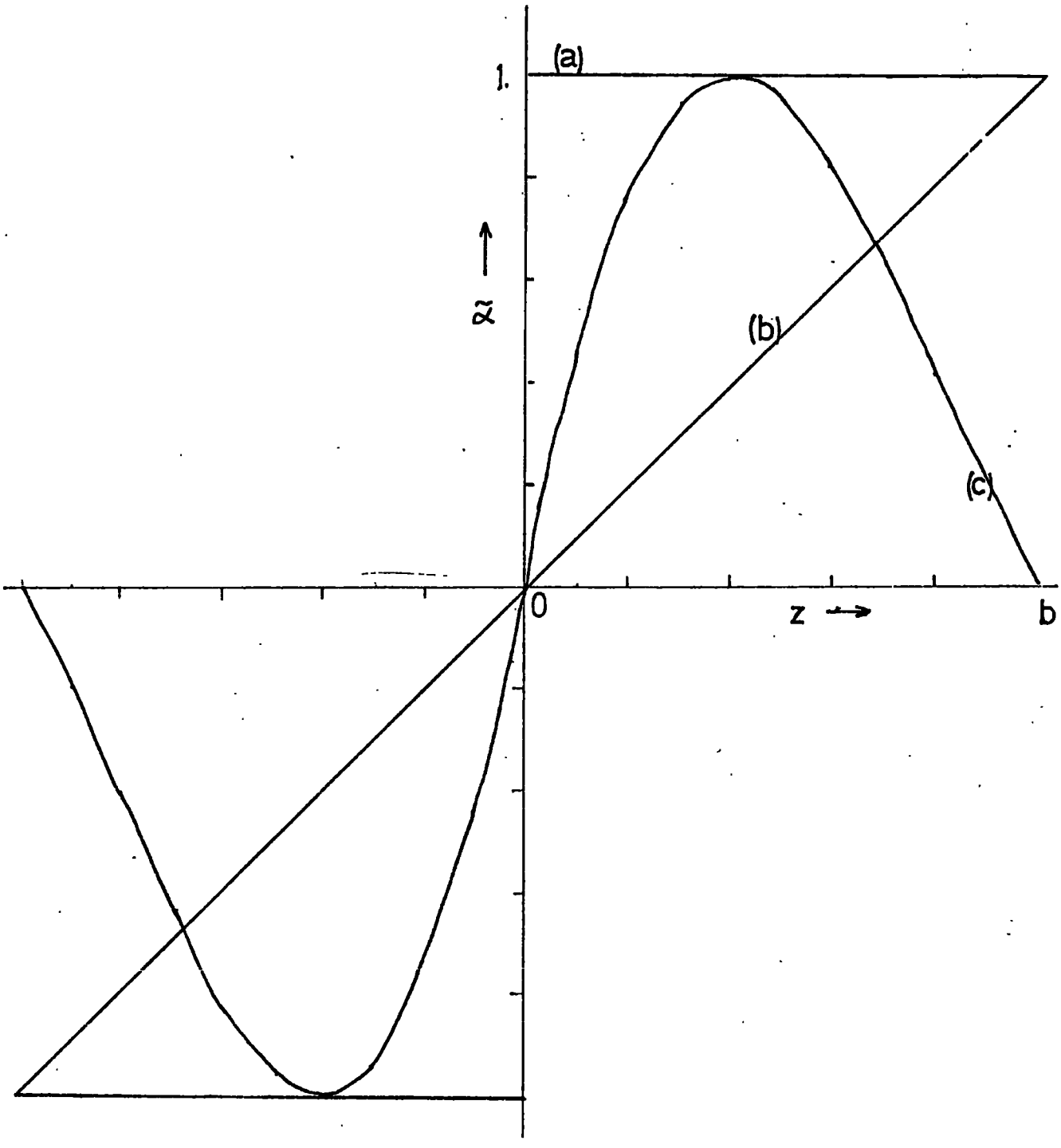

(a) PARKER 1971

(b) STIX 1975

(c) PRESENT WORK

FIG 6.1

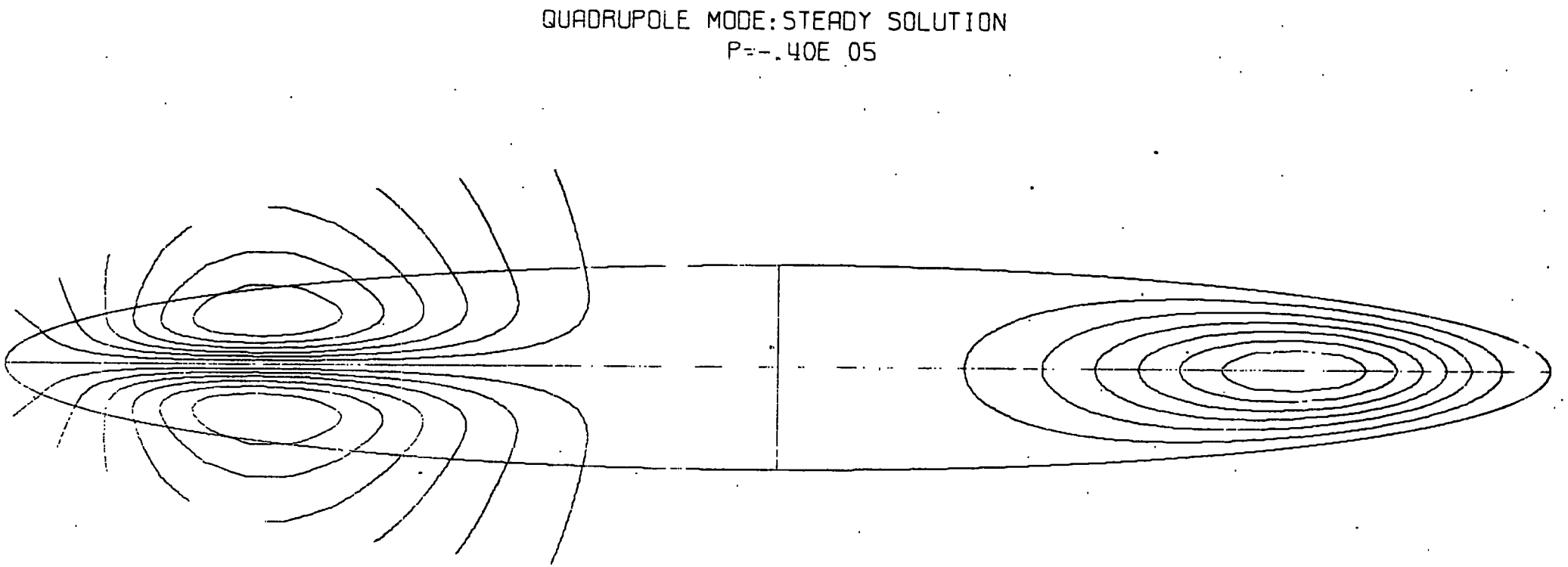

FIG 6.2

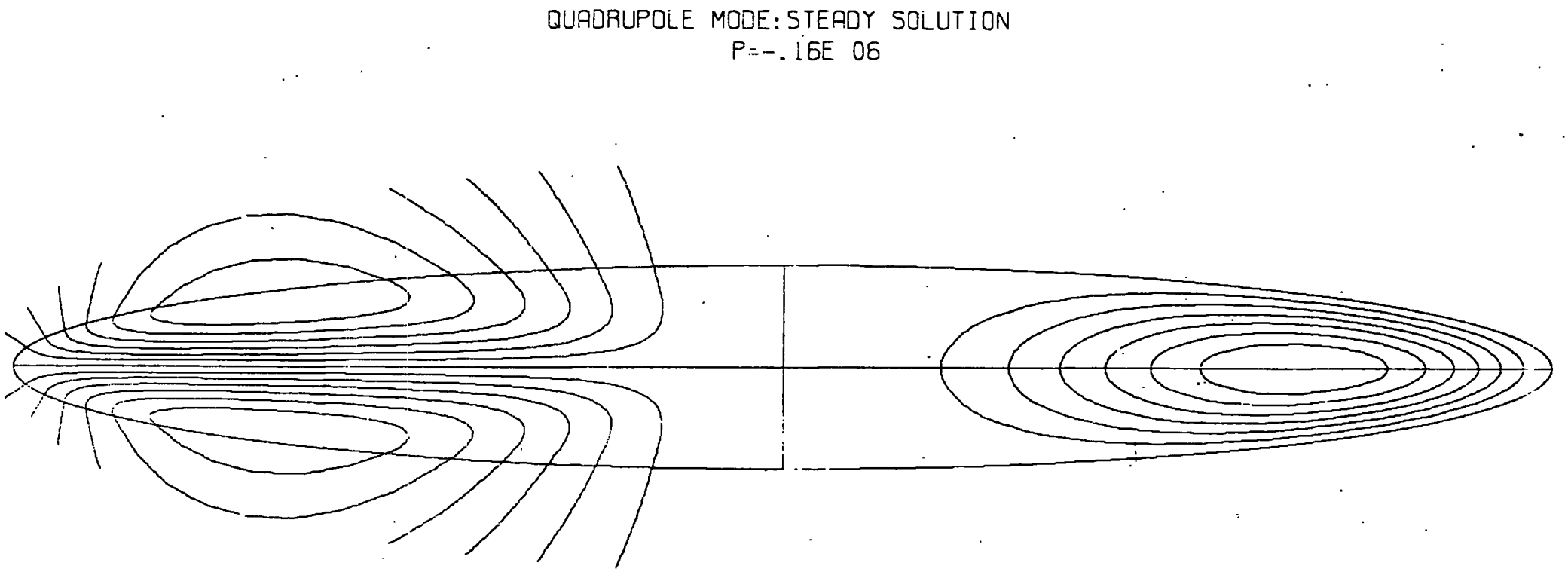

FIG 6.3

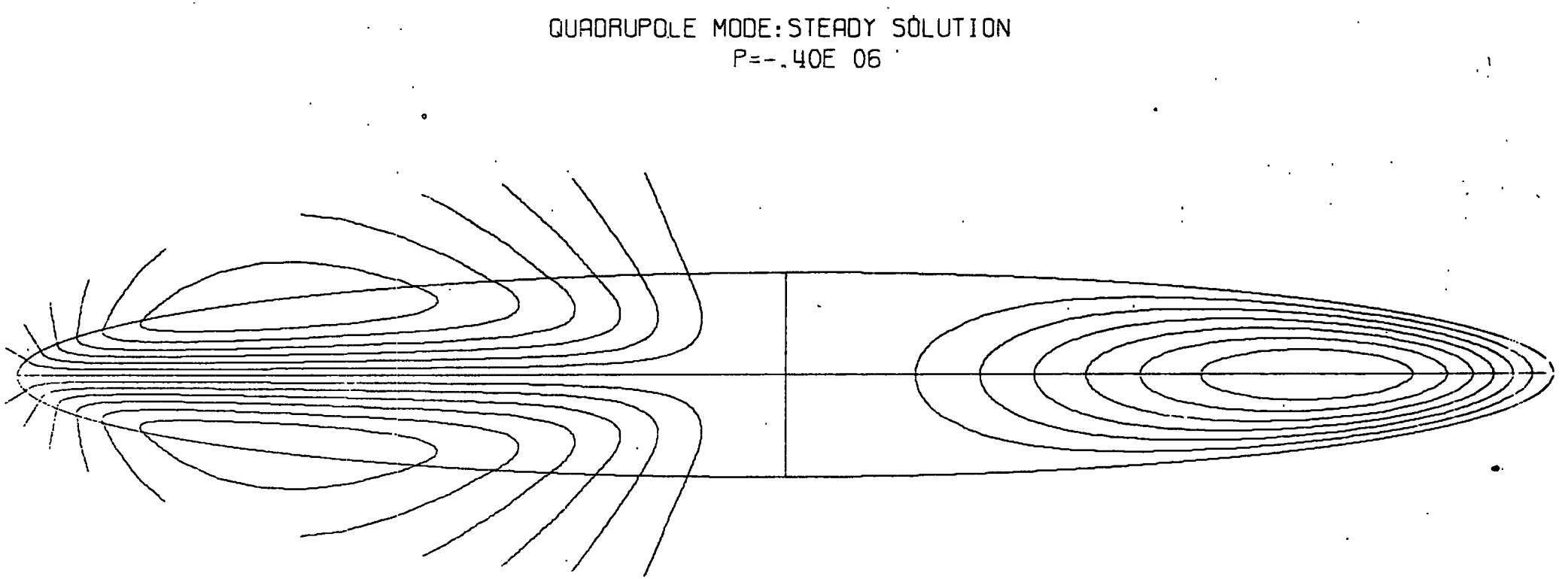

FIG 6.4

QUADRUPOLE MODE: STEADY SOLUTION
P=-.10E 08

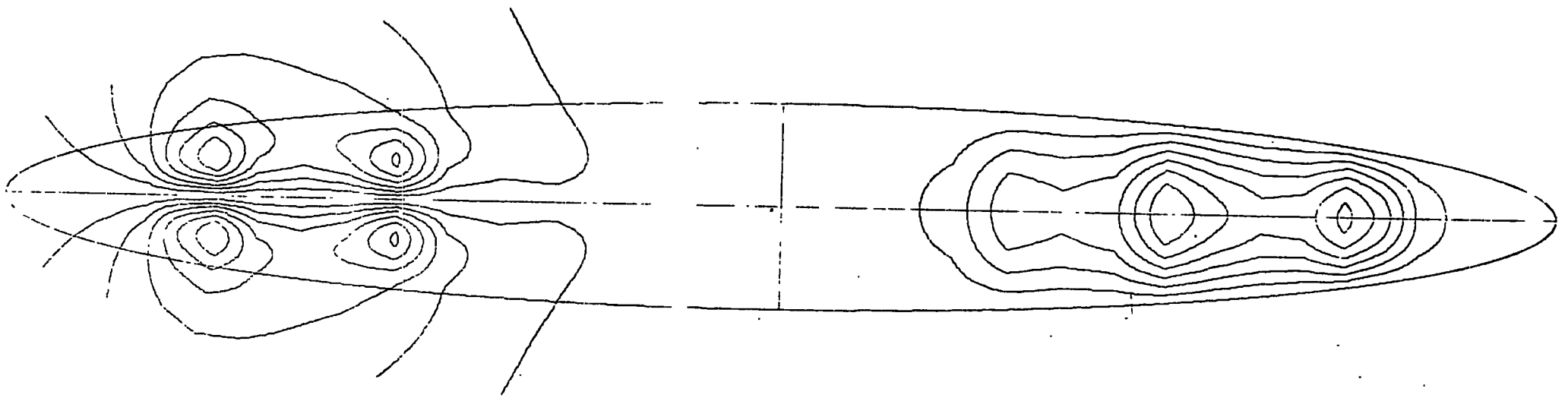

FIG 6.5

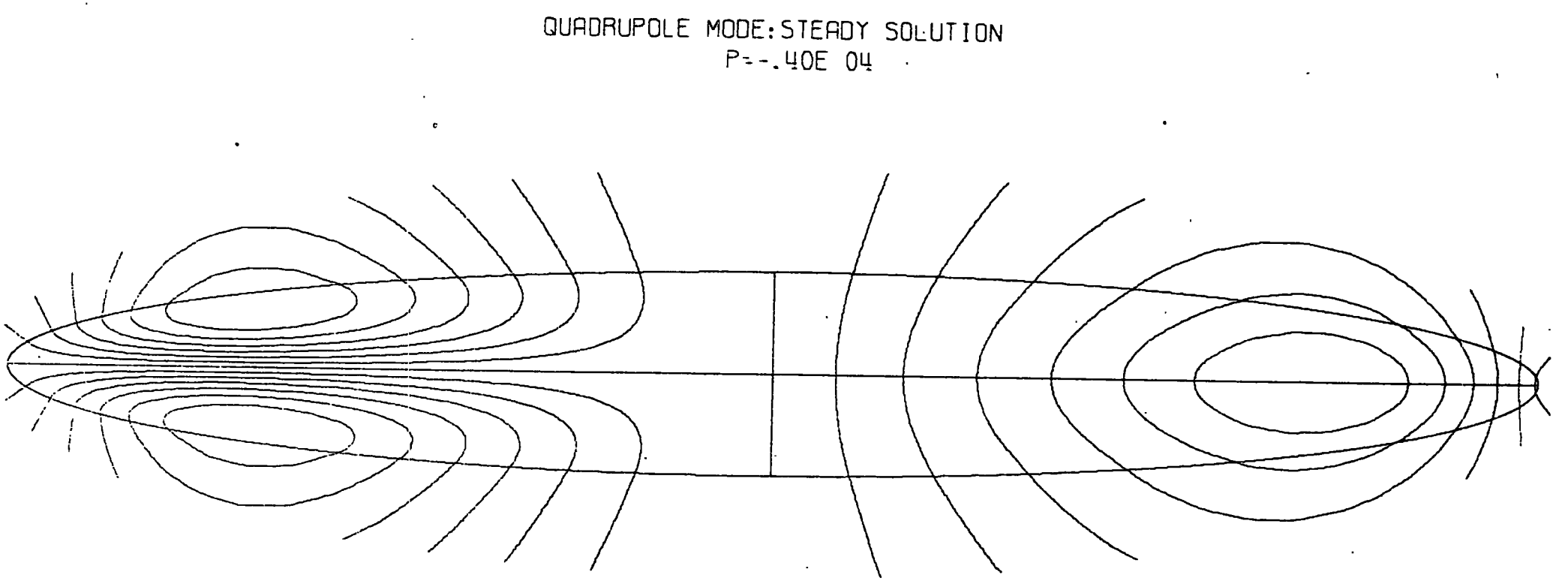

FIG 6.6

QUADRUPOLE MODE: STEADY SOLUTION
P=-.15E 05

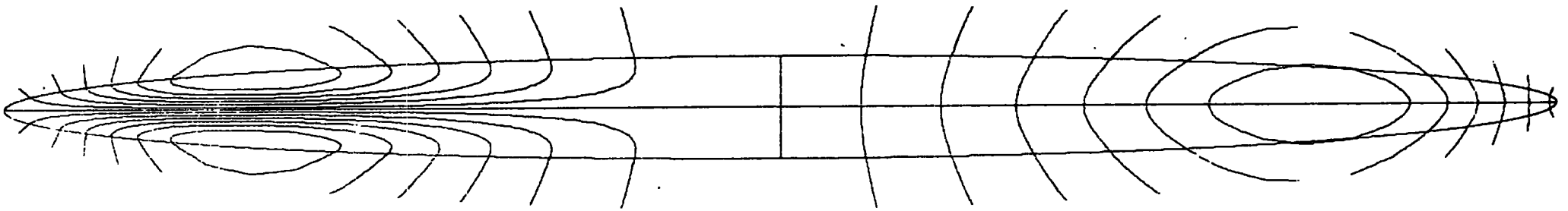

FIG 6.7

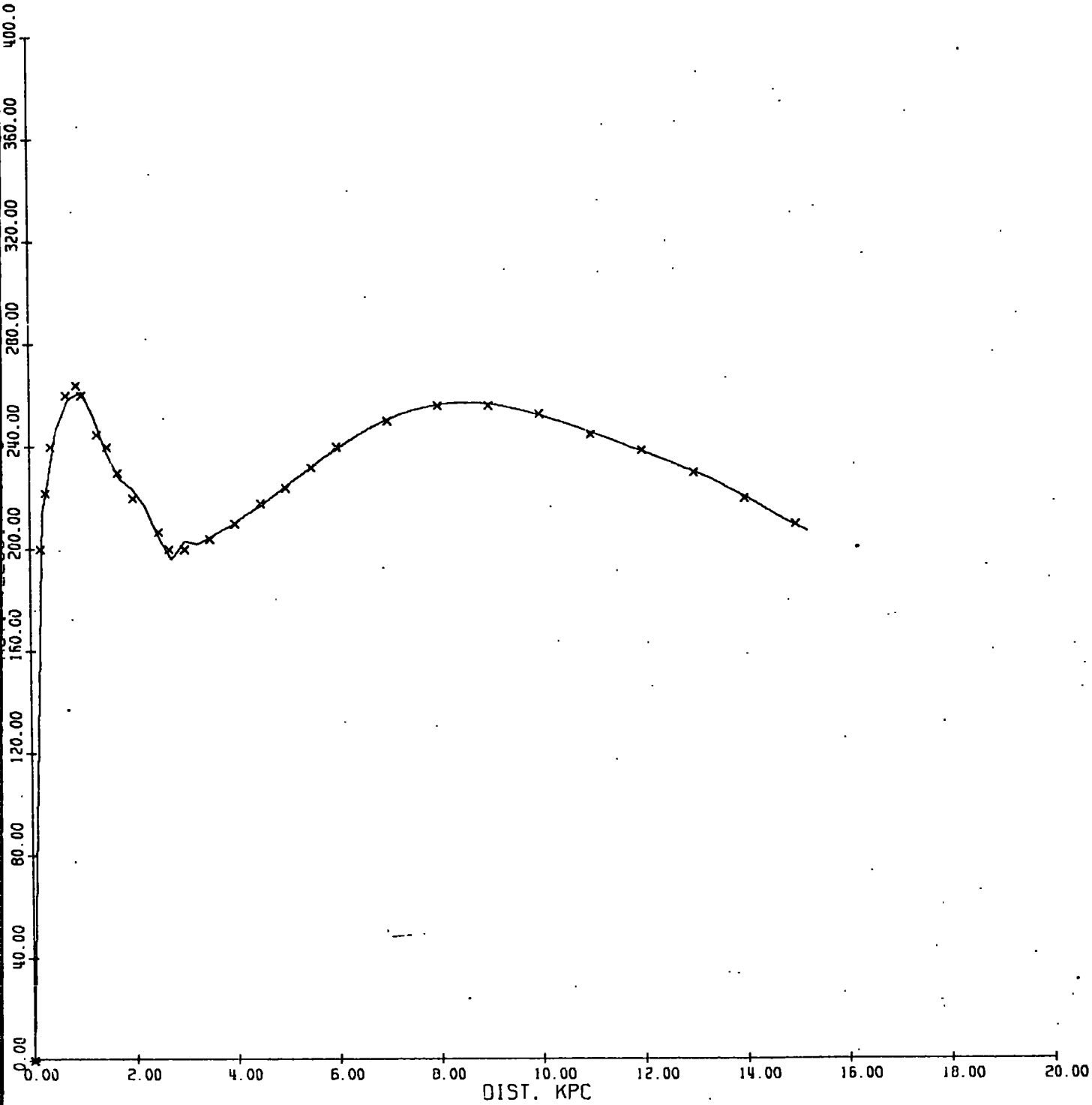
400.0
360.00
320.00
280.00
240.00
200.00
160.00
120.00
80.00
40.00
0.00
0.00
2.00
4.00
6.00
8.00
10.00
12.00
14.00
16.00
18.00
20.00
DIST. KPC

IG 6.8

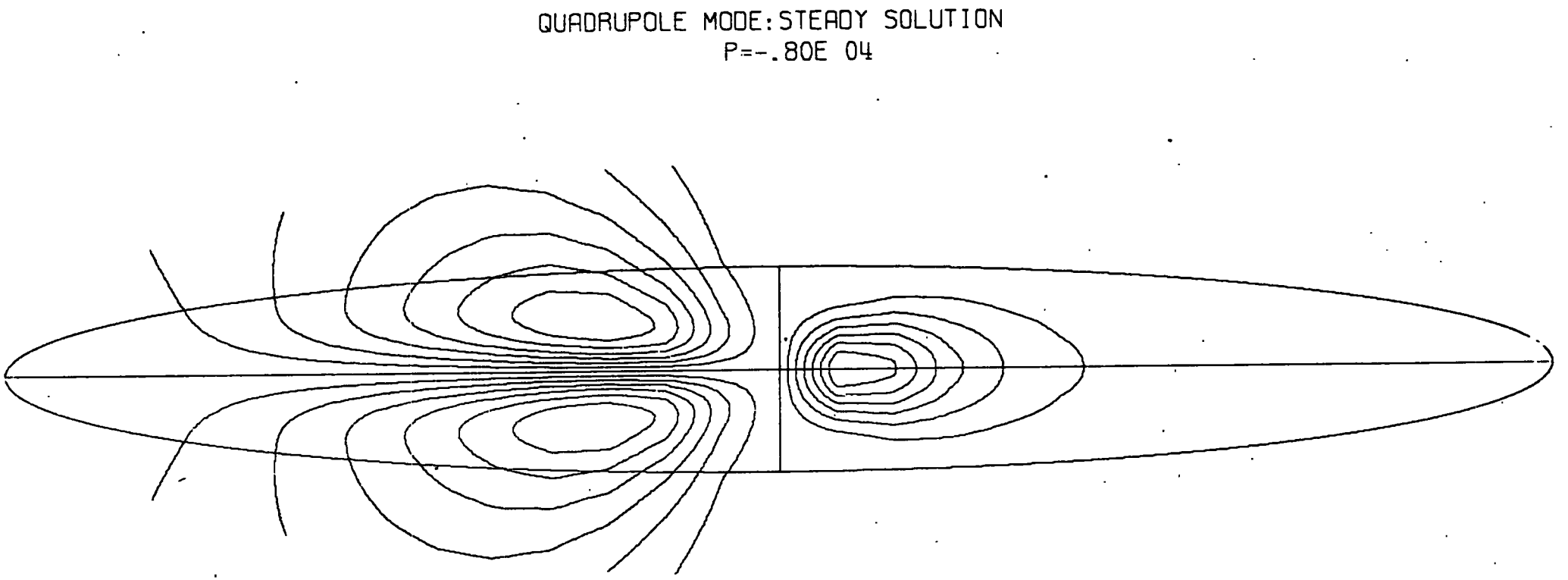

FIG. 6.9

QUADRUPOLE MODE:STEADY SOLUTION
P=-.20E 05

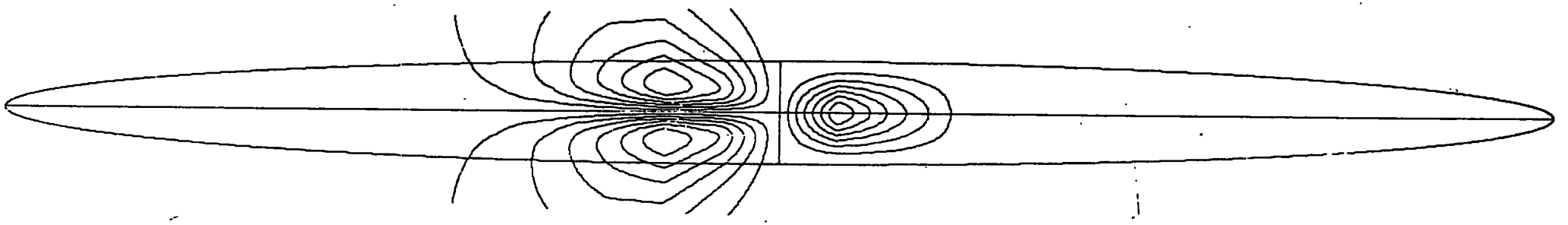

FIG 6.10

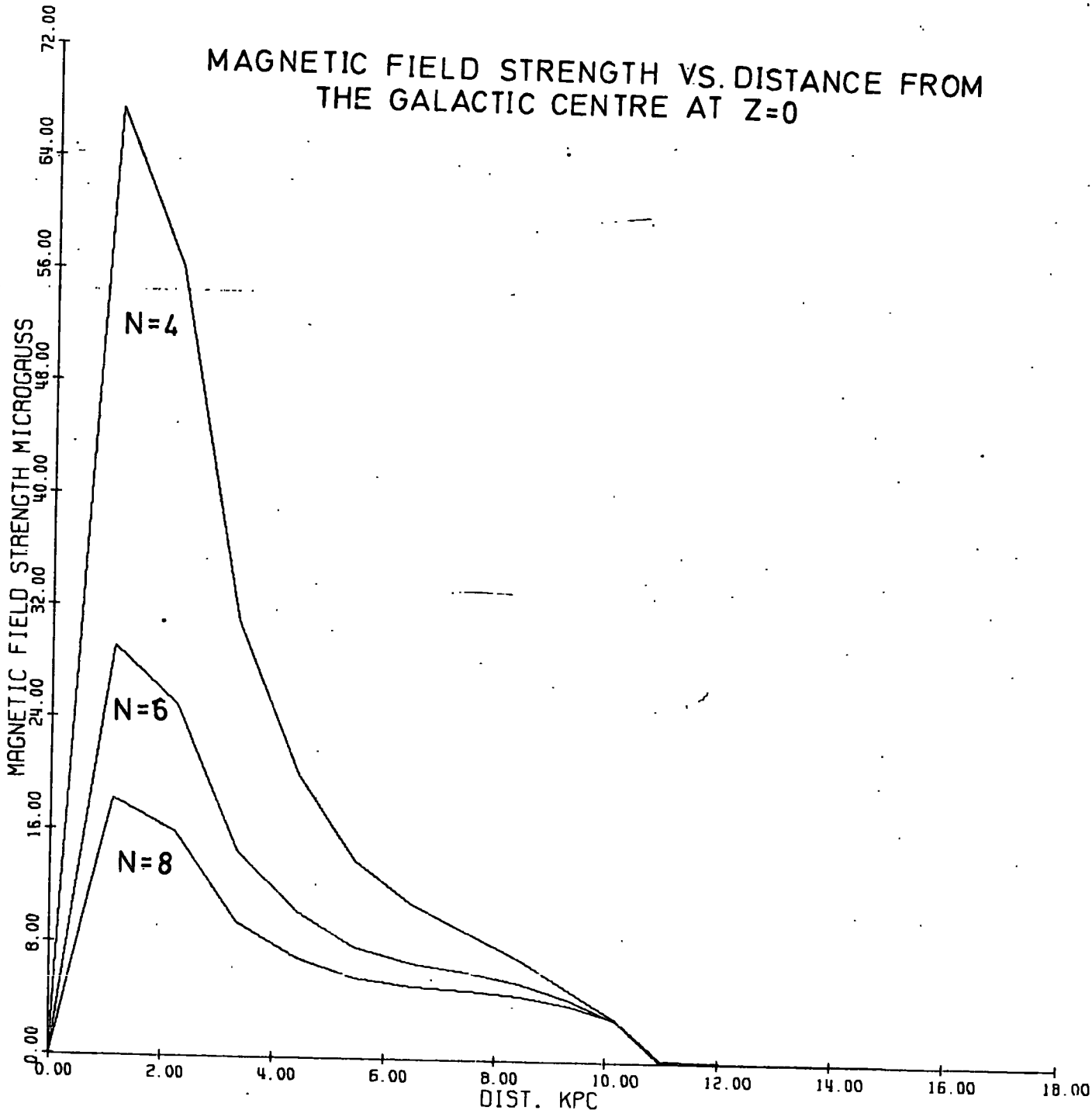
MAGNETIC FIELD STRENGTH VS. DISTANCE FROM THE GALACTIC CENTRE AT Z=0
MAGNETIC FIELD STRENGTH MICROGAUSS
72.00
64.00
56.00
48.00
40.00
32.00
24.00
16.00
8.00
0.00
N=4
N=6
N=8
0.00
2.00
4.00
6.00
8.00
10.00
12.00
14.00
16.00
18.00
DIST. KPC

FIG 6.11

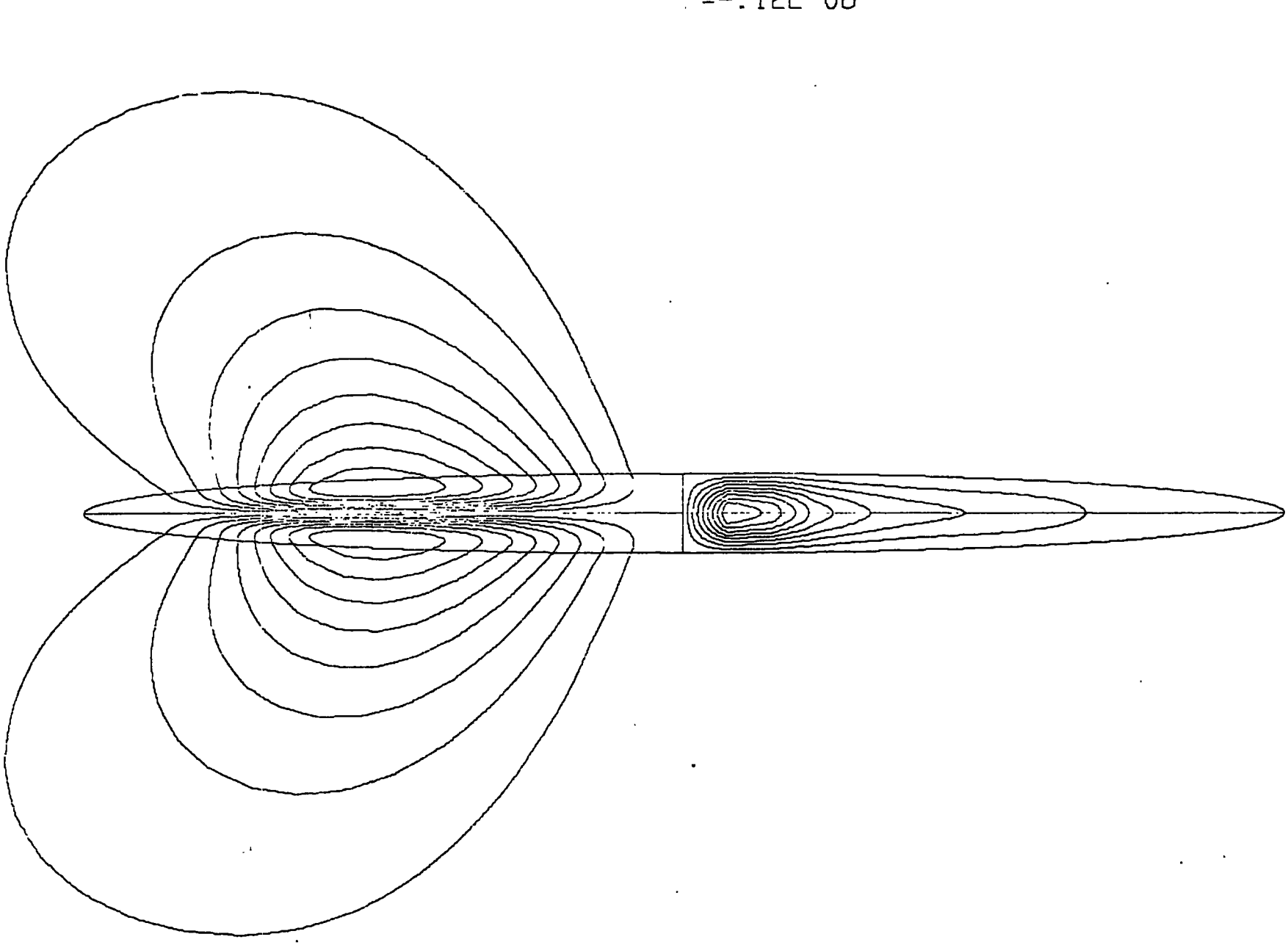

FIG 6.12

Chapter Seven. The Propagation of Ultra-High-Energy Cosmic Rays in the Proposed Field Model

7.1 Introduction

The consequences of our field model for the propagation of ultra-high energy cosmic rays are investigated by means of calculating the trajectories of particles leaving earth. This technique has previously been used by Thielheim and Langhoff (1968), and Karakula et al (1972), and Osborne et al (1973). They have considered 'conventional' field models which are characterized by a semi-empirical nature. Unlike a model predicted from the dynamo mechanism, a conventional model possesses no poloidal component.

Our model is concerned with the averaged large-scale component of the field, but the small-scale fluctuating component may also be important to the present problem. The irregularities in the Galactic magnetic field appear to be on scales ranging from 10 pc to 100 pc, which are comparable to the scales of turbulent motions. At a rigidity of 10^{18} eV a particle in a 3 μG magnetic field has a Larmor radius 300 pc. Therefore, at rigidities $\gtrsim 10^{18}$ eV it seems reasonable to neglect the effect of the small-scale fluctuating component of the field.

7.2 Calculation of Trajectories

The Lorentz force F acting on a charged particle q, moving with velocity $\underset{\sim}{v}$ in a magnetic field $\underset{\sim}{B}$ is

$$\underset{\sim}{F} = q/c(\underset{\sim}{v} \wedge \underset{\sim}{B}) \qquad (7.2.1)$$

c is the speed of light. Cgs units are used. The acceleration on the particle is given by

$$\frac{\underset{\sim}{a}}{c^2} = 9.25 \times 10^{17} (\hat{\underset{\sim}{v}} \wedge \underset{\sim}{B}) \frac{\underset{\sim}{z}}{\epsilon} \; kpc^{-1} \qquad (7.2.2)$$

where $\underset{\sim}{a}$ is the acceleration (kpc s^{-2}), c the speed of light (kpc s^{-1}), $\hat{\underset{\sim}{v}}$ the instantaneous unit velocity vector, B the magnetic field (μG), Z the atomic number, and E the energy of the energy of the particle (eV).

A simple time-stepping procedure is employed to calculate the trajectory. At the beginning of each time step the acceleration is calculated using (2). Since the acceleration is not constant during the time step an effective acceleration is calculated. This is equal to the acceleration at the mid-point of the step, and is calculated by a parabolic extrapolation using the acceleration at the two previous steps. The effective acceleration is now used to calculate the position and velocity at the end of the step. The length of the time step is reduced until the trajectory no longer depends upon it. Rounding errors can accumulate and become important if the trajectories are sufficiently lengthy. They manifest themselves through the loss of normalization of the instantaneous unit velocity vector.

The field model, described in section 6.6 spans an oblate spheroidal region whose semi-major axis is 25.8 kpc and semi-minor axis 21 kpc. It is complicated to perform the trajectory calculation in any geometry other than a Cartesian one, so we must specify the field in Cartesian co-ordinates. Components of the field are first found in cylindrical polar co-ordinates (r, ϕ, z) at each point on the oblate spheroidal grid (θ, x). We find the components of the poloidal field are

$$B_r = -\cos\theta\left(\frac{x^2+f_0^{-2}}{x^2+\cos^2\theta/f_0^2}\right)^{1/2} B_\eta + \frac{x\sin\theta}{(x^2+\cos^2\theta/f_0^2)}\, B_\xi \qquad (7.2.3)$$

$$B_z = \frac{x\sin\theta}{(x^2+\cos^2\theta/f_0^2)}\, B_\eta + \cos\theta\left(\frac{x^2+f_0^{-2}}{x^2+\cos^2\theta/f_0^2}\right)^{1/2} B_\xi \qquad (7.2.4)$$

where $$B_\eta = \frac{(x^2+f_0^{-2})}{b\,(x^2+\cos^2\theta/f_0^2)^{1/2}}\left[\frac{\partial A}{\partial x} + \frac{x\,A}{(x^2+f_0^{-2})}\right] \qquad (7.2.5)$$

and $$B_\phi = \frac{1}{b(x^2+\cos^2\theta/f_0^2)^{1/2}}\left[\frac{\partial A}{\partial \theta} + A\cot\theta\right] \qquad (7.2.6)$$

The notation has been explained in Chapter Five. The toroidal field is, of course, $B\phi$.

At the beginning of the program for calculating trajectories the field values (Br, $B\phi$, Bz) are read in for each point on the oblate spheroidal grid. During each time step of the trajectory calculation the field values are found in the following way:

(i) Given the position of the particle (x', y, z). the corresponding position on the oblate spheroidal grid (θ, x) is found from the inverse of the transformations given in section 5.2.

(ii) (Bx', By, Bz) is evaluated from the relevant (Br, $B\phi$, Bz) value

7.3 Results

The path lengths in the disk and deflections have been calculated for sets of 800 trajectories at prescribed energies. The particles (antiprotons) have been set off from earth in directions on a uniform grid in galactic co-ordinates (l^{II}, b^{II}). If it is assumed that cosmic ray sources are uniformly distributed in the disk, then the intensity of cosmic rays expected from a certain direction is proportional to the path length in the disk in that direction. Figures 7.1 to 7.3 show the path length distribution in Galactic co-ordinates for energies of 2×10^{18}, 2×10^{19}, and 10^{20} eV. The contours are equi-spaced and range typically from 1 kpc to 10 kpc in value. Figures 7.4 to 7.6 show the relevant deflections. The contour levels are marked in degrees. Even at the highest energies significant deflections occur in certain directions.

7.4 Discussion

The distribution of path lengths gives some idea of the expected anisotropies in arrival directions of particles if they are of Galactic origin.

The lack of observed anisotropies at these energies suggests that these particles, if they are protons, cannot be of galactic origin. Our result does not differ from that deduced from conventional models.

Judging from the deflections we have calculated, it would seem wiser to choose cut-offs at $E = 2 \times 10^{19}$ eV and $b^{II} = 45°$ for extra-galactic correlation searches. The deflections are somewhat larger than we have anticipated in Chapter Three. This is because of the poloidal field component of the model.

If the boundary conditions are adjusted to suit the case of a conducting intergalactic medium (section 6.5) then the stronger toroidal component of the field will penetrate the surface of the disk. For this model the deflections are much larger, so, unless the intergalactic medium is empty, the small-scale features of the distribution of the arrival directions of ultra-high-energy cosmic rays will probably give no information about their sources.

If the primary cosmic rays ($E > 10^{19}$ eV) are heavier particles (say iron nuclei) then their rigidities are $10^{17} - 10^{18}$ V. We have not ruled out the possibility that these primaries are of Galactic origin. This applies also for the conventional models.

References

Thielheim, K.O. and Langhoff, W. 1968, J. Phys. A: Gen Phys, 1, 694

Karakula, S. et al, 1972 J. Phys. A: Gen Phys, 5 904

Osborne, J.L. et al 1973 J. Phys. A: Math Nucl. Gen. 6 421

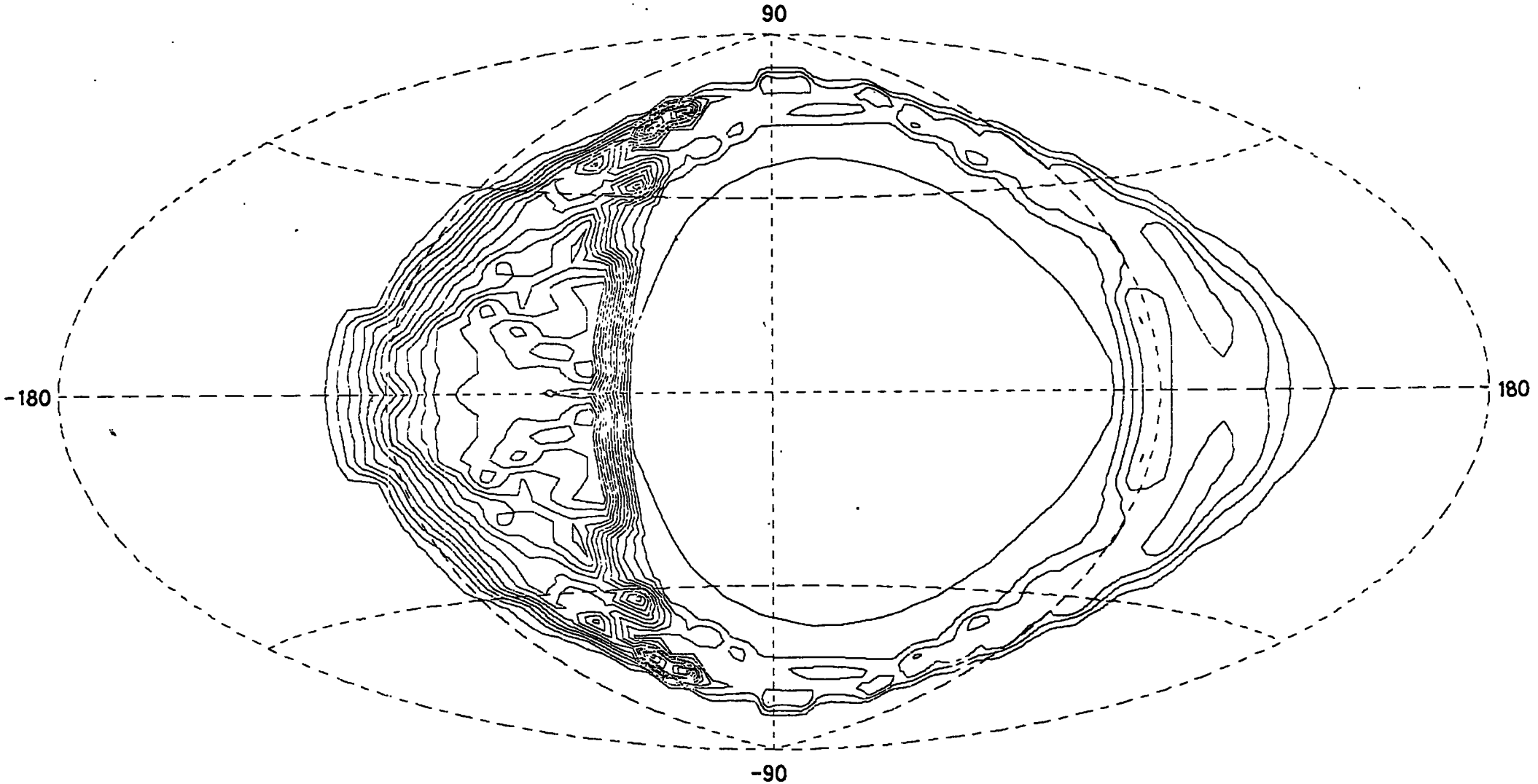

FIG 7.1

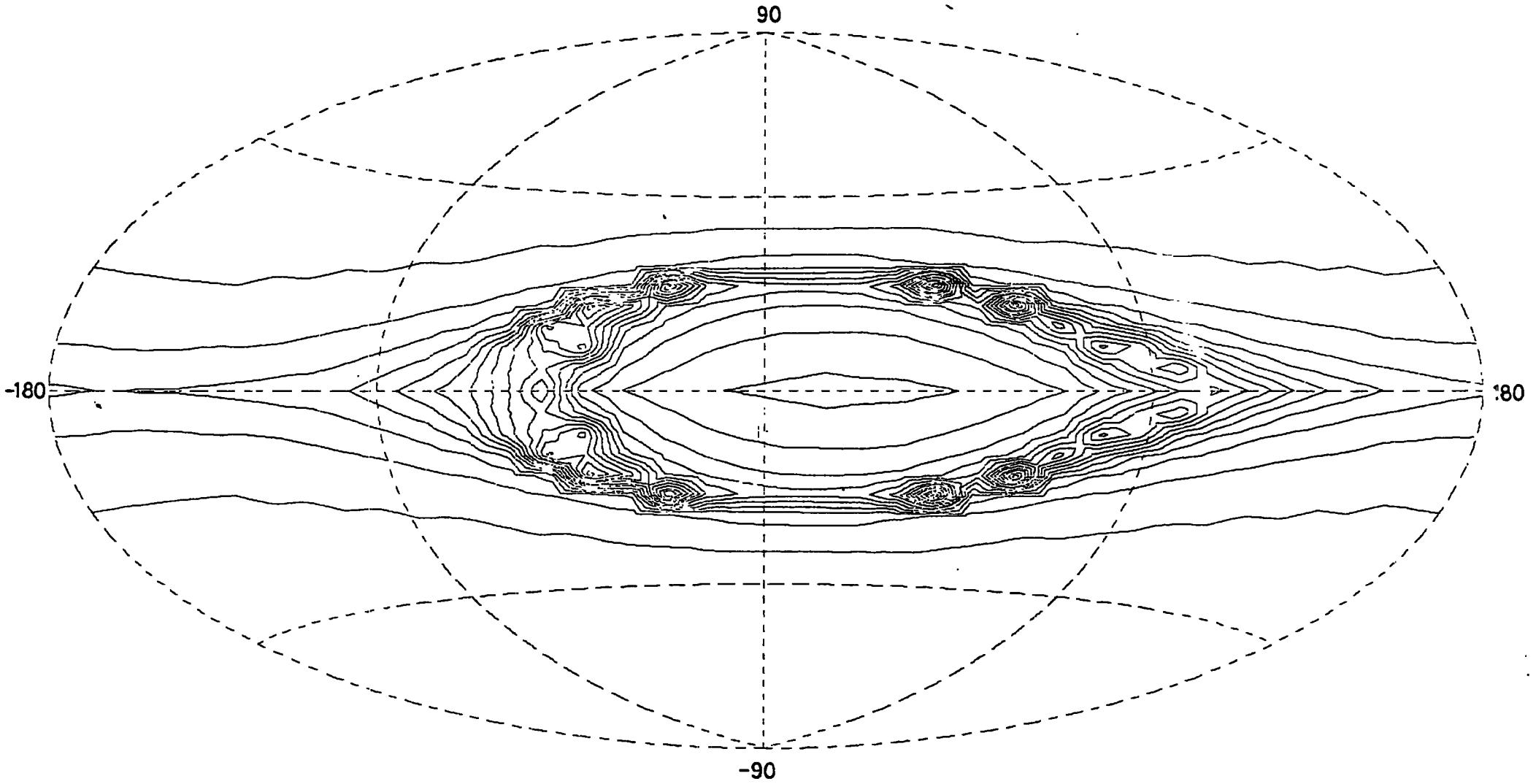

FIG 7.2

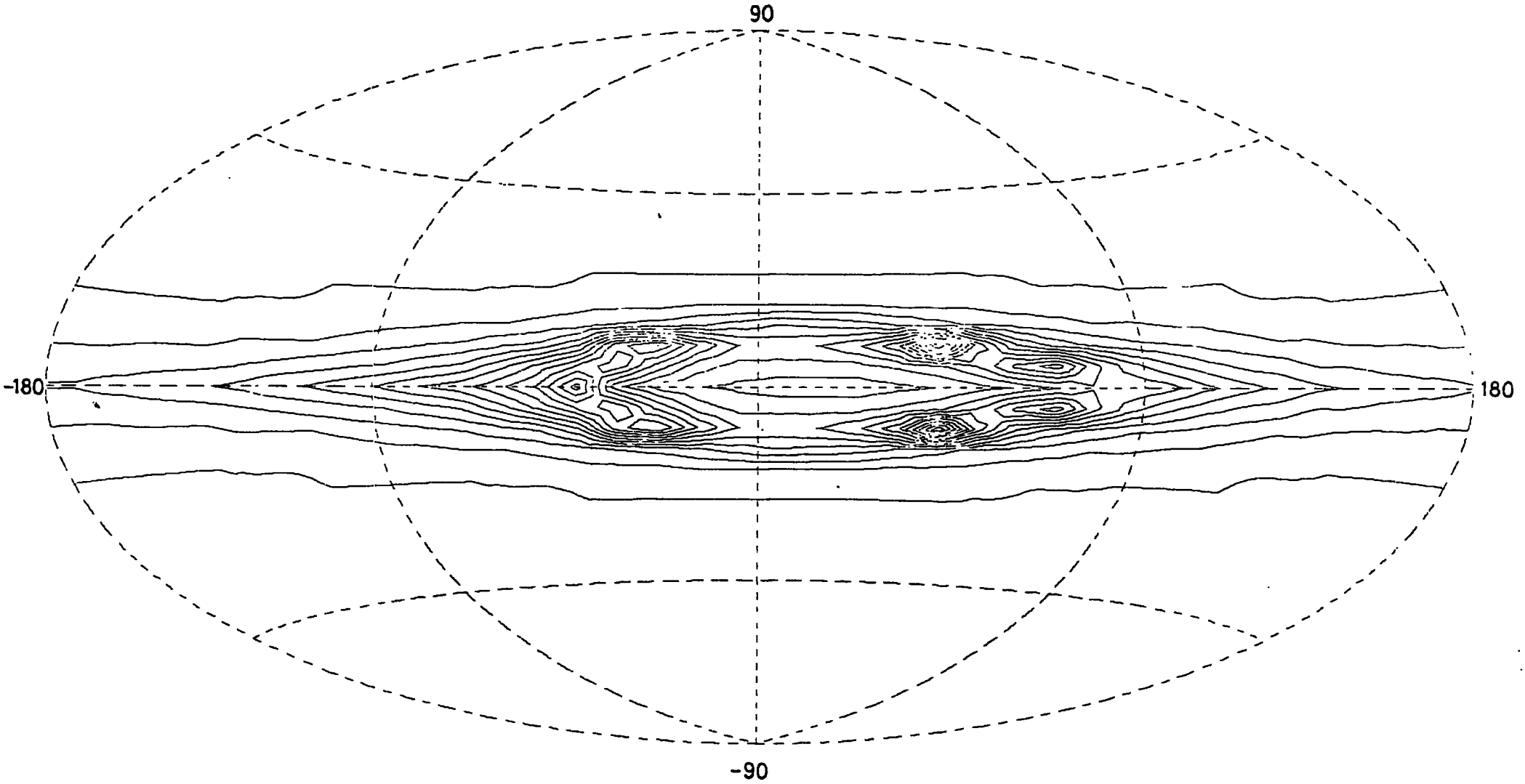

FIG 7.3

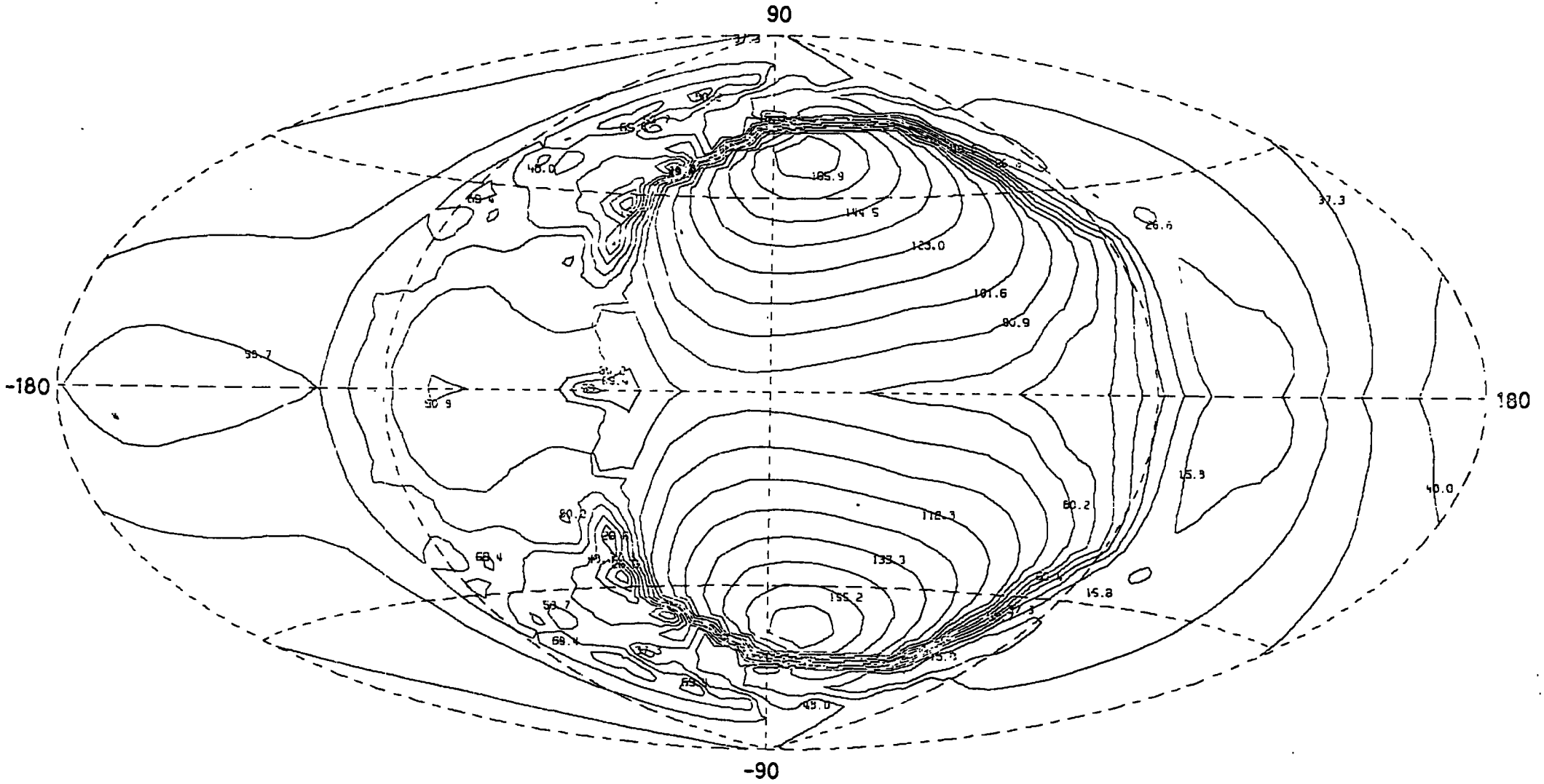
90
-180
180
-90
185.9
144.5
123.0
101.6
80.9
59.7
50.9
118.3
133.3
155.2
80.2
60.2
15.8
15.5
26.6
37.3
40.0
45.0

FIG 7.4

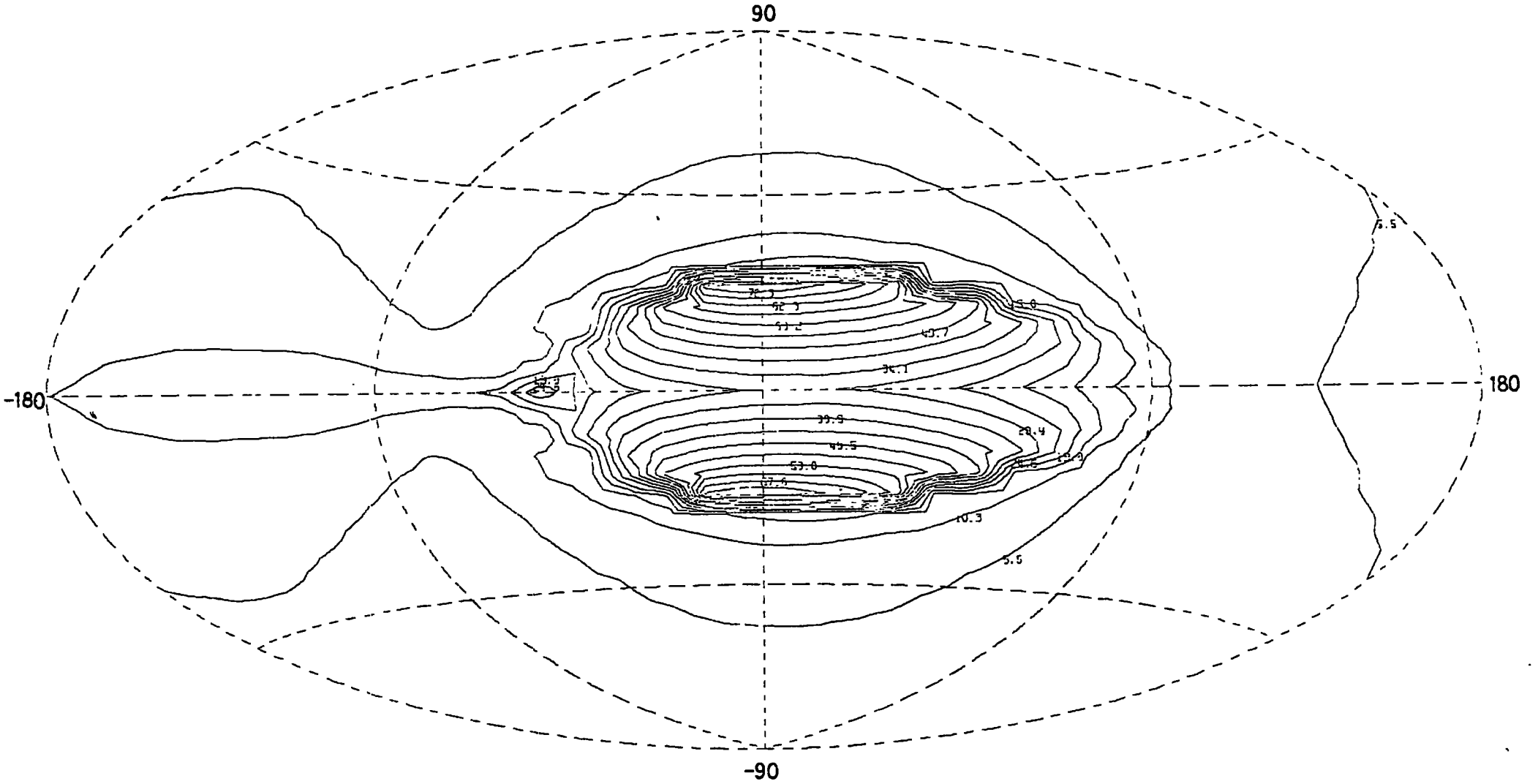

FIG 7.5

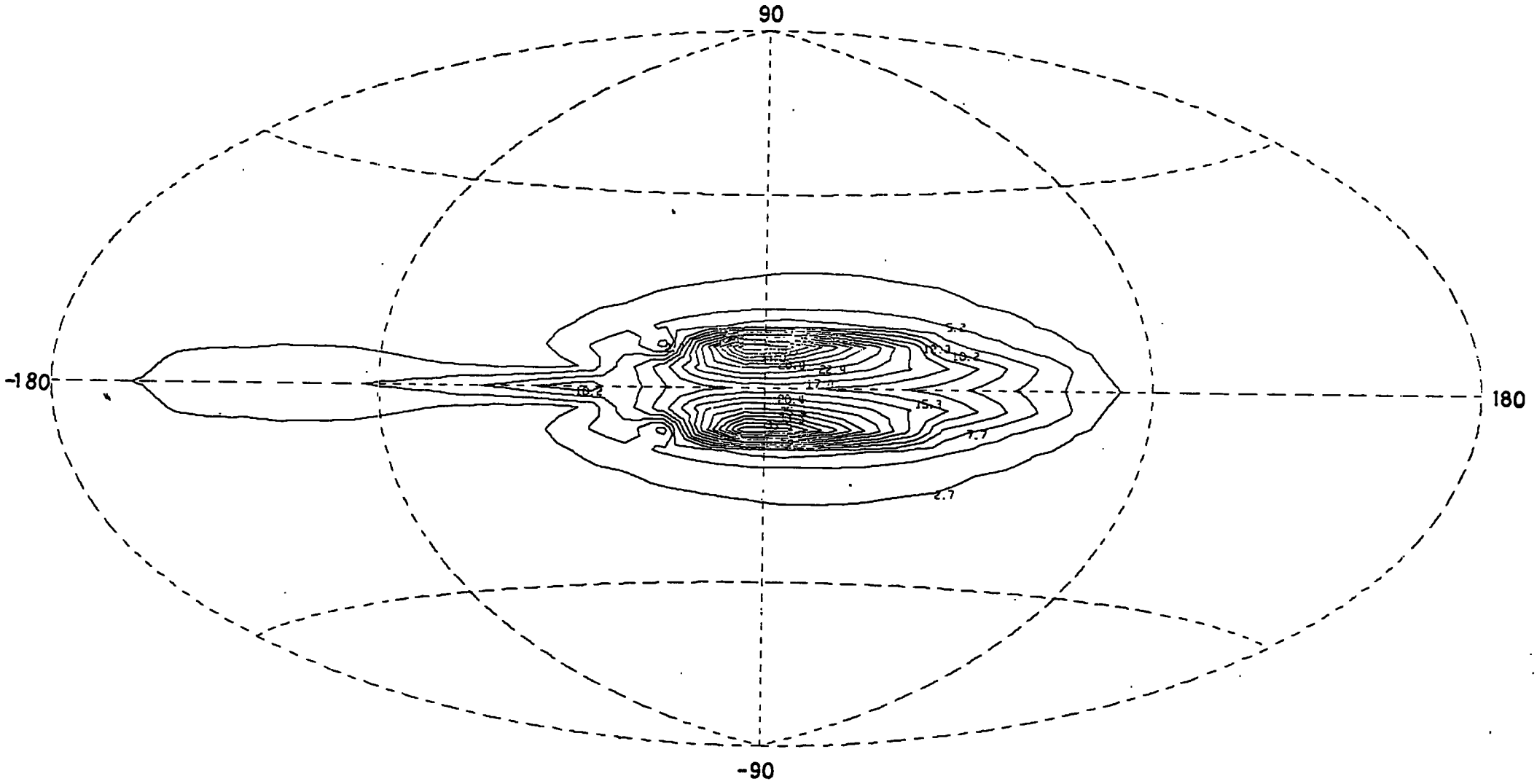

FIG 7 S

Chapter Eight. Comparison with Observations

8.1 Introduction

Synchrotron radiation is emitted wherever an electron having a relativistic velocity encounters a magnetic field. The emission for an ensemble of electrons is

$$\epsilon \propto \int n_e B_\perp^{(\gamma+1)/2} dl \qquad (8.1.1)$$

where the integral is along the line of sight γ is the spectral index of the differential energy spectrum of the relativistic electrons. $B_\perp$ is the magnetic field strength perpendicular to the line of sight. A complete treatment of the subject is given by Pacholczyk (1970).

In galaxies the sources of relativistic electrons are very probably encountered in the galactic plane and perhaps towards the galactic centre. If the propagation of the electrons is by some effective diffusion mechanism or by a combination of diffusion and convection one would expect that the electron density, n_e , would fall off towards the edges of the galaxy and that, because their rate of energy loss increases with energy, their energy spectrum would be steeper in the outer parts. For simplicity in the present comparison we take n_e and γ as constant, the latter being set equal to 2.8 in agreement with the mean spectral index of the overall continuum emission from spiral galaxies. Our results will represent, therefore, upper limits to the extent of the synchrotron radiation from galaxies.

Comparison will be made with two field models:

(a) the model used in Chapter Seven, which is characterized by ... empty intergalactic medium,

(b) the model which has a conducting intergalactic medium, and has been described in Chapter Six.

Figure 8.1, which shows the field model for (b) can be compared with Figure 6.11, which shows the field model for (a). For model (b) the diffusivity of the intergalactic medium is the same as the galaxy, and is $\sim 10^{26}$ cm^2 s^{-1}. No turbulent motions are prescribed outside the galaxy so this diffusivity is of an ambipolar nature. Noting that the ambipolar diffusivity of the interstellar medium is $\sim 10^{22}$ cm^2 s^{-1}, where the density of ionized matter (protons or electrons) is 10^{-1} -10^{-2} cm $^{-3}$ (Bridle and Venugopal, 1969) one expects a density 10^{-5} -10^{-6} cm^{-3} to be appropriate for the intergalactic medium of model (b). The critical density required to close the universe (for a Hubble constant Ho = 50 km s^{-1} Mpc) is $\sim 10^{-5}$ cm^{-3}.

8.2 Calculation of the Synchrotron Radiation

The calculation for the emission expected within the Galaxy is first described. Taking a direction (l^{II}, b^{II}) in Galactic co-ordinates, the unit vector, $\hat{\underset{\sim}{a}}$, along the line of sight is

$$\hat{\underset{\sim}{a}} = (-\cos l^{II} \cos b^{II}, -\sin l^{II} \cos b^{II}, \sin b^{II}) \qquad (8.2.1)$$

This is for a right-handed Cartesian co-ordinate system. Note that

$$B_\perp = B \sin\phi = |\hat{\underset{\sim}{a}} \wedge \underset{\sim}{B}| \qquad (8.2.2)$$

where ϕ is the angle the magnetic field vector mades with the line of sight. Let $\underset{\sim}{x}_e$ be the position vector of the earth. The position vector of a point at a distance l along the line of sight is

$$\underset{\sim}{r} = \underset{\sim}{x}_e + l\,\hat{\underset{\sim}{a}} \qquad (8.2.3)$$

The manner in which the field is specified in Cartesian co-orindates has already been described in Section 7.2.

$B_\perp$ can be calculated at each point along the line of sight and the integral evaluated numerically using Simpson's rule. The region which the field occupies has also been described. By evaluating the integrals for slightly smaller regions the convergence of their values can be tested. It was found that the results do not depend upon the extent of the region used.

For the calculation of the emission from the external galaxy the situation is more straightforward: integrals are evaluated along the lines of sight in the (θ, x) plane. As a check upon the calculations the emission from the line of sight through the galactic centre can be compared for the Galaxy and an external galaxy. Both should, of course, be the same, apart from small differences arising from the emission in the anticentre for the Galaxy. This is found to be the case. A step length of 0.1 kpc was used for all the integrations.

8.3 Comparison with the Synchrotron Radiation of the Galaxy

The survey map of the synchrotron radiation of the Galaxy at 150 MHz is shown in figure 8.2 (Landecker and Wielebinski, 1970). The emissions expected from models (b) and (a) are shown also upon a sinusoidal projection of the entire sky in figures 8.3 and 8.4. Galactic co-ordinates are used and each projection employs the same phase convention, which is set up in figure 8.2. The field models have been normalized to 3 μG at earth, but the emission is not normalized. The constants of proportionality for conversion of the predicted results to brightness temperature depends upon the frequencies of observation. The conversion factors, by which the emission for the predictions is multiplied, are quoted for relevant frequencies in table 8.1. These results follow from formulae appearing in Felten and Morrison (1968). The value of the electron flux (Io) has been taken as a constant, and equal to the observed value at earth ($80\ E^{-2.8}\ m^{-2}\ st^{-1}\ s^{-1}\ Gev^{-1}$)

TABLE 8.1

Frequency MHz	Conversion Factor ^{o}K/contour unit
150	2.5
610	4.3×10^{-2}
1415	3.7×10^{-3}

The most striking feature of the predictions is their lack of symmetry about the plane perpendicular to the equator at the Galactic centre. Individually the toroidal and poloidal components of the fields give rise to a symmetric contribution, but the combined contribution is asymmetric. In model (b), where the toroidal field penetrates the surface of the disk, the degree of asymmetry is less than in model (a). This is because the role of the toroidal field is more dominant in model (b) than model (a). The observations also show some asymmetry, but this may be understood in terms of spiral structure. In particular the observations in the plane show more emission at $l^{II} = 90^{o}$ (spiral in) than $l^{II} = 270^{o}$ (spiral out) but the converse is true for the models.

In view of the probable dependence of the disk emission upon spiral structure and the dependence of the predictions upon the model parameters, such as distributions of $\tilde{\eta}$ and $\tilde{\alpha}$ and the factor by which turbulence is suppressed, it is not realistic to make a detailed comparison. However, for the emission at high latitudes the situation is more favourable. The contribution predicted from the fields outside the disk depend upon their potential nature, being largely independent of the model parameters.

The fall-off in emission with Galactic latitude at $l^{II} = 0$ is faster for model (a), but slower for model (b), than for the observations. This suggests that it is not possible to account for the observed high latitude emission if the intergalactic medium is empty. The contribution from the disk component does, of course, confuse the situation somewhat, but by comparing with the observations of external galaxies one can overcome this difficulty.

8.4 Comparison with the Synchrotron Radiation from External Galaxies

Observations of five edge-on galaxies (NGC 891, 4631, 4244, 4565 and 5907) have been made by Ekers and Sancisi (Sancisi, private communication, October 1975). The two which are of the greatest interest are NGC 891 and 4631. They have been studied at 6 cm and 21 cm with resolutions of 8" and 30". The others have been studied only with the lower resolution of 1' so it is not possible to make comparisons. Figure 8.5 shows the observed map of NGC 4631 at 610 MHz, which has been redrawn from results communicated by Sancisi. Figure 8.6 is taken from Sancisi et al (1974) and shows the observed emission for NGC 891. Naturally one must make the assumption that these galaxies are very similar to our own. This is probably a good assumption for NGC 891 but more doubtful for NGC 4631, since there appears to be some evidence for tidal interaction of this galaxy with a neighbouring one (Baldwin, personal communication, November 1976).

The emissions expected from models (a) and (b) are shown in figures 8.7 and 8.8 respectively. Equispaced logarithmic contours are plotted in each case. The conversion factors relevant for the observations of NGC 4631 (at 610 MHz) and NGC 891 (at 1415 MHz) appear in table 8.1. The observed and predicted profiles for both galaxies and models are compared in figure 8.9.

The slight asymmetry in the observations above and below the plane may be of an instrumental origin. The predicted profiles have been convolved with Gaussians of half-widths .4 kpc and 2.4 kpc which are appropriate to the resolution of NGC 891 and 4631 respectively. The curves in each case have been normalized to the same maximum value.

The predicted profile for model (a) falls off considerably more rapidly than the observed profile for NGC 891. The situation is not so clear for NGC 4631 where the resolution is poorer. In view of the poorer resolution for NGC 4631 and complications arising from the possible gravitational interaction of this galaxy, it is wiser to base conclusions upon the comparisons with NGC 891. For model (b) the predicted profile falls off less rapidly than the observed profiles for both galaxies. These findings reinforce the suggestion made earlier on the difficulty of accounting for the observed high-z emission in terms only of a poloidal potential field. It is emphasized that the potential nature of this field primarily determines the fall-off, and its strength, which is model dependent, is not so important.

8.5 Discussion

Before summarizing the results of the comparisons some remarks are made concerning the problem of intergalactic gas. Field (1974) has reviewed the evidence for an intergalactic gas. Several rich clusters of galaxies (e.g Coma) have been found to be x-ray sources. If the emission mechanism is thermal bremsstrahlung (TB) then the observations give positive evidence for an intracluster gas (ICG). The x-ray data for Coma are consistent with TB from an ICG having $T = 0.9 \times 10^8$ K and mass $(2\text{-}5) \times 10^{14}$ $M_\odot$. This mass of gas is not sufficient to resolve the virial mass discrepancy of the cluster.

Observations of the diffuse x-ray background are sensitive to gas with $T = 10^6 - 10^{10}$ K. Silk and Tarter (1973) have predicted the contributions of clusters to the diffuse x-ray background and have tentatively concluded that the de Vaucouleurs' groups of galaxies (de Vaucouleurs, 1976) should be TB x-ray sources with $T = 10^5$ K to 10^7 K, containing sufficient ICG to bind the groups and close the universe. Field has suggested that a decisive test would be the observations of soft x-rays from such groups. If the temperature of the ICG is somewhat lower say $T = 10^4 - 10^6$ K, then the TB would be between 1 eV and 100 eV, which is a difficult region to observe, since the lower end is obscured by starlight, and the upper end by interstellar absorption.

The galaxies we have discussed are members of nearby de Vaucouleurs' groups. It is of some interest to note that model (b) which can be interpreted as having the galaxy surrounded by ionized intergalactic hydrogen (density $10^{-5} - 10^{-6}$ particles cm^{-3}) accounts for the high-z synchrotron emission observed in some galaxies. It is not difficult, however, to construct models which agree with observations. We have assumed a constant relativistic electron density throughout the entire region considered, so the results of the comparison with NGC 891 (figure 8.9) places an upper limit on the way this electron density must fall off in order to obtain agreement. This probably casts doubt on the realism of model (b). The ionized gas surrounding the galaxy is envisaged to be in hydrostatic equilibrium, thermal pressure maintaining the gas against gravitational collapse. Dynamic effects may play an important role here, the gaseous disk of the galaxy being inflated by cosmic ray pressure, and perhaps a galactic wind blowing fields and matter outwards.

One may also expect the fields to influence the motions of a very tenuous intergalactic gas. By introducing a diffusion mechanism for the relativistic electrons in model (b) it is possible that some conflict would arise between the predictions and observations. Given this, it would then be necessary to try and include the more complicated dynamic effects we have mentioned.

References

Bridle, A.H. and Venugopal, V.R. 1969 Nature 224 No 5219 545

Felten, J.E. and Morrison, P.M. 1968 Ap J 146 686

Field, G.B. 1974 IAU Sym 63, 13 "Confrontation of Cosmological Theories with Observation"

Landecker, J.L. and Wielebinski, R. 1970 Aust J Phys Astrophys Suppl 16 1

Sancisi et al 1974 Preprint University of Groningen

Silk, J. and Tarter, J. 1973 Astrophys J 183 387

de Vaucouleurs 1976 Stars and Stellar systems Vol IX 557 "Galaxies and the Universe" Ed by Sandage, A. et al

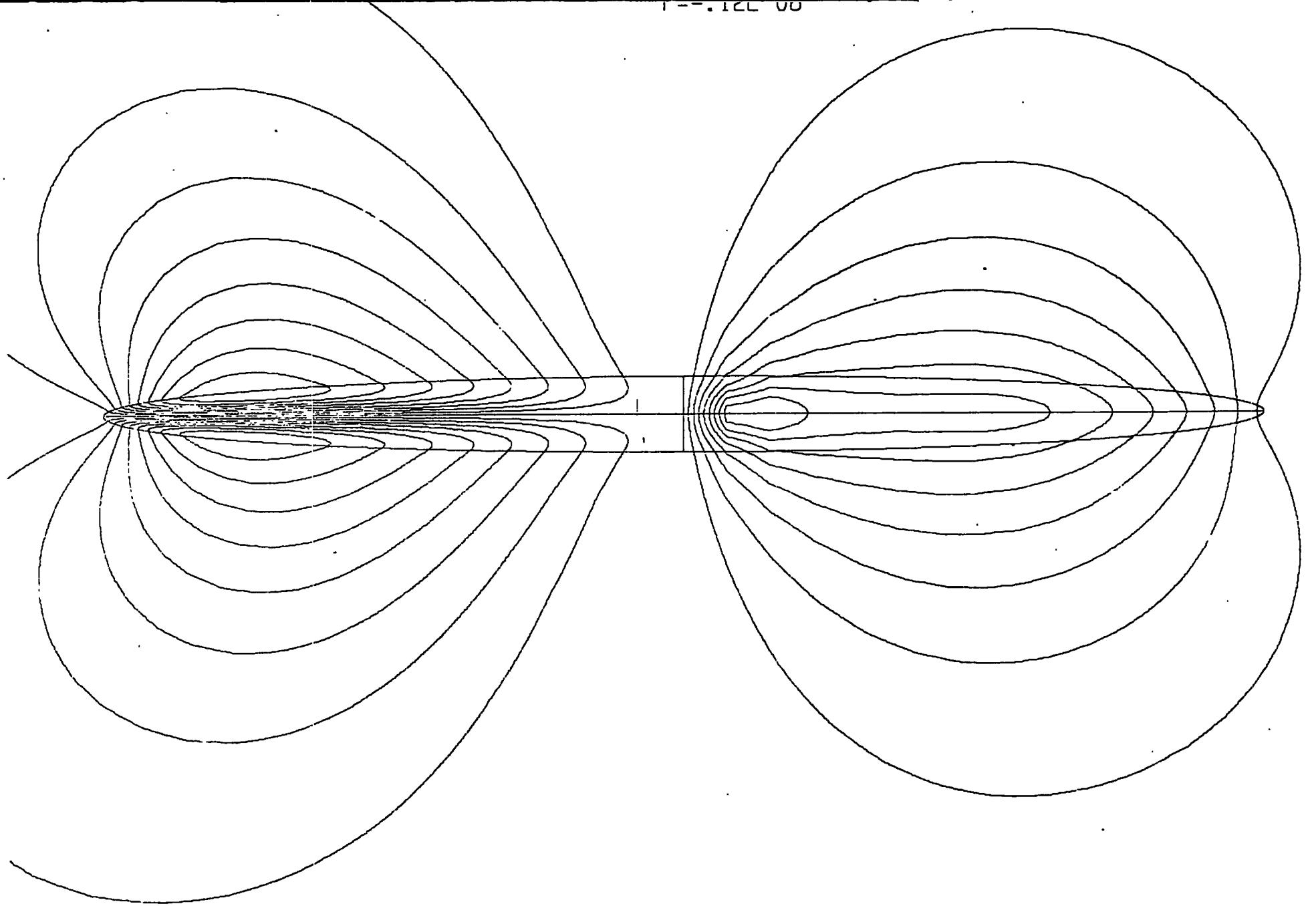

FIG 8.1

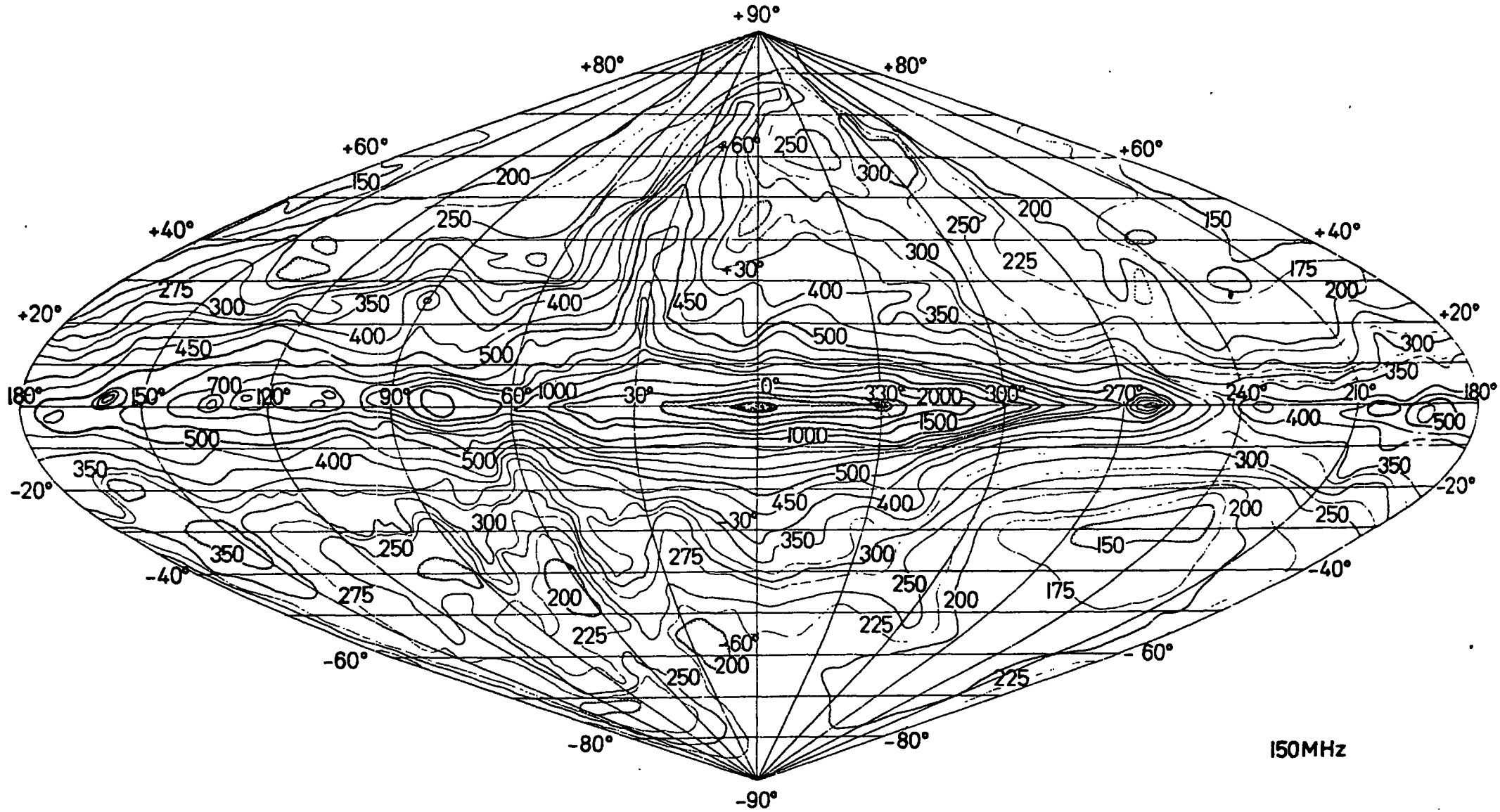
+90°
+80°
+80°
+60°
+60°
+60°
+40°
+40°
+30°
+20°
+20°
180°
150°
120°
90°
60°
30°
0°
330°
300°
270°
240°
210°
180°
-20°
-20°
-40°
-40°
-60°
-60°
-80°
-80°
-90°
150
200
250
300
225
175
275
350
400
450
500
700
1000
2000
1500
150MHz

FIG 8.2

Synchrotron emission for the galactic dynamo model (b)

Contour level incremental factor = 1.25

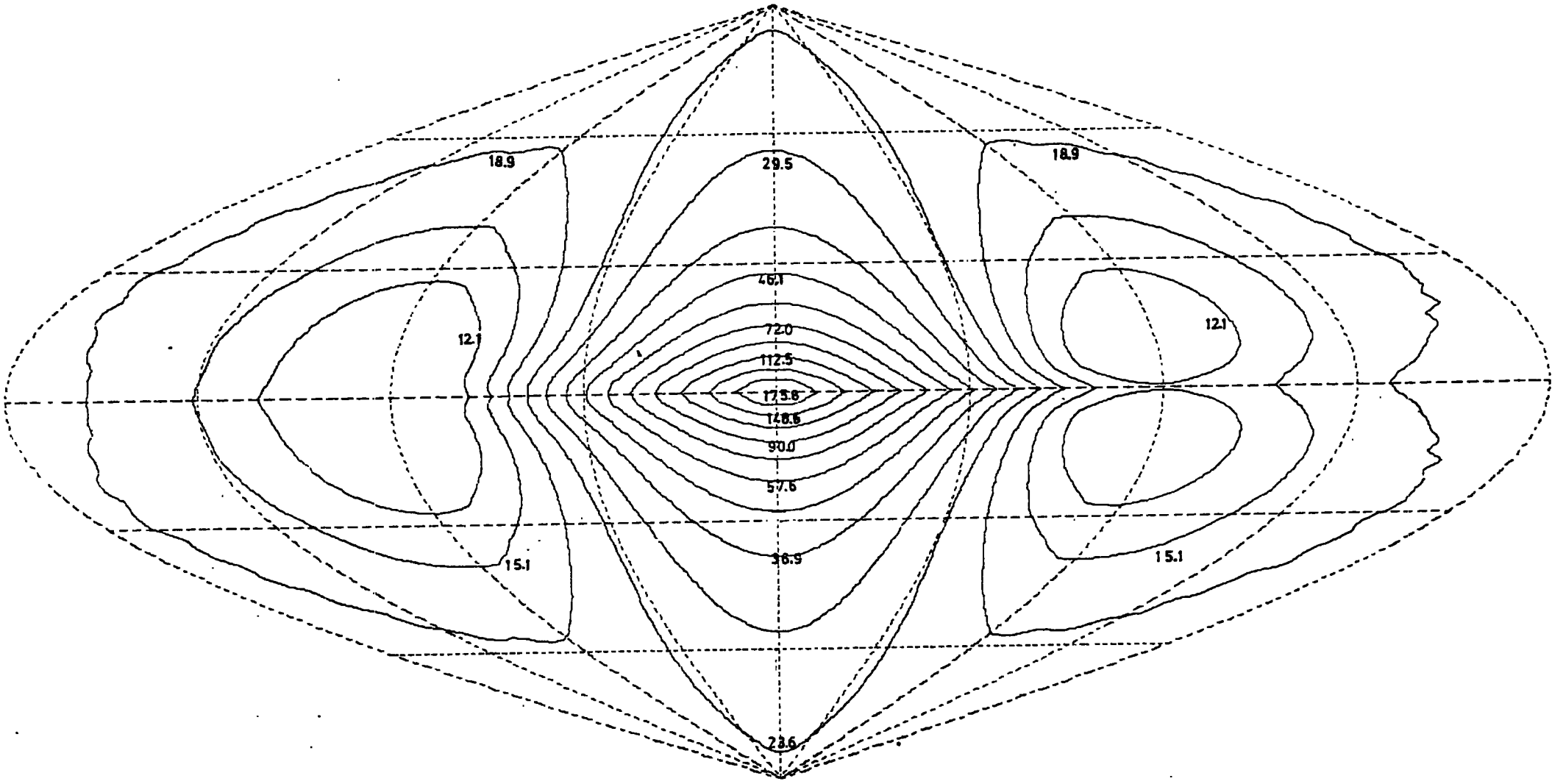

FIG 8.3

Synchrotron emission for the galactic dynamo model (a)

Contour level incremental factor = 1.5

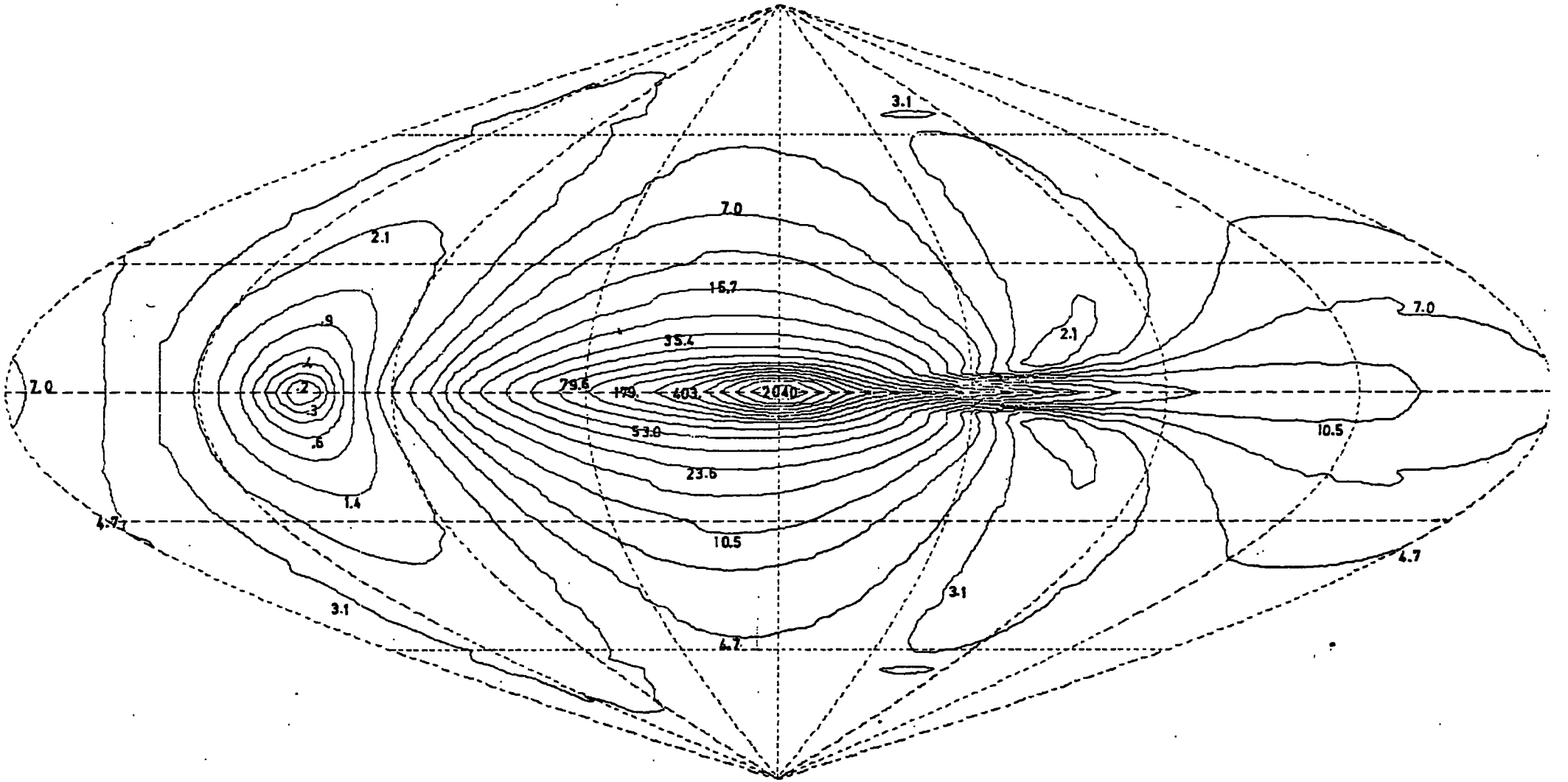

FIG 8.4

RADIO CONTINUUM EMISSION FOR N.G.C.4631 AT 610 MHZ

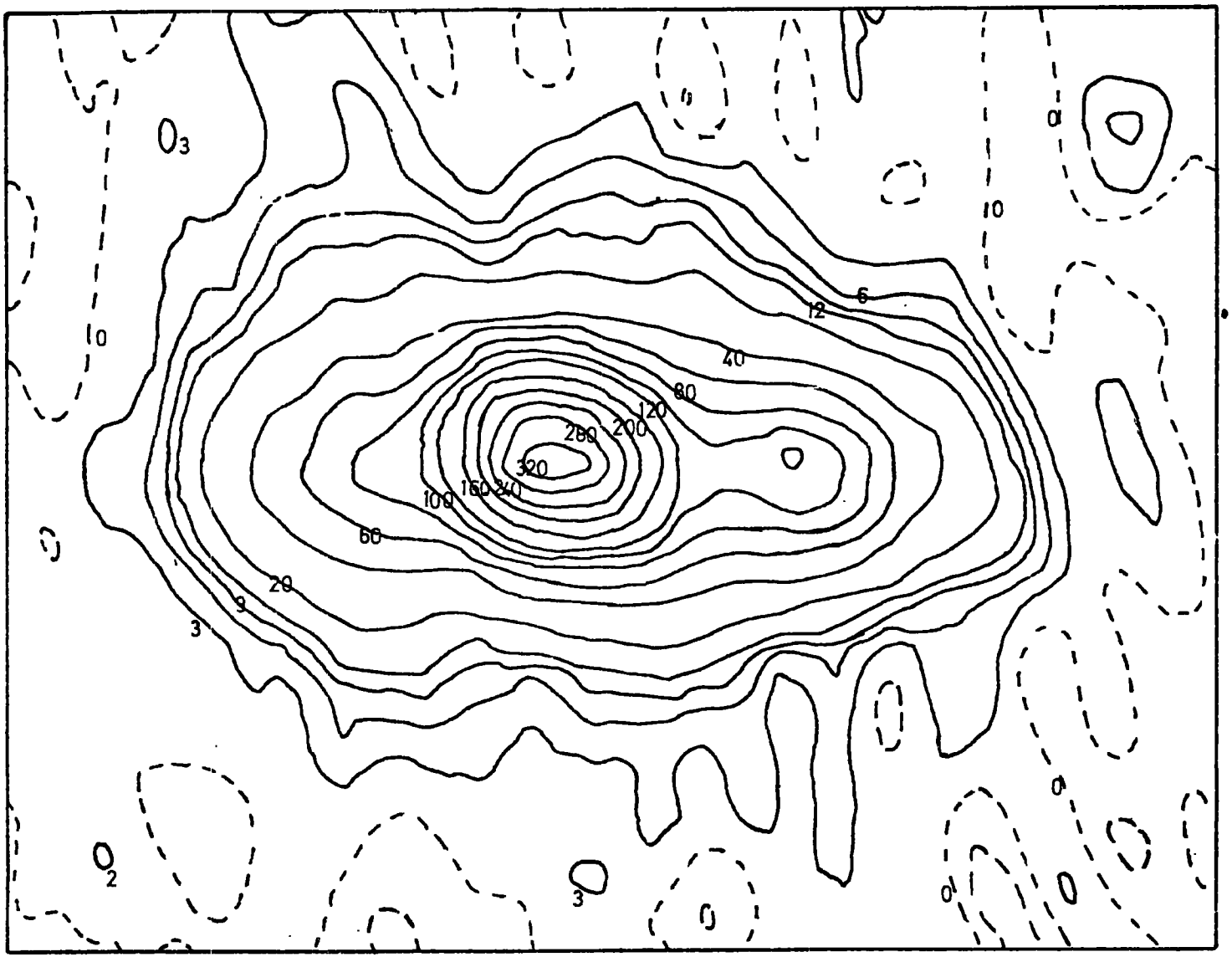

HPBW 58" x 107"

SCALE = 4'.8 / MM

FIG 8.5

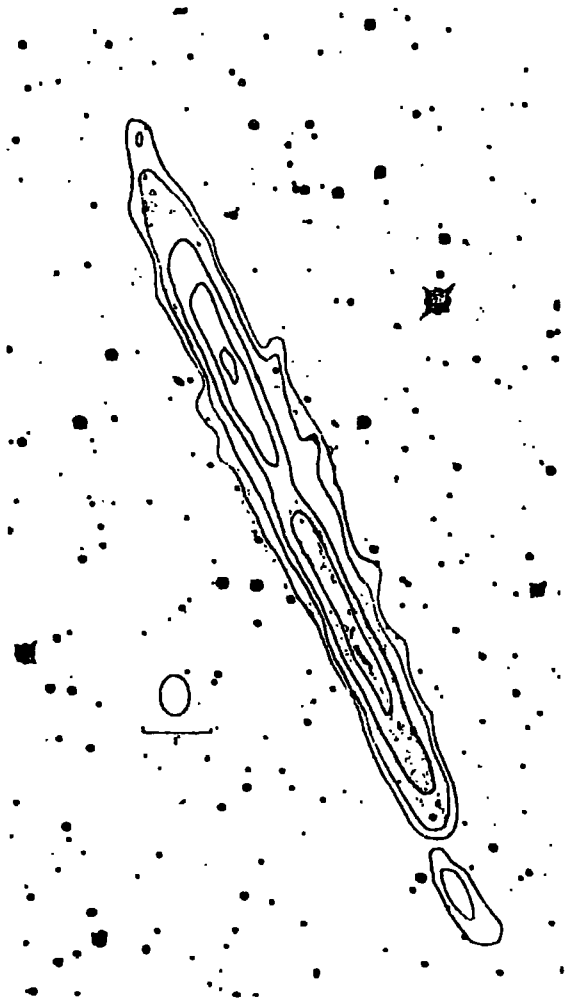

Figure 1:

Distribution of HI column density in NGC 891. The contours (0.2, 0.4, 1.2, 2.0, 2.8) are in units of 3 x 10^{21} cm^{-2}. These values are underestimates of the actual column densities, because of HI self-absorption and absorption against the radio-continuum emission from the disk of the galaxy itself. The beam-size is shown by the small ellipse. The map is based on incomplete data and therefore preliminary.

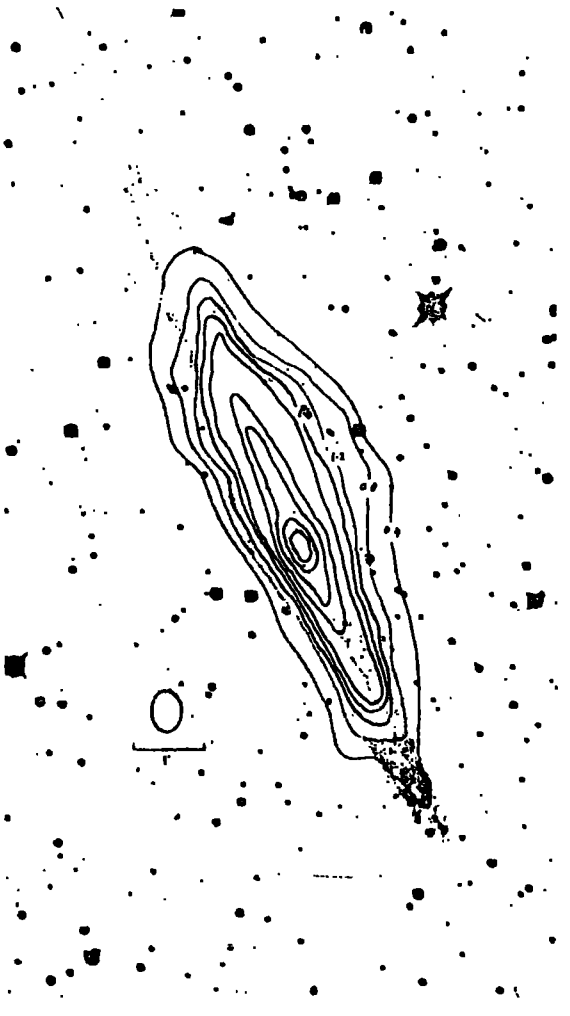

Figure 2:

Map of the radio continuum emission at 1415 MHz. The contour unit is 5 m.f.u./beam (≈ 4 K). The contour interval is 0.4 from 0.4 to 2.0 and 2.0 from 4.0 on. The spatial resolution is approximately the same as in the HI map.

FIG 8.6

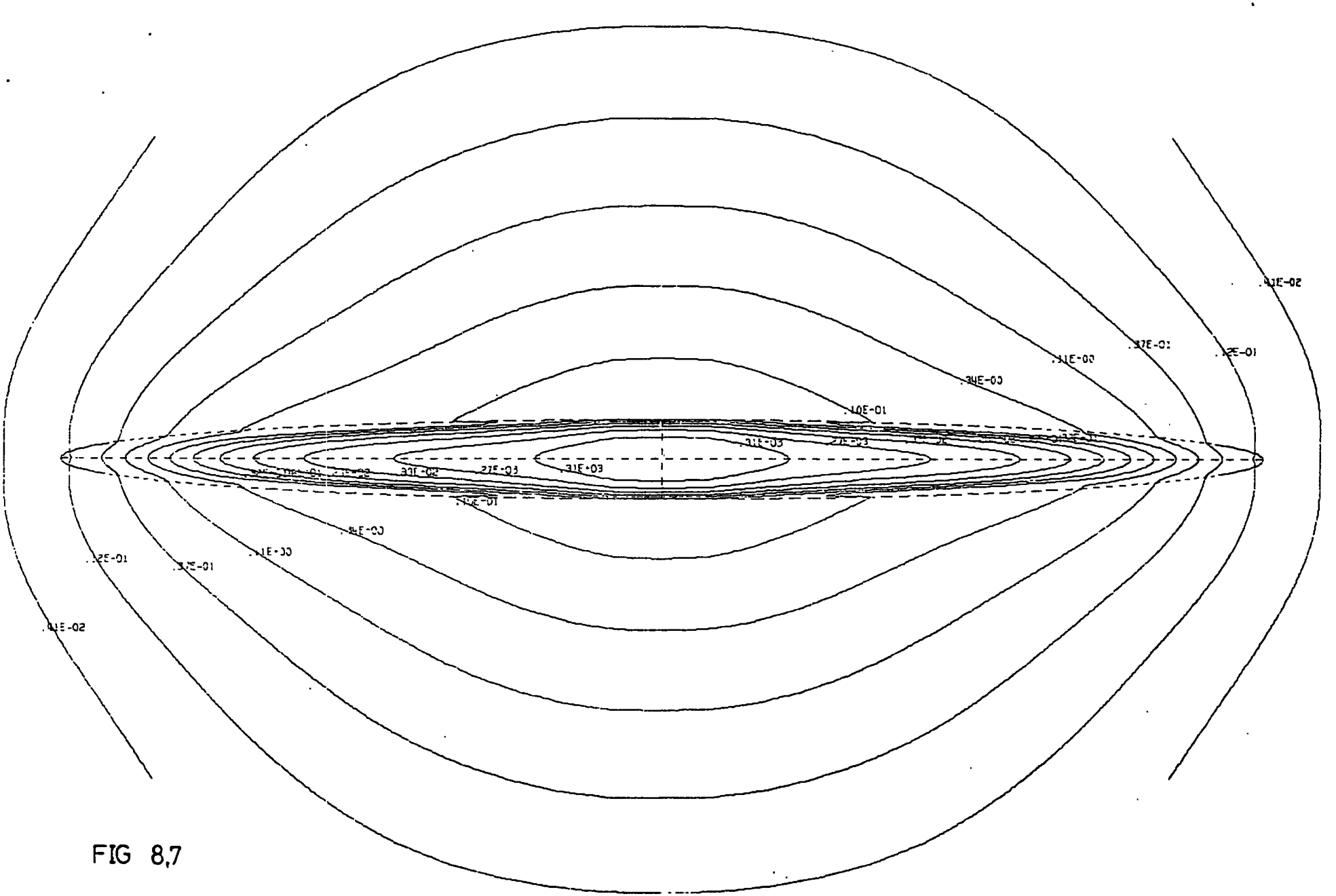

FIG 8,7

SYNCHROTRON EMISSION FOR THE GALACTIC DYNAMO (B)

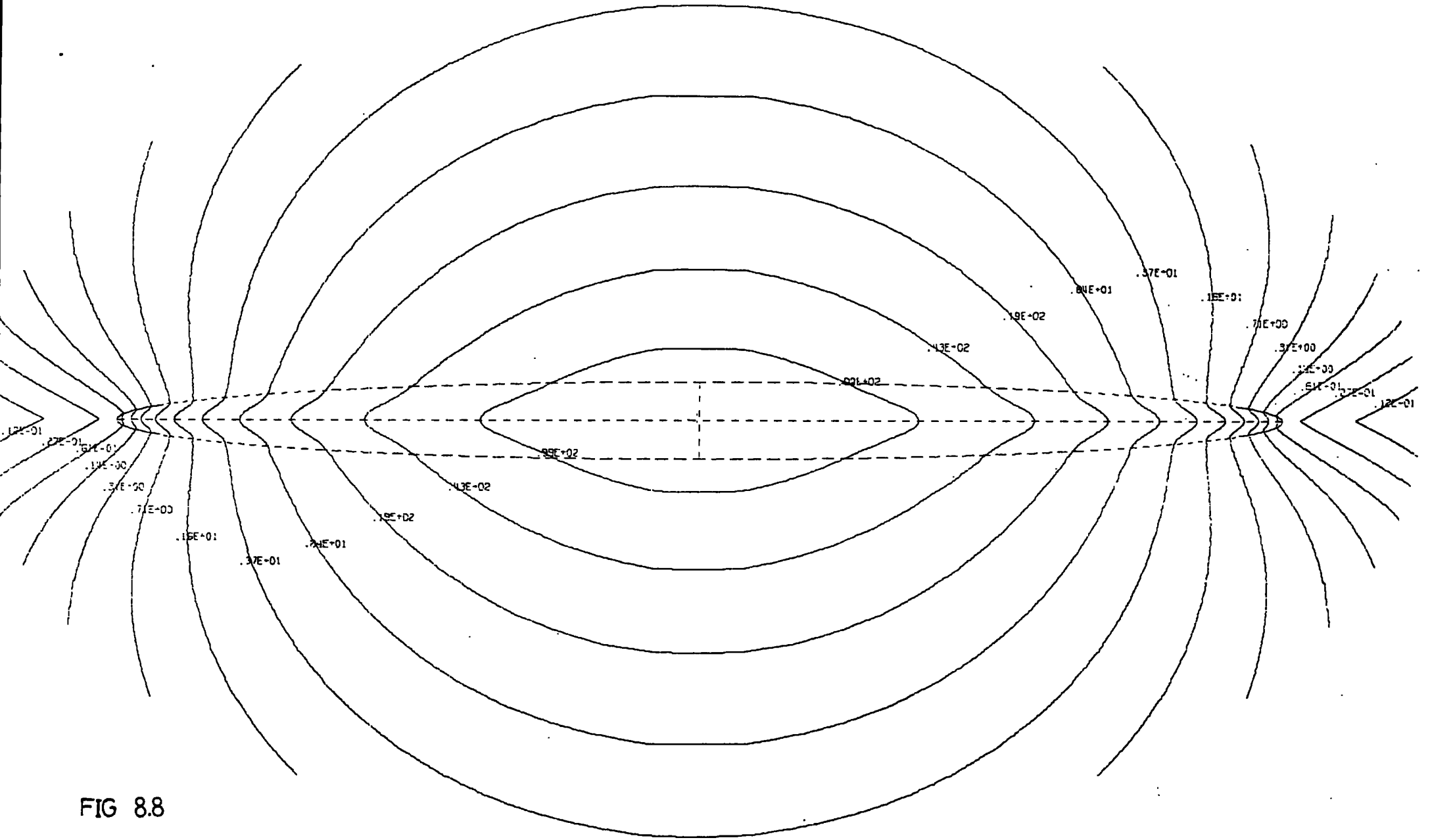

FIG 8.8

Comparison between predicted profile of dynamo models (a) and (b) and the observations of NGC 4631 and NGC 891.
x observations above the galactic plane ---- unconvolved profile
⊙ " " below " " " ____ convolved profile

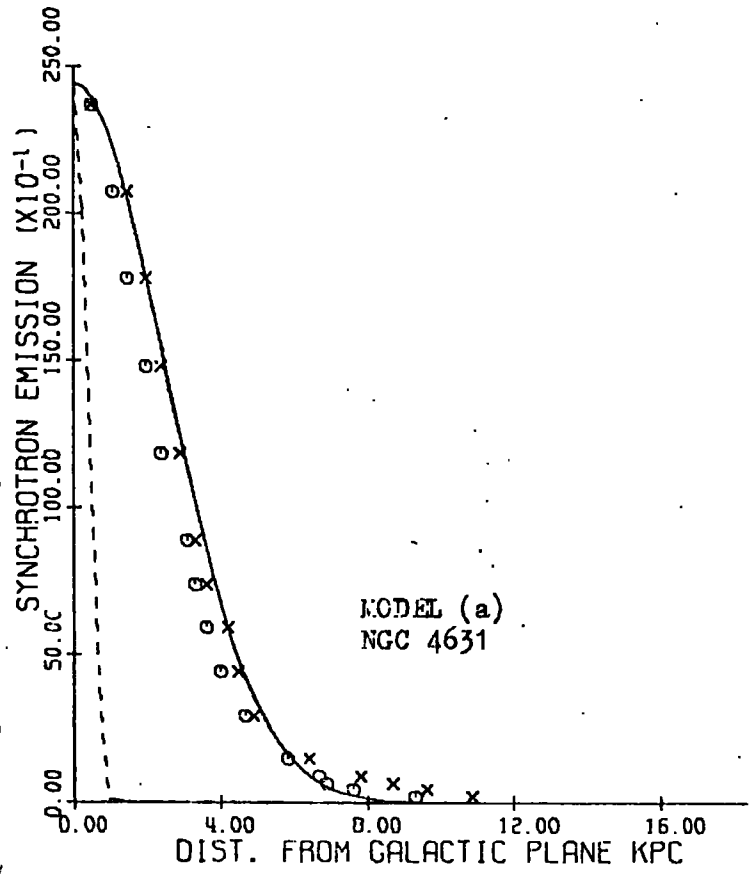

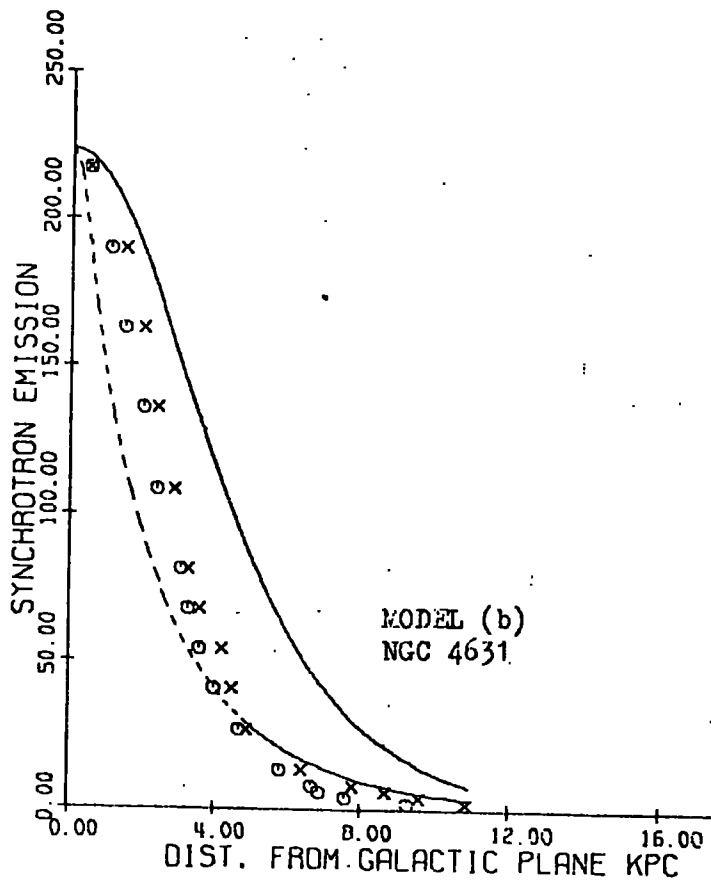

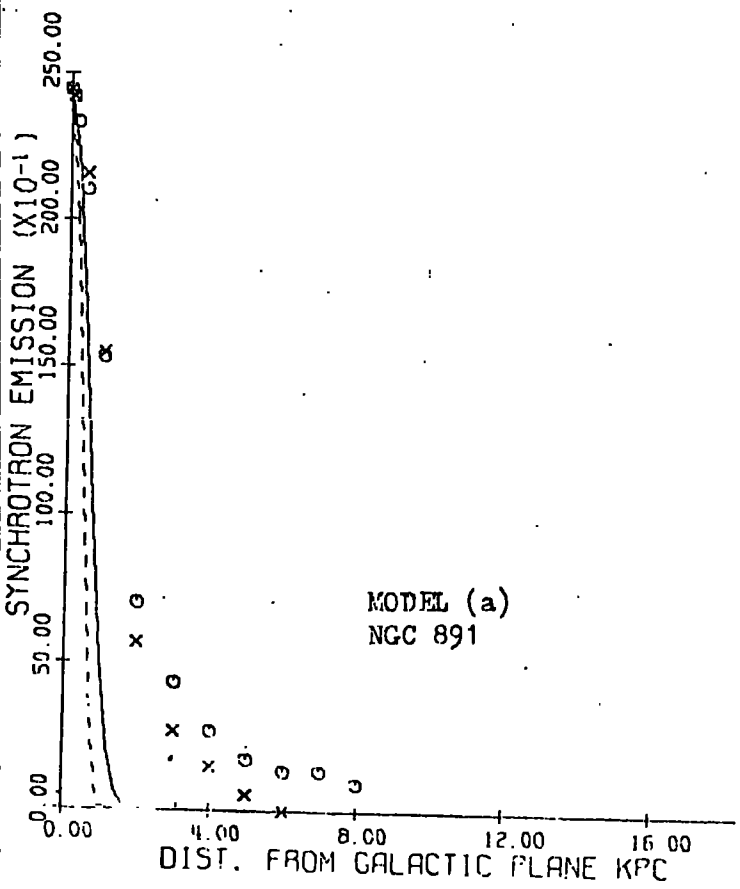

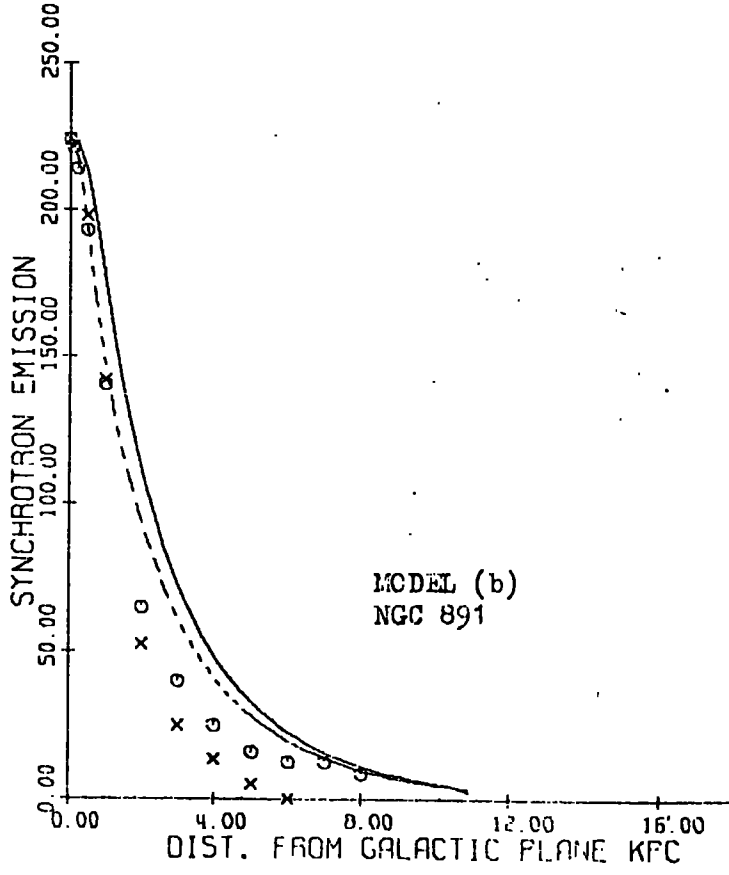

FIG 8.9

Chapter Nine. Conclusions

Dynamo action can occur in the galaxy. The galaxy can act as an $\alpha\omega$-dynamo, the steady quadrupolar mode being preferred. Oscillating solutions also occur, but require higher dynamo numbers for their excitation. Some attempt has been made to include nonlinear effects into the dynamo model, but this is far from satisfactory. The observed variation of the magnetic field in the disk inferred from the synchrotron radiation from the Galaxy is considerably less than predicted by the linear model. It is not clear whether the back-reaction of the magnetic field on the small-scale turbulent velocity field or on the large-scale velocity field dominates. The former effect has been investigated only in an arbitrary manner, a more sophisticated treatment awaiting further developments in turbulent magnetohydrodynamics. Good observations exist for the rotation curves of galaxies and provide incentive for developing the numerical techniques required for investigating the latter effect. There is no reason to believe that the suppression of turbulence can block dynamo action or that the occurrence of turbulence in a rotating cosmic body cannot alter the electromagnetic state of that system, as Piddington has suggested. The galactic magnetic field does not appear to be primordial but a consequence of present conditions.

Only axisymmetric solutions to the dynamo equation have been considered. However, the existence of spiral structure in the galaxy suggests that macroscopic regeneration induced by large-scale nearly symmetric fluid motions may be important. The approach provided by mean field electrodynamics to the problem is deceptively simpler than that of Braginskii's nearly symmetric dynamo approach, but the dynamic problems encountered in mean field electrodynamics are more difficult involving the fundamentals of turbulence theory. It is possible that both macroscopic and microscopic regeneration affect the nature of the galactic dynamo.

It is not possible to explain the observed synchrotron radiation from external galaxies on the basis of an essentially kinematic model and an empty intergalactic medium. Although it is possible to explain the observations by altering the model so that the intergalactic medium is conducting this is not interpreted as evidence for such a passive ionized medium in view of the physical implausibility of such a model. The results do suggest that ionized gas exists outside the denser galactic disk, but whether this is a global medium out of which galaxies may have formed and perhaps of sufficient density to bind clusters of galaxies or whether this has been issued from the galactic disk remains undecided. The escape of magnetic field by diffusion into the passive intergalactic medium of the model may have little relevance to the real case; instead it is envisaged that the magnetic field at the surface of the disk may dominate the motions of a tenuous intracluster plasma, both field and gas evaporating from a disk inflated by cosmic ray pressure. Observations of radio polarization of the synchrotron radiation from edge-on galaxies may be made in the near future and should distinguish between kinematic and dynamic models for the magnetic field. The kinematic model will give rise to a larger degree of polarization than a dynamic one, as a consequence of the large-scale regular field outside the disk.

As for the propagation of ultra-high-energy cosmic rays in the galaxy the kinematic dynamo model would rule out a galactic origin for primaries of a predominantly proton composition, in agreement with conventional field models. The poloidal field of the dynamo model is too weak to have any trapping effect upon the high energy particles. In the case of an empty intergalactic medium it is possible for small-scale correlations to provide source information particularly at high latitudes ($b^{II} > 45^{o}$).

However, it seems that significant amounts of ionized gas exist beyond the disk, weakening this possibility considerably. It is not clear how much dynamic effects might alter the picture, and seems wise to keep an open mind about the problem of extragalactic versus galactic origin for these particles.

In conclusion, dynamo theory can provide an adequate basis for building models of the galactic magnetic field which provide the most plausible explanation for its existence, and serve to unify diverse astrophysical observations both in the fields of cosmic ray astrophysics and radio astronomy.

APPENDIX I

The Parametric Equations of the Equal-Area Hammer Projection

This projection of the entire sky, also known as the equal-area Aitoff projection (although Hammer made the first construction, see Steers, 1962), is commonly used in Astrophysics. Its parametric equations, however, do not appear readily available in the literature on map projections. We have therefore made the following derivation, (Fong and White, unpublished) the results of which should prove useful to those wishing to use this projection in computer graphics.

To obtain this projection the following operations are necessary. The hemisphere shown in figure 1 is projected onto the (x, y) plane, and then the co-ordinate system is rotated so that the pole no longer appears at the centre, but at the circumference. We have the equations

$$\begin{aligned} z &= \cos\theta = \cos\theta' \cos\phi' \\ y &= \sin\theta \sin\phi = \cos\theta' \sin\phi' \\ x &= \sin\theta \cos\phi = \sin\theta' \end{aligned} \qquad \text{AI (1)}$$

and, referring to figure 2, we make the equal-area requirement that

$$dA = a^2 \sin\theta \, d\theta \, d\phi = \ell \, d\phi d\ell \qquad \text{AI (2)}$$

Then

$$\tfrac{1}{2} d(\ell^2) = -a^2 d(\cos\theta) \qquad \text{AI (3)}$$

$$\ell = a'(1 - \cos\theta)^{1/2} \qquad \text{AI (4)}$$

where $a' = \sqrt{2}\, a$

We set

$$\begin{aligned} X &= \ell \cos\phi \\ Y &= \ell \sin\phi \end{aligned} \qquad \text{AI (5)}$$

To cover the entire sky we perform the final transformations

$$\theta_s = \theta' \qquad \phi_s = 2\phi' \qquad \text{AI (6)}$$

and

$$X_L = 2Y \qquad Y_L = X$$

whence

$$l = a' \left(1 + \cos\theta_s \cos\phi_s/2 \right)^{1/2}$$

AI (7)

and

$$\tan\phi = \cot\theta_s \sin\phi_s/2$$

This has the effect of stretching, by a factor of 2, the original circular projection in the X_L axis, giving the familiar elliptical shape of the final projection. Substituting equations (6) and (7) into equations (5), and simplifying, shows that the equal-area Hammer projection $(\theta s, \phi s) \rightarrow (X_L, Y_L)$ is given by the equations

$$X_L = 2a'b \cos\theta_s \sin\phi_s/2$$

$$Y_L = a'b \sin\theta_s \qquad \text{AI (8)}$$

where

$$b = \left(1 + \cos\theta_s \cos\phi_s/2 \right)^{-1/2}$$

$$-\pi/2 < \theta_s < \pi/2$$

$$-\pi < \phi_s < \pi$$

We have put the operations which can be performed manually to produce the projection into a mathematical form.

As a check, it can be now shown that the equations do represent an equal-area projection. It is found that the Jacobian

$$\begin{vmatrix} \partial X_L / \partial\theta_s & \partial X_L / \partial\phi_s \\ \partial Y_L / \partial\theta_s & \partial Y_L / \partial\phi_s \end{vmatrix} = a^2 \cos\theta_s$$

as expected. The family of curves are shown in figure 3.

Reference

Steers, J.A. 1962 An Introduction to the study of map projections p 161-164 Univ of London Press Ltd

FIG. 1.

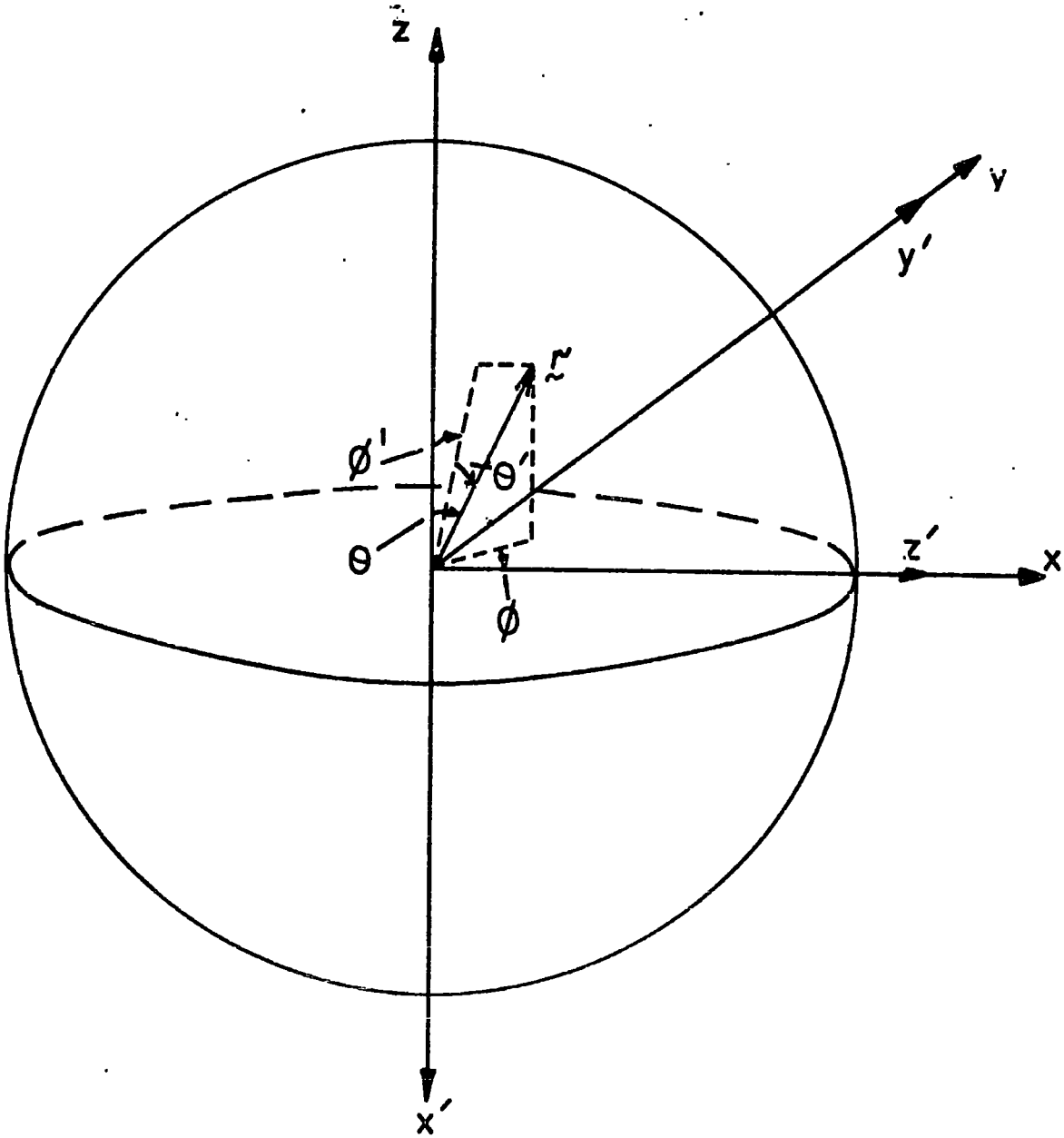

FIG. 2.

EQUAL-AREA AZIMUTHAL PROJECTION

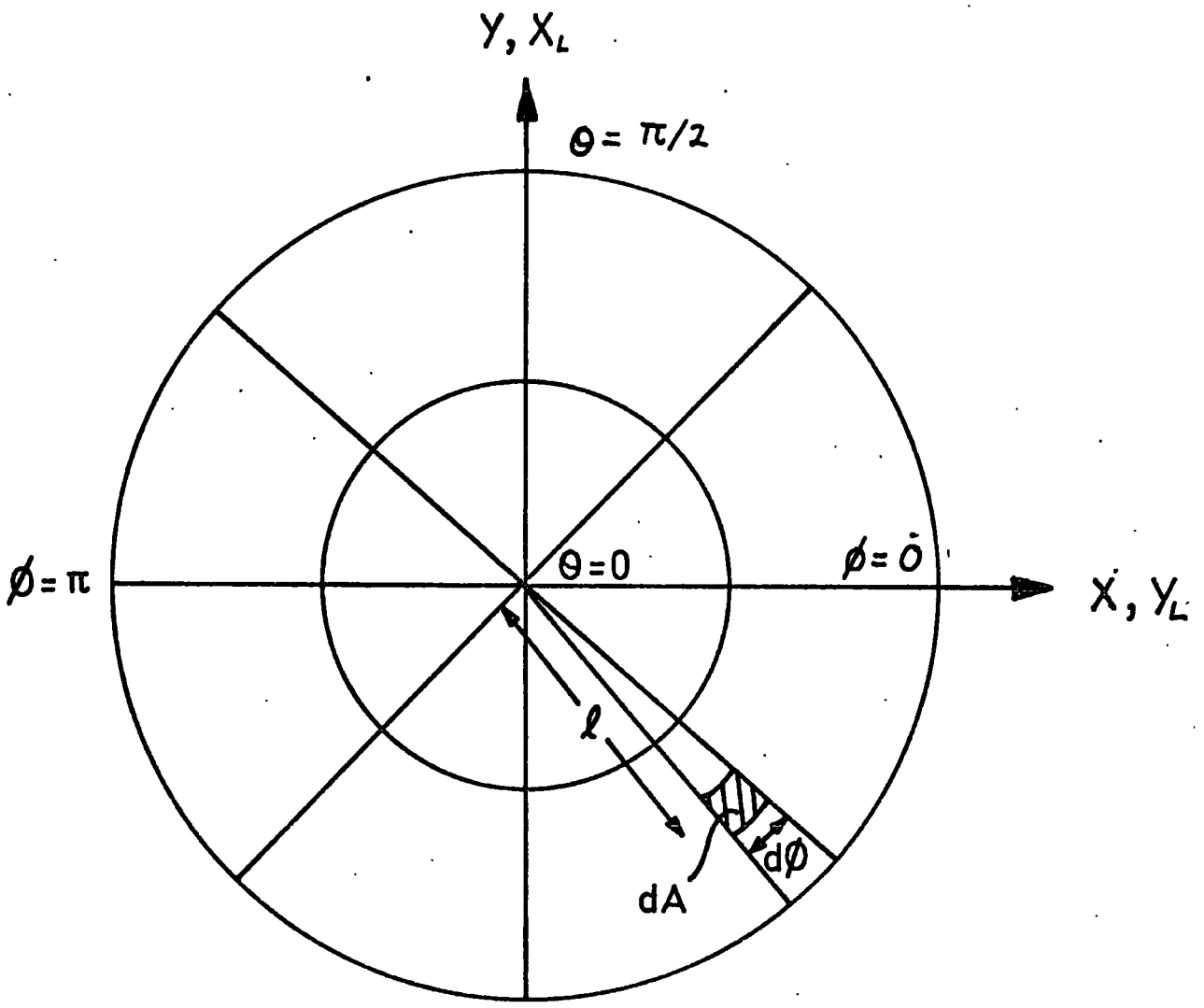

FIG.3.

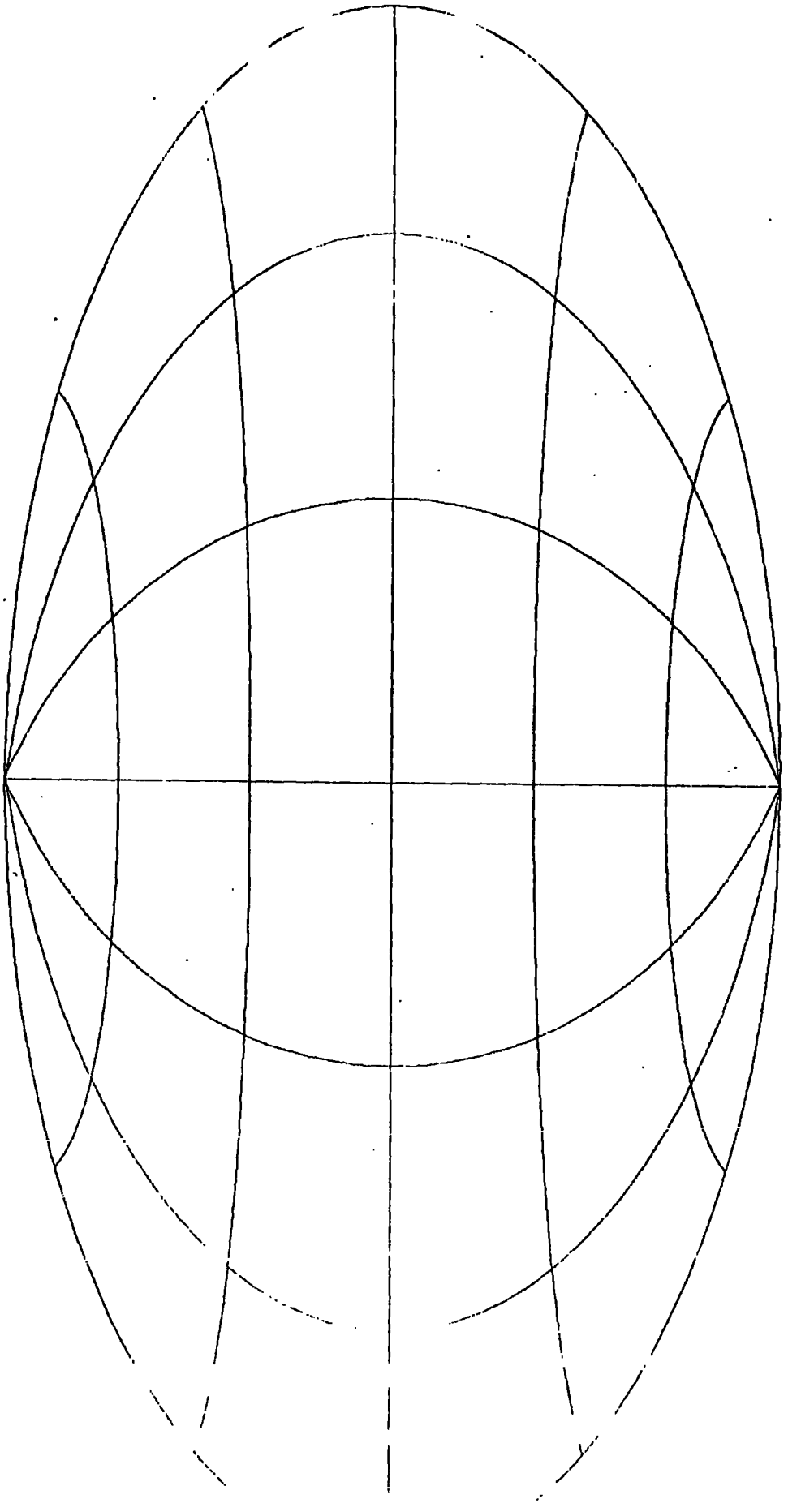

APPENDIX II

The Random Magnetic Field Model

Kiraly (personal communication, November 1974) has suggested the following derivation for the random small-angle multiple scattering of a proton in a magnetic field. The field model consists of uncorrelated fields of dimension $\bar{z}$. Each cell has a constant field strength and the overall directional distribution of the field is isotropic.

The path of a high-energy proton projected on the xz-plane is considered.

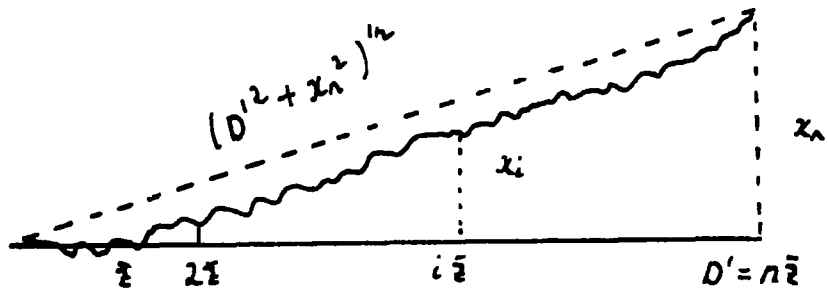

The angular deflection the xz-plane (yz-plane) for a high-energy proton is α_{ix} (α_{iy}) in the i^{th} cell. We expect $\langle \alpha_{ix}^2 \rangle = \langle \alpha_{iy}^2 \rangle = \alpha^2$ but $\langle \alpha_{ix} \rangle = \langle \alpha_{iy} \rangle = 0$. The angular bracket denotes the expectation value. Then

$$x_i = \sum_{\nu=0}^{i-1} (i\bar{z} - \nu\bar{z})\,\alpha_{\nu x}$$

$$= \bar{z} \sum_{\kappa=1}^{i} \kappa\,\alpha_{i-\kappa,x}$$

AII (1)

Consequently $\langle x_i \rangle = 0$, but

$$\langle x_i^2 \rangle = \bar{z}^2 \Big\langle \sum_{\kappa,\kappa'=1}^{i} \alpha_{i-\kappa,x}\, \alpha_{i-\kappa',x} \Big\rangle$$

$$= \bar{z}\,\alpha^2 \sum_{\kappa=1}^{i} \kappa^2 = \frac{i(i+1)(2i+1)}{6}\,\bar{z}^2\alpha^2$$

$$\simeq \alpha^2 \bar{z}^2 i^3/3 \qquad \text{AII (2)}$$

Similarly $\langle y_i^2 \rangle = \alpha^2 \bar{z}^2 i^3/3$. The total deflection

$$\langle \beta^2 \rangle = (\langle x_n^2 \rangle + \langle y_n^2 \rangle)/D^2$$

where $D = (D'^2 + x_n^2 + y_n^2)^{1/2}$ is the straight line distance.

For small-angle scattering

$$x_n^2 + y_n^2 \ll D'^2 \qquad \text{AII (3)}$$

then $D' \sim D$, and

$$\langle \beta^2 \rangle = 2\alpha^2 D/3\bar{z} \qquad \text{AII (4)}$$

Since we have isotropy i.e. $\langle \beta_x^2 \rangle = \langle \beta_y^2 \rangle = \langle \beta_z^2 \rangle = \frac{\langle \beta^2 \rangle}{3}$,

and constant fields in each cell then

$$\alpha_{ix}^2 = \beta_{iy}^2 \bar{z}^2/(100 E_{19}^2) \;,\quad \alpha_{iy}^2 = \beta_{ix}^2 \bar{z}^2/(100 E_{19}^2)$$

where $E_{19}(10^{19}$ eV), B (10^{-9} Gauss), $\bar{z}$ (Mpc), α (radians)

In these units

$$\alpha^2/\bar{z} = \langle \beta^2 \rangle \bar{z}/(300 E_{19}^2) \qquad \text{AII (5)}$$

and for β ($= \langle \beta^2 \rangle^{1/2}$) in degrees, we find

$$\boxed{\beta \simeq 2.7\, K\, E_{19}^{-1}\, D^{\frac{1}{2}}} \qquad \text{AII (6)}$$

where $K^2 = \langle \beta^2 \rangle \bar{z}$ is the propagation parameter.

For the path length difference we proceed as follows: let $\delta' = L - D'$, where L is the length of the path in space, and $\delta = L - D$.

$$\delta = \delta' - \frac{1}{2}\left(\frac{x_n^2}{D'} + \frac{y_n^2}{D'} \right) \qquad \text{AII (7)}$$

because of (3).

Since

$$\delta' = \sum_{i=1}^{n} \left[\left(\bar{z}^2 + (x_i - x_{i-1})^2 + (y_i - y_{i-1})^2 \right)^{1/2} - \bar{z} \right]$$

$$= \frac{1}{2\bar{z}} \sum_{i=1}^{n} \left[(x_i - x_{i-1})^2 + (y_i - y_{i-1})^2 \right] \qquad \text{AII (8)}$$

and

$$\langle (x_i - x_{i-1})^2 \rangle = \langle (y_i - y_{i-1})^2 \rangle$$

$$= \bar{z}^2 \left\langle \left(\sum_{\nu=0}^{i-1} (i-\nu)\alpha_{\nu x} - \sum_{\nu=0}^{i-2} (i-1-\nu)\alpha_{\nu x} \right)^2 \right\rangle$$

$$= \bar{z}^2 \left\langle \left(\alpha_{i-1,x} + \sum_{\nu=0}^{i-2} \alpha_{\nu x} \right)^2 \right\rangle$$

$$= \alpha^2 \bar{z}^2 i \qquad \text{AII (9)}$$

one obtains

$$\langle \delta' \rangle = \frac{1}{2\bar{z}} 2\alpha^2 \bar{z}^2 \sum_{i=1}^{n} i = \alpha^2 \bar{z} n^2/2$$

$$= \frac{\alpha^2}{2\bar{z}} D'^2$$

and finally

$$\langle \delta \rangle = \frac{\alpha^2}{2\bar{z}} D'^2 - \frac{1}{2}\left(\frac{2\alpha^2}{3\bar{z}} D'^2 \right)$$

$$= \frac{1}{6} \frac{\alpha^2}{\bar{z}} D'^2 \simeq \frac{1}{6} \frac{\alpha^2}{\bar{z}} D^2 \qquad \text{AII (10)}$$

using (5) we conclude

$$\boxed{\langle \delta \rangle = 1800\, \kappa^2 E_0^{-2} D^2} \qquad \text{AII (11)}$$

where $\langle \delta \rangle$ is in years.

Skilling (private communication) has reached essentially the same results by Fourier analysing the magnetic field.

APPENDIX III

The Simplified Maximum Likelihood Evaluation of the SN Hypothesis

The principle of maximum likelihood (see Kendall, 1951) is applied to evaluate the SN hypothesis discussed in Chapter Three. The likelihood function which is formulated has been suggested by Kiraly (personal communication February 1975). Let c be the intensity parameter, which characterizes the intensity of ultra-high energy cosmic rays produced by a SN. It is assumed to be the same for all SN_e . Let $\nu = 1, 2, \ldots N$ index the observed air shower lines, and $i = 1, 2, K_\nu$ index those SN_e whose circles (radius 5°) have intersections with the shower line. Let α_ν (hours) denote the right-ascension (RA) of the shower, and δ_ν its declination. We set $x_\nu = \alpha_\nu/24$. The probability density for the ν^{th} shower being in the position x_ν is, without normalization,

$$P'_\nu(x_\nu) = 1 + \sum_{i=1}^{K_\nu} h_{\nu_i}(x_\nu) \qquad \text{AIII (1)}$$

$$h_{\nu_i}(x_\nu) = g_{\nu_i}(x_\nu)\, c \cos\delta_\nu \qquad \text{AIII (2)}$$

$$g_{\nu_i}(x_\nu) = \begin{cases} R_{\nu_i}^{-\chi} & |x_\nu - x_{\nu_i}| \leq \Delta\nu_i \\ 0 \quad \text{if} & |x_\nu - x_{\nu_i}| > \Delta\nu_i \end{cases} \qquad \text{AIII (3)}$$

Diagramatically:

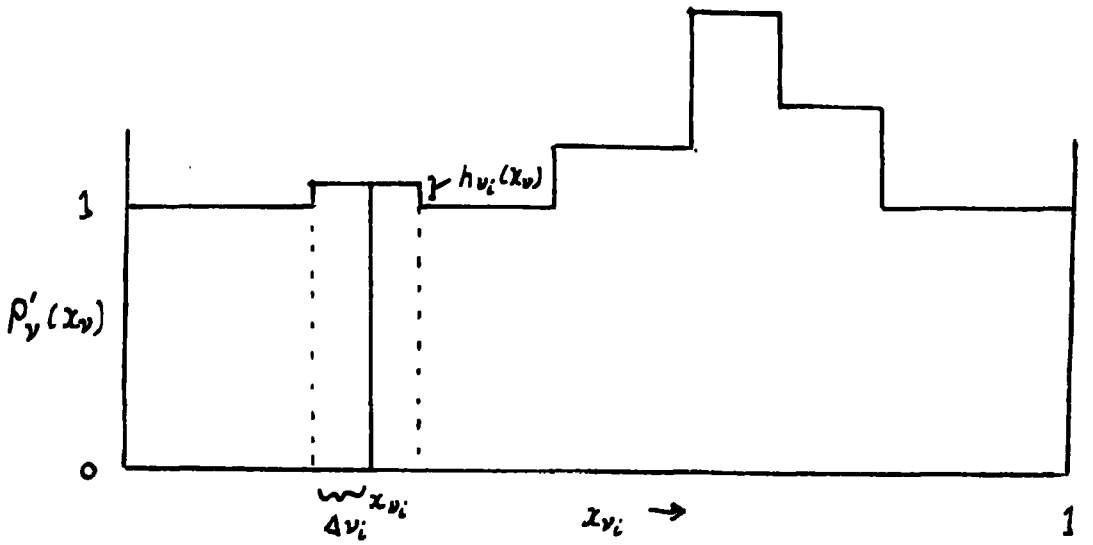

R_{ν_i} is the distance of the SN which contributes at x_{ν_i}. $K = 2$ takes account of the inverse square law, whereas $K = 4$ would also make allowance for the reduction flux due to propagation effects caused by magnetic fields (see AII). The $\cos\delta_\nu$ factor appearing in (2) allows for coverage effects.

The normalized probability density is

$$\rho_\nu(x_\nu) = \left(1 + \sum_{i=1}^{K_\nu} h_{\nu_i}(x_\nu)\right) \Big/ \left(1 + 2\sum_{i=1}^{K_\nu} \Delta\nu_i\, c\, R_{\nu_i}^{-K} \cos\delta_\nu\right)$$

$$= (1 + c\cos\delta_\nu\, s_\nu) / (1 + c\cos\delta_\nu\, \bar{s}_\nu)$$

AIII (4)

where

$$s_\nu = \sum_{i=1}^{K_\nu} q_{\nu_i}(x_\nu)$$

$$\bar{s}_\nu = \sum_{i=1}^{K_\nu} \Delta\nu_i\, R_{\nu_i}^{-K} \qquad \text{AIII (5)}$$

The likelihood function $L(c)$ is

$$L(c) = \log \prod_{\nu=1}^{N} P_\nu(x_\nu) \qquad \text{AIII (6)}$$

and maximizing with respect to c we find

$$\frac{\partial L}{\partial c} = \sum_{\nu=1}^{N} \frac{(s_\nu - \bar{s}_\nu)\cos\delta_\nu}{(1 + c\, s_\nu \cos\delta_\nu)(1 + c\,\bar{s}_\nu \cos\delta_\nu)} = 0 \qquad \text{AIII (7)}$$

The maximization is achieved numerically, taking a suitable range for c. The maximum value c_{max} of c and $L(c_{max})$ is determined for the actual data. $L(c_{max})$ is the probability density of finding c_{max}, relative to the c = 0 case. The quantile of $L(c_{max})$, which is found by Monte Carlo methods (i.e assigning random values of RA to the showers), tests the hypothesis: it is the probability that we have wrongly rejected the null hypothesis.

In order to estimate both the propagation parameter (K, discussed in Appendix II) and the intensity parameter it is necessary to extend the likelihood function to two dimensions (K, c). L (K, c) is then maximized with respect to both K and c. To achieve this a time 'window' selection is performed, for varying values of K, before determining the maximum value of c. The selection was carried out by allowing those events whose time delays δ' satisfied

$$\delta/2 \leq \delta' \leq 2\delta \qquad \text{AIII (8)}$$

where δ is given by AII (11). The random sets of air showers are now also assigned the actual arrival times in a random order.

Reference

Kendall, M.G. 1951 The Advanced Theory of Statistics vol II p 12-21
C Griffin & Co Ltd Third Ed.

APPENDIX IV

The Eigenvalue Approach to the Dynamo Problem

Stix (1975) has formulated this approach, which is outlined. We mention a way of incorporating this approach for the imposition of boundary conditions for the initial-value problem.

The external magnetic field

$$\underset{\sim}{B}_p = -\nabla\psi \qquad \text{AIV (1)}$$

In the axisymmetric case

$$\psi = e^{\lambda t} \sum_{n=1}^{\infty} A_n P_n(\eta) Q_n(i\xi) \qquad \text{AIV (2)}$$

satisfies the boundary condition at infinity. The time dependence, t, is separated into the exponential factor. P_n and Q_n are Legendre polynomials of the first and second kind, respectively.

The internal toroidal field is represented by

$$B = e^{\lambda t} \sum_{n=1}^{\infty} b_n(x) P_n^1(\eta) \qquad \text{AIV (3)}$$

$b_n(1) = 0$ for all n satisfies the condition that no currents flow outside the disk.

The internal poloidal field is represented by the toroidal vector potential A = (0, 0, A) where

$$A = e^{\lambda t} R \sum_{n=1}^{\infty} a_n(x) P_n^1(\eta) \qquad \text{AIV (4)}$$

The boundary condition on $a_n(x)$ is found by equating the external and internal poloidal field components, using the orthogonality of P_n and P_n^1, and eliminating A_n. The result is

$$(1+1/\beta_0^2)\left.\frac{da_n}{dx}\right|_{x=1} + a_n(1)\left[1 - n(n+1)\,Q_n(i\beta_0)\Big/\left.\frac{d}{dx}Q_n(ix\beta_0)\right|_{x=1}\right] = 0$$

AIV (5)

Equations (3) and (4) are substituted into equations (5.4.5) and (5.4.6), which are multiplied by $(x^2+\eta^2/\beta_0^2)\,P_\nu^1(\eta)$ and integrated over the η interval (-1, 1). The results are

$$\lambda \sum_n F_{n\nu} b_n = -R_m \sum_n K_{n\nu} + \frac{N_\nu}{\nu^2}\left[(x^2+\beta_0^{-2})\frac{d^2 b_\nu}{dx^2} + 2x\frac{db_\nu}{dx} + \frac{b_\nu}{1+x^2\beta_0^2} - \nu(\nu+1)\,b_\nu\right]$$

AIV (6)

and

$$\lambda \sum_n F_{n\nu} a_n = R_m \sum_n G_{n\nu} + \frac{N_\nu}{\nu^2}\left[(x^2+\beta_0^{-2})\frac{d^2 a_\nu}{dx^2} + 2x\frac{da_\nu}{dx} + \frac{a_\nu}{1+x^2\beta_0^2} - \nu(\nu+1)\,a_\nu\right]$$

AIV (7)

where

$$F_{n\nu} = \int_{-1}^{1}(x^2+\eta^2/\beta_0^2)\,P_n^1 P_\nu^1\,d\eta$$

AIV (8)

$$K_{n\nu} = \frac{1}{\nu^2}\int_{-1}^{1} s\left[\frac{\partial\omega}{\partial x}\frac{\partial}{\partial\eta}(s a_n P_n^1) - \frac{\partial\omega}{\partial\eta}\frac{\partial}{\partial x}(s a_n P_n^1)\right] P_\nu^1\,d\eta$$

$$G_{n\nu} = b_n \int_{-1}^{1} 2x\,(x^2+\eta^2/\beta_0^2)\,P_n^1 P_\nu^1\,d\eta$$

$$N_\nu = 2\nu(\nu+1)/(2\nu+1)$$

The integrals are worked out using orthogonality and recurrence relations, and are listed in the appendix of Stix's paper.

To test Stix's calculation we proceeded as follows. The problem was first simplified by setting $\lambda = 0$, and only the steady modes occur. (6) and (7) become

$$AX = 0 \qquad \text{AIV (9)}$$

where X is the column vector consisting of values of a_n (x) and b_n (x) at grid points, for each harmonic. For (a_n, n = 0, 2, 4 .. N), (b_n, m = 1, 3, 5 .. N + 1) the quadrupole mode is obtained, and (a_n = 1, 3, 5 .. N + 1), ($b_{\ }$, $_{\ }$ = 0, 2, 4, N) the dipole mode is obtained. The split occurs since the integrals in (8) vanish if $n - \nu$ is odd. This arises because of the symmetry properties of $\tilde{\alpha}$ and $d\tilde{\omega}/ds$ with respect to z = 0. At x = 0, η has a discontinuity, and for regularity it is required that a_n and b_n for all even n and da_n/dx and db_n/dx for all odd n are zero.

To determine $a_n(x)\big|_{x=1}$ the following relations are used (Roberts and Stix, 1972):

$$a_\lambda(1-\Delta x) = a_\lambda(1) - \Delta x \left.\frac{da_\lambda}{dx}\right|_{x=1} + \frac{\Delta x^2}{2!}\left.\frac{d^2a_\lambda}{dx^2}\right|_{x=1} \cdots \qquad \text{AIV (10)}$$

$$(x^2+f_0^{-2})\left.\frac{d^2a_\lambda}{dx^2}\right|_{x=1} + 2x\left.\frac{da_\lambda}{dx}\right|_{x=1} + a_\lambda\left[\frac{1}{1+x^2f_0^2} - \lambda(\lambda+1)\right] = 0 \qquad \text{AIV (11)}$$

(7), (10) and (11) give the required result:

$$a_\lambda(1-\Delta x)/a_\lambda(1) = 1 + \frac{\Delta x}{1+f_0^{-2}}\left[a_\lambda(1)\left(1 - \lambda(\lambda+1)\right.\right.$$

$$\left.\left. P_\lambda(if_0x)/\left.\frac{d}{dx}P_\lambda(if_0x)\right|_{x=1}\right.\right] \qquad \text{AIV (12)}$$

We can now set up the matrix A (in (9)) and determine the dynamo number (R_m^2) for the quadrupole mode. The value of R_m for which the first zero of $|A|$ occurs gives the result. This was determined by trial and error, using a standard NAG Library program to find $|A|$. Ten harmonics and ten grid points were taken. Our determinant was therefore 200 x 200. The result $P \approx -58{,}000$ is in reasonable agreement with the initial value problem result (-63,000). Stix solves the more general eigenvalue problem $AX = \lambda BX$.

We now consider if it is advantageous to incorporate some of these techniques into our initial-value formulation. Noting that

$$A(\eta, 1-\Delta x) = e^{\lambda t} R \sum_{n=1}^{N} a_n (1-\Delta x) P_n^1(\eta)$$

we can determine $a_n(1-\Delta x)$ for all n from the values of $A(\eta, 1-\Delta x)$ on the finite-difference grid. This would obviously involve the same amount of work as the method we have already described for the imposition of boundary conditions, unless the matrix in concern is positive definite (in which case over-relaxation could be used). Given $a_n(1-\Delta x)$, $a_n(1)$ are determined from (12) which give $A(\eta, 1)$.

For the external solution, however, the situation is definitely more favourable. Given $a_n(1)$, A_n are determined (once the internal and external values of the poloidal field are equated) which give ψ and consequently $\underset{\sim}{B}p$. This would be more efficient computationally than the method of interpolation we have employed, and greater accuracy could probably be achieved.

References

Stix, M. 1975 Astron & Astrophys 42, 85

Roberts, P.H, Stix, M. 1972 Astron & Astrophys 18 453

Acknowledgements

The author wishes to thank Professor A.W. Wolfendale for making available the facilities of the Physics Department of the University of Durham, and the Science Research Council for its financial support.

He expresses gratitude to Dr. J.L. Osborne for his guidance and encouragement during the period of research for this thesis.

The author acknowledges valuable discussions with Dr. J. Baldwin, Dr. R. Ellis, Dr. R. Fong, Mr. D.K. French, Professor J. Linsley, Professor M. Rees, Dr. J. Skilling, Dr. A. Watson, and Professor A.W. Wolfendale. Professor J. Linsley, Dr R. Sancisi, and Dr. A.Watson are thanked for providing the author with observational data prior to publication. The author has received advice and help also from Mr. P. Kiraly, Professor P.H. Roberts, and Dr. A.M. Soward to whom he is particularly grateful. The facilities and assistance of staff at the Durham University Computer Unit have been appreciated.

Finally, the author wishes to thank his sister Mrs G. Lockett for skilfully typing this thesis.